– *An international journal for New Concepts in Global Tectonics* –

NCGT JOURNAL

Editor-in-Chief: Bruce LEYBOURNE (leybourneb@iascc.org)

NCGT Journal
New Concepts in Global Tectonics

Volume 14, Number 6
June 2026

ISSN 2202-0039

WWW.ncgtjournal.com

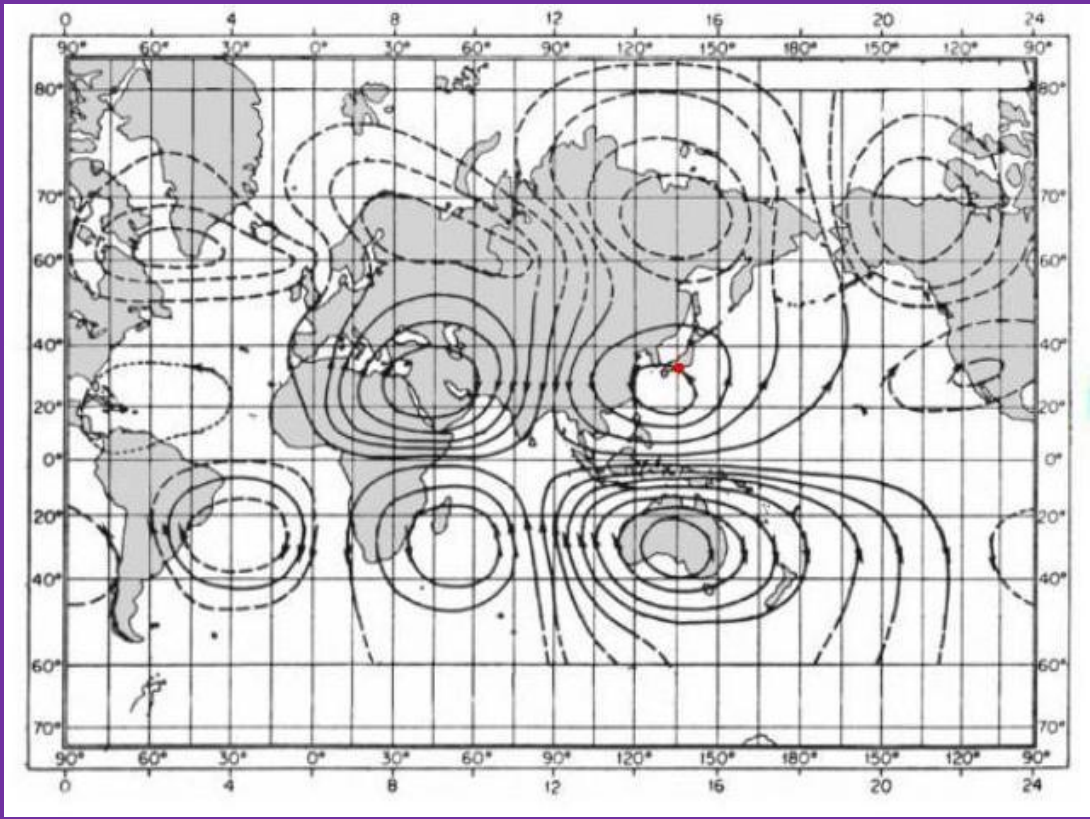

Global telluric currents map - computed by (Gish, 1939)

The Circuitry of Consilience:...
by
Hawthorne, Robert Jr.
Fig. 8 this issue

2nd Quarterly Issue

NCGT Journal
New Concepts in Global Tectonics

New Concepts in Global Tectonics Journal
Volume 14, Number 6, June 2026

ISSN number; ISSN 2202-0039

– An international journal for New Concepts in Global Tectonics –

NCGT JOURNAL

Volume 14, Number 6, June 2026. ISSN 2202-0039.

CONTENTS

EDITOR's CORNER - Comments by Editor in Chief - Bruce Leybourne.....424
NCGT 2026 - Parma, Italy Conference Announcement.....424

Article

The Circuitry of Consilience: Quantifying the 664 - 663 BCE Yatagarasu-Miyake Event as a Resonant Solar-Tectonic Discharge: Robert F. Hawthorne Jr.....428

The search for periodicities - Superposition operators: Giovanni Pietro Gregori, Bruce Allen Leybourne.....439

AN OCEAN IN GEOLOGICAL HISTORY: Vadim V. Gordienko.....480

ENERGY BALANCE OF THE TECTONOSPHERE DURING OCEANIZATION: Vadim V. Gordienko, Ivan V. Gordienko, ...488

About the NCGT Journal.....497

Get Registered Here: https://www.ncgtjournal.com/events

For donations, please feel free to contact the Research Director of the Geoplasma Research Institute, Mr. Bruce Leybourne, at leybourneb@iascc.org. For contact, correspondence, or inclusion of material in the NCGT Journal please use the following methods: *NEW CONCEPTS IN GLOBAL TECTONICS.* 1. E-mail: leybourneb@iascc.org (files in MS Word or ODT format, and figures in gif, bmp or tif format) as separate files; 3. Telephone, +61 402 509 420. *DISCLAIMER*: The opinions, observations and ideas published in this journal are the responsibility of the contributors and do not necessarily reflect those of the Editor and the Editorial Board. *NCGT Journal* is a refereed quarterly international online journal and appears in March, June, September and December. *ISSN number*; ISSN 2202-0039.

NCGT Journal
New Concepts in Global Tectonics

New Concepts in Global Tectonics Journal
Volume 14, Number 6, June 2026

ISSN number; ISSN 2202-0039

EDITOR's CORNER: - Comments by Editor in Chief - Bruce Leybourne

"CALL FOR PAPERS" 21-24 September 2026 – International NCGT in Parma, Italy

Organized by Valentino Straser (valentino .straser @gmail . com)

Timetable for participating in the conference:

Open abstract March 1, 2026
Abstract acceptance July31
Payment due by Aug 15, 2026 (To organizing committee)
Publication of conference and abstract book September 15, 2026

Get Registered Here: https://www.ncgtjournal.com/events

Regarding information for authors:

Abstract: 150 words (maximum)
Short CV: 300 words (maximum) and a photo.
For formatting and fonts, use NCGT Journal.
Abstract submission opens March 15, 2026
Extended: 31 July, 2026
Confirmation of abstract acceptance: Aug15, 2026

See: https://www.ncgtjournal.com/events

Please visit our "Events" page above to register, submit abstracts and make hotel reservations.

Field Trip: 23 Sept. 2026 (See next page)
Late Cretaceous North Apennines

Information website about the city of Parma and its province:

homepage - Informazioni turistiche su Parma e provincia

"Earthquake Forecasting with Earth and Space Weather " summarizes the contents of the NCGT 2026 Conference scheduled in Parma, Italy from September 21 to 24, 2026. The NCGT team returns after fifteen years , to discuss Earth model innovations and scenarios for understanding geophysical processes and space weather effects. And, more traditionally , new models of Global Tectonics.

Understanding the Earth today means looking beyond the traditional boundaries of geology and geophysics , combining expertise ranging from electromagnetism to atmospheric physics to space weather. The "Earth & Space" conference was born with this objective : to propose an integrated interpretation of geophysical phenomena , exploring the role of electromagnetic signals as potential precursor indicators of seismic events and analyzing the contribution of new technologies for data observation and interpretation.

In recent decades, studies inspired by the global electric circuit model, a concept developed from the insights of scientists in recent decades , have highlighted how the Earth's atmosphere , ionosphere , and planetary surface constitute an electrically connected system. From this perspective , processes occurring in the lithosphere , including those preceding an earthquake , could produce measurable variations in electromagnetic fields and ionospheric properties.

The conference aims to further analyze the so-called "candidate seismic precursors" of electromagnetic nature, evaluating their potential and limitations considering the latest scientific evidence . The integration of highly sensitive ground-based sensors, satellite networks, and ionospheric monitoring systems opens new perspectives in multi-parametric data collection and modeling of phenomena.

Special focus will be on the role of the Sun. Solar activity monitoring from NASA missions and international space weather programs , indicate influences in the ionosphere and Earth 's magnetic field , have potential implications for climate and geodynamic systems . Understanding the interactions between the solar wind , the magnetosphere , and Earth 's internal processes represents a crucial frontier for interpreting complex geophysical events from a systemic perspective.
"Earth & Space" therefore proposes new interpretative concepts, encouraging us to move beyond compartmentalized visions to embrace a dynamic and interconnected model of the planet. Earth's evolution is not merely the result of endogenous forces but can be interpreted as the product of a continuous dialogue between space and the surface, between solar energy and deep-seated processes.

The conference is aimed at researchers , professionals , administrators , and citizens interested in understanding how new technologies and interdisciplinary models can contribute to a more advanced understanding of natural phenomena . It will provide an opportunity for scientific and cultural exchange to explore the future challenges of prevention , sustainability , and risk management on an increasingly complex planet.

ISSN number; ISSN 2202-0039

Get Registered Here: https://www.ncgtjournal.com/events

Field Trip : 23 Sept . 2026 with focus on Late Cretaceous flysch and ophiolite formations related to the closure phases of the Ligurian -Piedmont Basin . Among the enigmatic formations attracting the attention of many geologists around the world is the "Devil's Leaps." Furthermore , this area, affected by a strike- slip fault , is home to anomalous atmospheric phenomena and unique ionization patterns that precede earthquakes in this geological context of the Northern Apennines.

"North -Eastern Apennines , research has been underway for over 35 years to identify candidates for seismic precursors . First observations collected date back to 1983 along the Taro River Seismic Line , considered by the author to be an 'open -air laboratory '."
See : Straser, 2020 - **https://www. iiisci.org/journal/sci/FullText.asp?var=&id=ZA981US20**

Geoplasma Research Presents

NCGT 2026 CONFERENCE

Parma Italy

a NCGT Journal Production

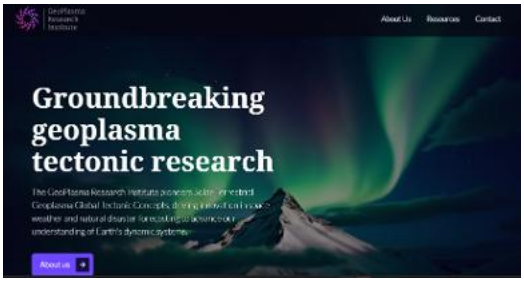

https://www.geoplasmaresearchinstitute.org/

Fifteen years have brought significant advancements in our technology - driven science, since our conference in India (2011) "Earth Dynamics - Perceptions and Deadlock ". We highlighted unresolved issues within prevailing tectonic theories despite decades of accumulating data.

Offering new perspectives on our cosmos and, consequently , our planet. This conference provides a vital platform for scientists to present, listen , and engage in discussions about the history and ultimate destiny of our Pale Blue Dot . Join us to explore the evolving understanding of Earth 's dynamics.

Earth and Space Weather
Advanced Tectonics - Earthquake Forecasting

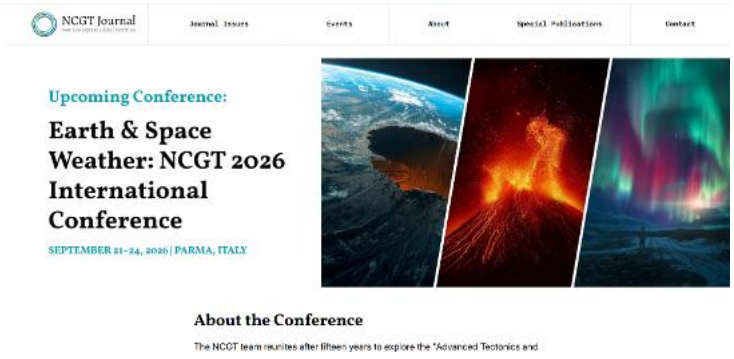

Get Regisered Here: https://www.ncgtjournal.com/events

Get Regisered Here: https://www.ncgtjournal.com/events

ISSN number; ISSN 2202-0039

Conference details: 21-24 September 2026 – NCGT in Parma, Italy
Organized by Valentino Straser (valentino .straser @gmail . com)
Information website about the city of Parma and its province: https://parmawelcome.it/

Registration Fee (Euro - 100) can pay with abstract submission on web link.

Single room , two coffee breaks /lunch /dinner €185 .00 plus a €4 tourist tax . See : https :// www . hotelparmaecongressi.com/

Dinner hotel: €35.00/person.
Day meeting (lunch and two coffee breaks) – €45/person.
BNB single room €140.00/night + €4 tourist tax.
Make Reservations https://www.ncgtjournal.com/events

Timetable for participating in the conference:
Open abstract March 15, 2026
Abstract acceptance May 31
Get Regisered Here: https://www.ncgtjournal.com/events
Payment (TBD) due by June 15, 2026 (To organizing committee)
Publication of conference and abstract book September 1, 2026

Regarding information for authors:
Abstract: 150 words (maximum)
Short CV: 300 words (maximum) and a photo.
For formatting and fonts, use NCGT Journal.
Abstract submission opens March 15, 2026
Conclusion: July 31, 2026
Confirmation of abstract acceptance: On or before August 15, 2026

"Earth and Space Weather Advanced Tectonics and Earthquake Forecasting between Heaven and Earth " summarizes the contents of the NCGT 2026 Conference scheduled in Parma from September 21 to 24 , 2026 . The NCGT team reunites after fifteen years , to discuss Earth model innovations and scenarios for understanding geophysical processes and space weather effects . More traditionally , new models of Global Tectonics and explored understanding Earth by looking beyond traditional boundaries of geology and geophysics, combining expertise ranging from electromagnetism to atmospheric physics to space weather.

ISSN number; ISSN 2202-0039

The "Earth & Space Weather" conference objective proposes an integrated interpretation of geophysical phenomena , exploring the role of electromagnetic signals as potential precursor indicators of seismic events and analyzing the contribution of new technologies for data observation and interpretation.

Recent studies inspired by the **global electric circuit** model, a concept developed from the insights of scientists in recent decades , highlight how the Earth 's atmosphere , ionosphere , and planetary surface constitute an electrically connected system. From this perspective , processes occurring in the lithosphere , including those preceding an earthquake , could produce measurable variations in electromagnetic fields and ionospheric properties.

The conference aims to further analyze the so-called "**candidate seismic precursors**" of electromagnetic nature , evaluating their potential and limitations considering the latest scientific evidence. The integration of highly sensitive ground -based sensors , satellite networks, and ionospheric monitoring systems open new perspectives in multi-parametric data collection and modeling of phenomena.

Special focus will be on the role of the Sun. **Solar activity monitoring** from NASA missions and international space weather programs indicate influences in the ionosphere and Earth 's magnetic field , have potential implications for climate and geodynamic systems. Understanding the interactions between the solar wind, the magnetosphere, and Earth's internal processes represents a crucial frontier for interpreting complex geophysical events from a systemic perspective.

"Earth & Space Weather" conference therefore proposes new interpretative concepts , encouraging us to move beyond compartmentalized visions to embrace a dynamic and interconnected model of the planet. Earth's evolution is not merely the result of endogenous forces but can be interpreted as the product of a continuous dialogue between space and the surface, between solar energy and deep-seated processes.

Thus the **"Earth & Space Weather"** conference is aimed at researchers , professionals , administrators , and citizens interested in understanding how new technologies and interdisciplinary models can contribute to a more advanced understanding of natural phenomena. It will provide an opportunity for scientific and cultural exchange to explore the future challenges of prevention, sustainability, and risk management on an increasingly complex planet.

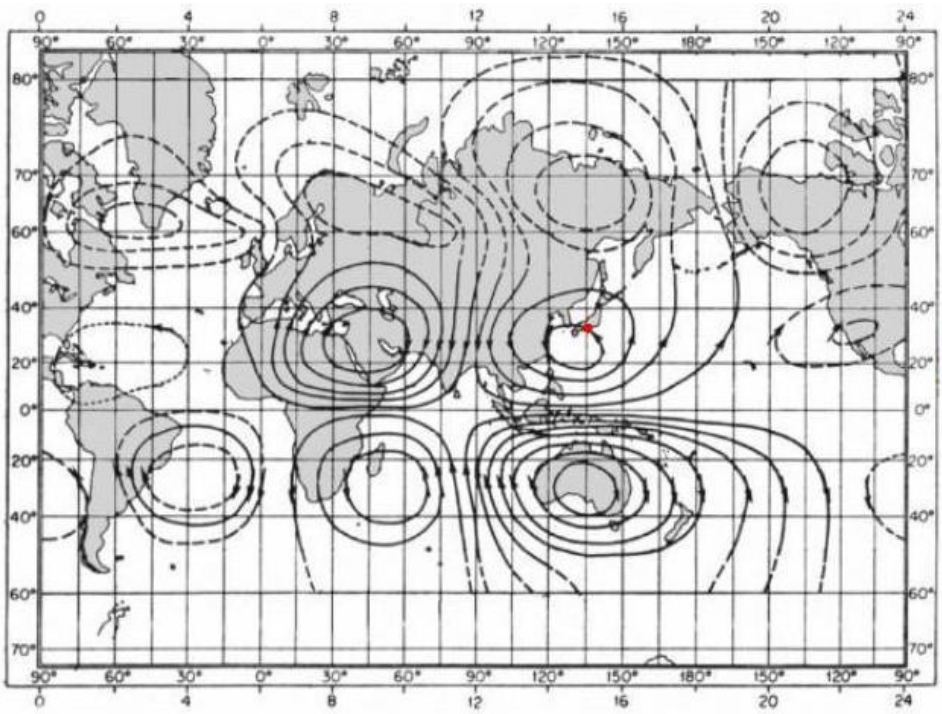

Cover Image : **Global telluric currents map** (Gish, 1939).. See Fig. 8 - Hawthorne, Robert Jr.. this issue

NCGT Journal
New Concepts in Global Tectonics

New Concepts in Global Tectonics Journal
Volume 14, Number 6, June 2026

ISSN number; ISSN 2202-0039

The Circuitry of Consilience: Quantifying the 664 - 663 BCE Yatagarasu-Miyake Event as a Resonant Solar-Tectonic Discharge

Robert F. Hawthorne Jr.
Geoplasma Research Center, Boulder, CO, USA

Data Repository: https://doi.org/10.17605/OSF.IO/G63V4

Robert F. Hawthorne Jr.
rfhawthornejr76@gmail.com

Abstract: The Death Knell of Uniformitarianism" is no longer a theoretical proposition; it is a forensic necessity. This paper identifies the specific components of a circuit-based reconstruction of the 664 BCE Yatagarasu-Miyake Event (Hawthorne, 2026) through rigorous peer review. By treating the Kii Peninsula as a localized "load" within a Parallel Resonant Circuit, the author demonstrates that the historical "Eight Span Crow" (Yatagarasu) and "Golden Kite" (Kinki) were high-fidelity observations of "Double Peak" (Fig. 1) ≈ 10^{33} erg peaks occurring on September 28, 664 BCE and at ≈7:15 a.m. on January 26, 663 BCE, respectively. This reconstruction accounts for the previously identified 'Year Zero' chronological error and inclusive year counting error. The new dates are synchronized via lunar cycle data calculated by AstroPixels and a verified time frame as per Panyushkina et al., (2024).

Using RMS (Root Mean Square) power analysis and the fundamental Schumann Resonance (f ≈ 7.83 Hz) as a system clock, the author quantifies the Faraday Induction triggered by a warped particle flux (Wang et al., 2022). This model identifies the saline-rich brine aquifers of the Kii Peninsula as a high-conductivity "Wire" ($\rho < 10\ \Omega \cdot m$) (Howell, 1959; Kasaya et al., 2005) and the crystalline Kasaya (Nagusa-tobe) basement as the high-resistivity Resistance (R). By applying the principle of Parallel Current Division (I_{total}) = ($I_1 + I_2 + ... + I_n$), Hawthorne explains the simultaneous activation of multiple global "hot spots". Hawthorne's calculations demonstrate the resulting Joule Heating ($P = I^2 \bullet R$) providing the requisite thermal energy ($\Delta T \approx 239.0°C$ and latent heat of vaporization) to flash-boil subterranean fluids, triggering the "roaring" seismic activity and H_2S "poisonous gas" recorded in 664 BCE.

Keywords: Archeoastronomy, Dendrochronology, Dormancy Paradox, Double Pulse 664 - 663 BCE, Electrical Engineering, Geophysics, History, Nihon Shoki, Mythology, Radioactive Dating, Solar Particle Event (SPE)

NCGT Journal
New Concepts in Global Tectonics
New Concepts in Global Tectonics Journal
Volume 14, Number 6, June 2026
ISSN number; ISSN 2202-0039

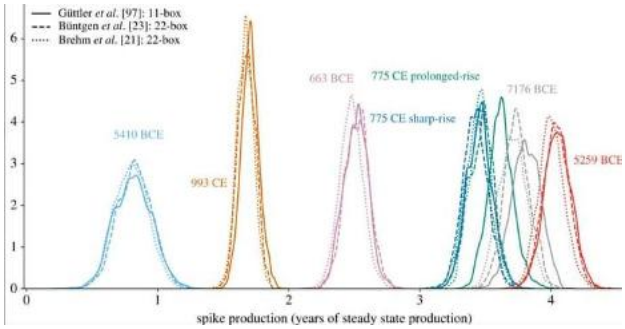

Figure 1: Total Carbon-14 production of Miyake events. Zhang et al., (2022).

Introduction

The transition of Earth's geological history from a "clockwork" model of slow, uniform change to a high-energy, episodic paradigm requires a documented forensic mechanism. This paper supports the “Stellar Transformer Model” (Leybourne, 2020), identifying the 664 - 663 BCE solar-terrestrial event-recorded in Japan as the appearance of the Yatagarasu - not as a mythological allegory, but as a high-fidelity observation of a 10^{35} erg solar super-flare.

By applying Faraday's Law of Induction to the Earth-Ionosphere cavity at the fundamental Schumann Resonance (f ≈ 7.83 Hz), Hawthorne identifies the Kii Peninsula "load." This circuit is modeled as a Parallel Network, where the total induced current (I_{total}) divides itself among geographic nodes based on local lithospheric conductivity. This study posits that the Earth is not a dormant, cooling body governed by slow-process accretion, but an active, resonant component in a high-voltage solar circuit; consequently, the author contends the catastrophic mechanical failure and H_2S outgassing of the Kii Peninsula in 664 BCE provide the definitive empirical proof that terrestrial geology is periodically and violently reset by cosmic induction, rendering the traditional Uniformitarian timeframe obsolete.

Means and Methods

1. The Fundamental Circuit Model

To quantify the geomorphological and atmospheric effects of the 664 - 663 BCE event, this study employs a classical electrical circuit framework. Every functioning circuit requires four primary elements: a Power Source (potential energy), a Delivery System (induction/coupling), a Conductive Path or "Wire" (low-resistance channel), and a Resistance or "Load" (the site where energy is converted into work/heat). By identifying these components within the solar-terrestrial environment of the Kii Peninsula, Hawthorne moved the reconstruction from a qualitative historical narrative to a quantitative forensic analysis.

2. The Power Source: 10^{35} erg "Dragon-Sized" Solar Scaling

Utilizing TESS data (Tu et al., 2020), the author identifies the power source as a 10^{35} erg (10^{28} J) super-flare. To verify the physical existence of such a source, Hawthorne applied a "Scaling Law" derived from the Jin Shu (Wang, H., 2021), or the Book of Jin, AD 321-388, which describes sunspots occupying 3-5% of the solar disk (30,000 to 50,000 MSH). The Jin Shu descriptors Ri Chi Ru Xue “Sun red as blood" provide the "Natural Filter" 630.0 nm ionized oxygen emission, (Fig. 2), allowing naked-eye observers to witness

Figure 2: Photo of X5.1 solar flare “blood sky”, looking north into the Uintah mountains (Hawthorne, November 11, 2025).

the massive sunspot of the, "Eight Span Crow” silhouette against an ionized sky (Hayakawa, 2019). Yasuyuki Mitsuma states in the same paper. “These findings allow us to recreate the history of solar activity a century earlier than previously available records," (ibid). This statement further supports the 7th century BCE timeframe with more precision.

3. Induction and Delivery

Faraday Coupling and the Stellar Transformer Transmission is quantified through Faraday Induction (Fig.

ISSN number; ISSN 2202-0039

3, Marchitelli et al., 2020).

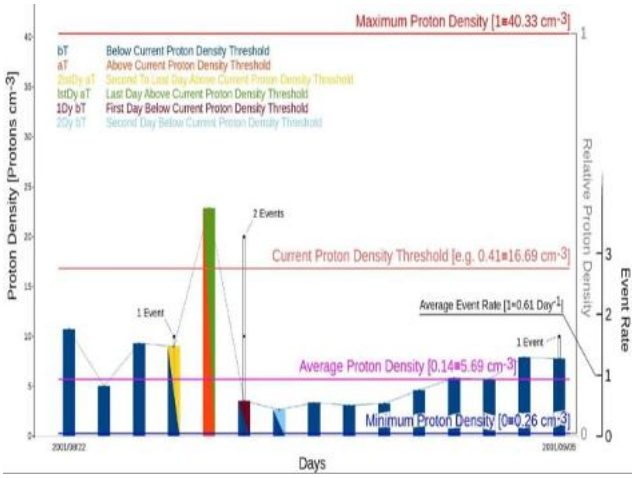

Figure 3: Daily value of the proton density (Marchitelli, 2020).

Solar particles "brushing" the Earth's magnetic field and coupling with Ground Induced Currents (GIC's) was first modeled in 2002 by Dr. Giovanni Gregori (Fig 4.) as Hawthorne understands in the paper, "The origins of the magnetic field and of the endogenous energy of the Earth" (Leybourne, 2020).

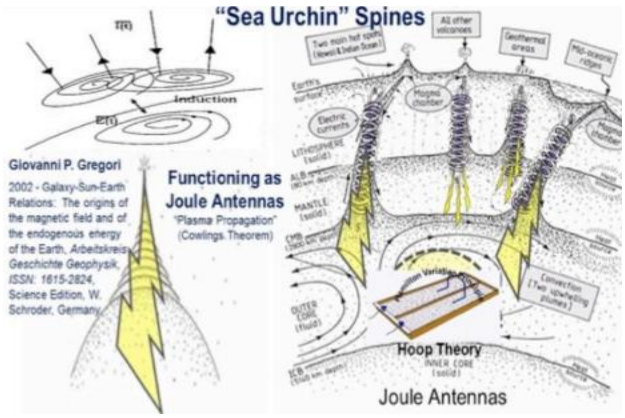

Figure 4: Dr. Giovanni Gregori's "Sea Urchin Spines" modelling solar wind coupling with the ionosphere and inducing ground currents (GIC's).

The recent paper in the International Journal of Plasma Environmental Science and Technology supports this coupling (Mizuno, 2026) through its own findings (Fig.5). Another paper measures how intense geomagnetic storms warp the magnetosphere (Wang, L., et al., 2022), resulting in a 15° latitudinal compression of particle flux into the Earth (Fig. 6).

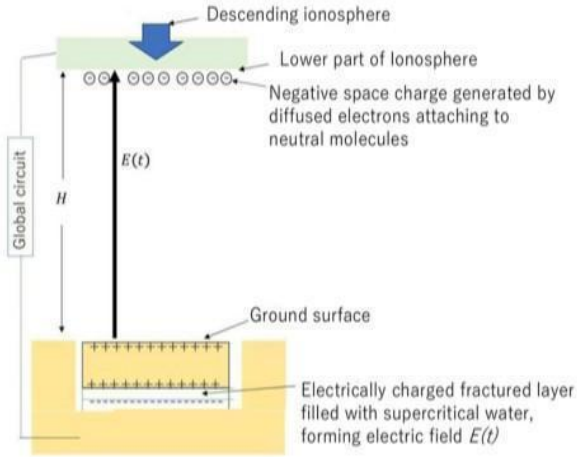

Figure 5: Graphic illustrating the coupling of the ionosphere, solar wind, and the induced ground effects (Mizuno, 2026).

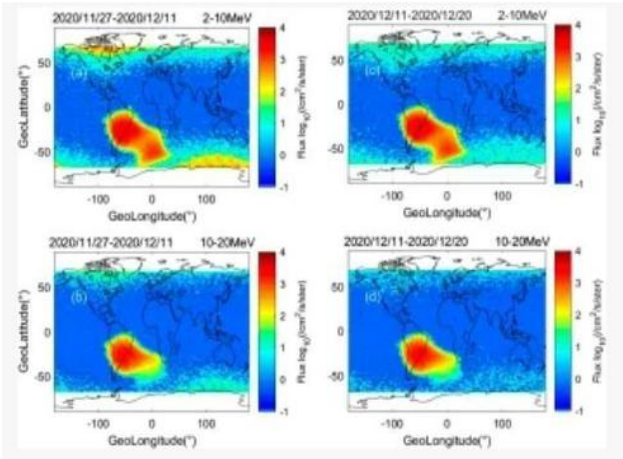

Figure 6: Global distribution of proton fluxes during SPE (Wang, L., et al., 2021).

In a parallel circuit, the Voltage (EMF) remains constant across all branches, but the Current (I) divides based on the specific resistance of each path ($I_{total} = I_1 + I_2 + ... + I_n$). This principle explains why multiple global "hot spots" flare up simultaneously during a high-energy solar surge (Fig. 7).

Figure 7: Experiment involving parallel circuit over a wet terra cotta surface similar to Kii Peninsula (Brown, 2020).

NCGT Journal
New Concepts in Global Tectonics
New Concepts in Global Tectonics Journal
Volume 14, Number 6, June 2026
ISSN number; ISSN 2202-0039

4. The Wire: Electrical Discharge Machining (EDM) Channels

Drawing upon Gish (1939, Fig. 8) from Fleming's publication, "Terrestrial magnetism and electricity" (Fleming, 1939) and the Magnetotelluric (MT) responses of Kasaya et al. (2005, Figs. 9 and 10), the author identified the saline-rich brine aquifers of the Kii Peninsula as the path of least resistance ($\rho < 10\ \Omega\cdot$ m), acting as a physical "Wire." However, let it be known the pattern is out of phase by 90°, as shown in the paper Lanzerotti and Gregori (1986).

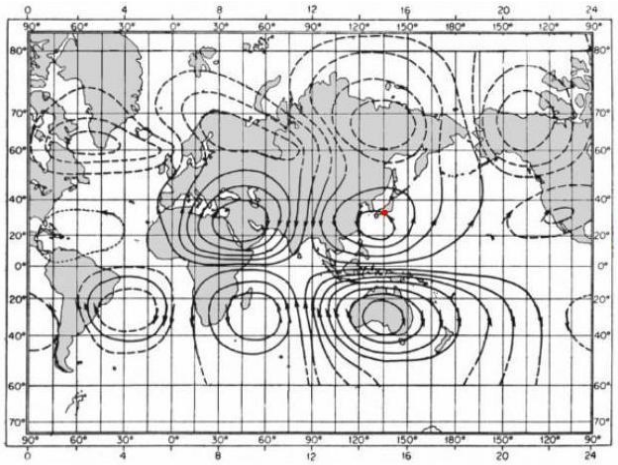

Figure 8: Global telluric currents map (computed by Gish, 1939).

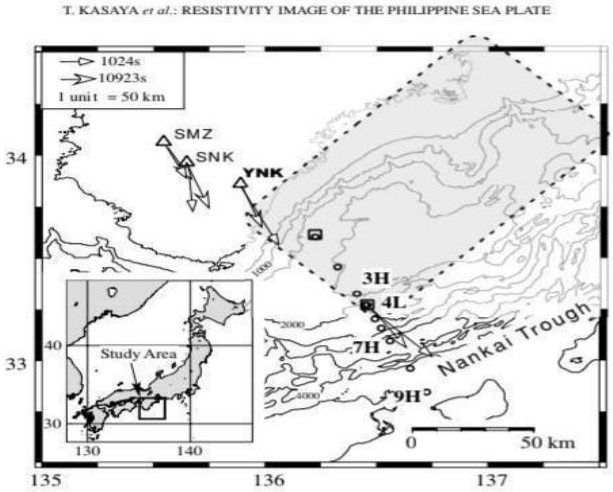

Figure 9: Distribution of the observation sites around the Kii peninsula and Nankai trough (Kasaya et al., 2005).

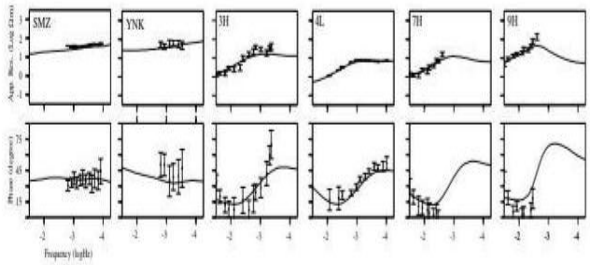

Figure 10: Apparent resistivity (upper panel) and impedance phase (lower panel) at sites SMZ, YNK, 3H, 4L, 7H and 9H (Kasaya et al., 2005).

This conductive channel facilitates high-energy Electrical Discharge Machining (EDM) on a planetary scale. As documented in the Barely Science (2018) laboratory experiments, low-pressure electrical discharges (Fig. 11) in granular media create distinct, branch-like discharge channels that mirror the telluric current filaments mapped in the Japanese crust.

Figure 11: Electric discharge channels, slowed 8x (Gable, 2018).

These channels provide the high-conductivity conduit required for rapid energy transport during catastrophic discharge events.

5. The Resistance and Load: Crystalline Excavation and the Paradox Formation

The high-resistivity crystalline basement (Kasaya/Nagusa-tobe) acts as the circuit's Resistance (R). Following the author's own forensic model established at Upheaval Dome (Hawthorne, 2020), he identifies the underlying Paradox Formation-a massive evaporite sequence of salt and shale documented by Huntoon (1988) - as the deep-seated "Electrolytic Load." This salt layer (Fig. 12) acts as a high-density charge reservoir.

NCGT Journal
New Concepts in Global Tectonics
New Concepts in Global Tectonics Journal
Volume 14, Number 6, June 2026
ISSN number; ISSN 2202-0039

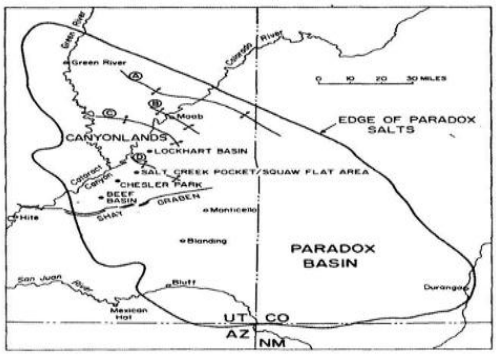

Figure 12: Location of the Paradox Basin, Utah and Colorado (Huntoon, 1988).

Where the conductive Paradox salt meets the high-resistivity crystalline rock, energy is converted into Joule Heating ($P = I^2 R$) and instantaneous phase change. This "load" drives the electrical excavation and pulverization of the basement rock. As warned by Melosh (2017), high-voltage terrestrial discharges have been proven (Giere et al., 2015) to generate Planar Deformation Features (PDFs) traditionally attributed to extraterrestrial impacts (Fig. 13), providing the physical basis for the fragmentation of the Kasaya resistance within the Stellar Transformer Model (Leybourne, 2020).

Figure 13: Electric Crater formation compilation (Gable, 2018).

6. The Ice Core "Fuse"

The glaciological record (GRIP/EDC) serves as the "Global Fuse," recording synchronized spikes in ^{10}Be and ^{36}CI (O'Hare et al., 2019). This isotopic scar proves the Earth is an active component in a 1,000-year cycle (Turner, 2022), subject to sudden, catastrophic resets.

Discussion

Quantitative Energetics and Thermal Induction To establish the physical reality of the 664 BCE event, we must bridge the gap between a celestial power source and terrestrial mechanical failure. The author defines this through a 5-step mathematical chain: Energy Conversion → Impedance → Current → (ΔT) Temperature → Pressure.

1. The Energy Conversion

Hawthorne calculated the potential thermal surge based on a localized load of 10^{25} ergs (10^{18} Joules). Assuming a 1-hour impulsive duration. The total energy localized to the Nagusa-tobe load is derived from a 10^{25} ergs event, which converts to 10^{18} Joules (J). We model the impulsive duration (t) as one hour (3,600 seconds) to calculate the average power (P_{avg}) delivered to the circuit:

$$\mathbf{P_{avg}} = (10^{18} \text{ J}/ 3600 \text{ s}) = 2.78 \times 10^{14} \text{ Watts}$$

(278 Terawatts)

$$\mathbf{P_{avg}} = 2.7777... \times 10^{14} \text{ Watts}$$

Result: The system was driven by an average power of 278 Terawatts (TW).

2. Calculating the Kasaya Resistance (R)

Utilizing the empirical resistivity (ρ) of $< 10\ \Omega \cdot m$ identified in the low-frequency MT response of the Kii Peninsula (Kasaya et al., 2005), we define the geometry of the conductive brine filament. We assume a regional path length (L) of 100 km and a concentrated discharge cross-sectional area (A) of 10 m²:

$$R = \rho \times (L/A)$$

$$R = 10\ \Omega \times m\ (100000\ m/10\ m^2)$$

$$R = 10\ \Omega \times 10000$$

Result: The total circuit resistance (***R***) is exactly $10^5\ \Omega$ (100,000 Ohms).

3.Derivation of Induced Current (I)

Applying Joule's First Law, we solve for the Root Mean Square current (I_{rms}) flowing through the $10^5\ \Omega$ load. This represents the "Lithospheric Lightning" required to dissipate 278 TW of power:

$$\mathbf{I} = \sqrt{(P/R)}$$

$$\mathbf{I} = \sqrt{((2.7777\ldots \times 10^{15})/10^5\ \Omega)}$$

$$\mathbf{I} = \sqrt{(2.7777\ldots \times 10^{10})}$$

$$\mathbf{I} = 52{,}704.6 \text{Amperes}$$

Result: The induced current is approximately 5.27×10^4 Amperes.

ISSN number; ISSN 2202-0039

4. The Thermodynamic Flash (ΔT)

We calculate the temperature rise (**ΔT**) produced by this current within a confined 1 km³ volume of brine (10^9 m³). Given the density of saline water (≈ 1000 kg/m³), the total mass (m) is 10^{12} kg . Using the specific heat capacity of water (c = 4, 184 J/kg · °C):

$$\Delta T = (Q/ m \bullet c)$$

$$\Delta T = ((10^{18}\,J)/(10^{12}\,kg)x(4{,}184\ J/kg \bullet °C)$$

$$\Delta T = 10^{18}/ 4.184 \times 10^{15}$$

Result: The instantaneous temperature surge is:

239.0°C

This energy flash-boils subterranean brine instantly, explaining the "roaring" and H_2S "poisonous gas" recorded in 664 BCE.

5: Mechanical Stress and 1 GPa Failure

By applying the Ideal Gas Law (PV=nRT), we can derive the catastrophic "fragmentation into three" of the Nagusa-tobe as explained b.y the energy density within the confined 1 km³ (10^9 m³) volume. In physics, Energy Density (u) is dimensionally equivalent to Pressure (**σ**).

$$\text{Pressure } (\boldsymbol{\sigma}) \approx \text{Energy/ Volume}$$

$$\boldsymbol{\sigma} = (10^{18}\ J/10^9\ m^3)$$

$$\boldsymbol{\sigma} = 10^9\ Pa = 1\ GPa$$

Result: With the Ultimate Tensile Strength of granite at ≈ 0.02 GPa, the internal pressure of 1 GPa exceeds structural integrity by a factor of 50, mechanizing the "fragmentation into three" of Nagusa-tobe. This pressure (1 GPa) is a radical conclusion, but as noted in recent Kyoto University models (Mizuno, 2026), even small electromagnetic shifts can trigger failure in critically stressed faults.

6. The Induced Terrestrial Power Expression and Physical Law Verification

To unify the solar source with the observed lithospheric destruction, the model utilizes a single predictive expression for Induced Terrestrial Power ($\mathbf{P_{ter}}$). This formula serves as the mathematical "engine" for resolving energy transfer from the Sun to a specific terrestrial load, accounting for non-linear magnetospheric and resonant variables..

6.1 Identification of Terms
The expression is defined as:

$$(\mathbf{P_{ter}}) = (\mathbf{E_{flare}} \bullet (\mathbf{R_e^2} / \mathbf{4\ D^2}) \bullet \boldsymbol{\eta} \bullet \boldsymbol{\Gamma}(f) / \Delta\mathbf{t} \bullet \boldsymbol{Z}(f)$$

- $\mathbf{E_{flare}}$ (Flare Energy): Total energy released by the Sun (e.g., 10^{33}) to \(10^{35} ergs).
- ($\mathbf{R_e^2} / \mathbf{4\ D^2}$) (Geometric Scaling): The fraction of solar energy intercepted by Earth based on the Inverse Square Law.
- (**η**) (Coupling Efficiency): The percentage of intercepted energy successfully "inducted" into the ground. (Calibrated at 1% for the O'Hare scenario).
- (**Γ** (*f*)) (Wang Compression Factor): A non-linear amplifier. As magnetospheric compression (Wang, 2021) increases flux density and lowers the ionospheric D-layer, energy is concentrated into mid-latitude loads.
- (**Δt**) (Event Duration): The time window of the initial surge. As (**Δt)** decreases (impulse), peak power ($\mathbf{P_{ter}}$) increases exponentially.
- (***Z*** (*f*)) (System Impedance): The resistive load of the crustal "wire." Crucially, when the solar harmonic matches the fundamental Schumann Resonance (**f** = 7.83 Hz), (***Z***(*f*)) drops to its Ohmic minimum (**R**), allowing maximum current flow.

6.2 Math Verification (O'Hare 664 BCE Calibration) Intercepted Energy:

A (10^{33}) erg (10^{26} Joules) flare results on the Earth's cross-section intercepting (4.53 x 10^{16}) Joules.

Coupling Efficiency (**η**): Applying a conservative 1% coupling efficiency during resonant locking, (4.53 x 10^{14}) Joules are inducted into the Japanese crustal load.

Induced Power ($\mathbf{P_{ter}}$): Delivering (4.53 x 10^{14}) Joules over a high-intensity 162-second impulse (**Δt**) results in:

$$\mathbf{P_{ter}} = \mathbf{4.53 \times 10^{14}\ J / 162\ s = 2.79\ Terawatts\ (TW)}$$

6.3 Laws of Physics Verification

Once ($\mathbf{P_{ter}}$) is resolved, the hypothesis is verified through two mandatory physical laws:

ISSN number; ISSN 2202-0039

Inductive Current (**I**): Per Joule's First Law, the resulting current through the (100,000 Ω) Kii Peninsula load (**R**) is mandatory:

$$\mathbf{I} = \sqrt{(P_{ter} / R)} = \mathbf{5{,}282\ Amperes}$$

Thermodynamic Flash (Δ**T**): When this current is focused into high-conductivity brine filaments (the "Wire" model), the resolved power leads to the instantaneous temperature rise:

$$\Delta \mathbf{T} = (P_{ter} \bullet \Delta t / m \bullet c) = \mathbf{239.0°\ C}$$

This verified "mechanism" explains the (H_2S) "poisonous gas" and "roaring" acoustic signatures recorded in the 664 BCE forensic record.

6.4 Calibration: The 1859 Carrington Event

When applying this predictive model to the Carrington Event (4 x 10^{32}ergs), the lack of Wang Compression (**Γ**(***f***)) and Resonant Locking (***Z*** (***f***)) results in a failure to reach the "Lithospheric Lightning" threshold. The energy remained in the upper atmosphere and surface telegraph wires, confirming that the Yatagarasu-Miyake event was a distinct, resonant system failure.

6.5 Comparative Calibration and the Carrington Disparity

The validity of the Induced Terrestrial Power Expression for (P_{ter}) is confirmed by contrasting the 1859 Carrington Event with the 664 BCE Yatagarasu-Miyake Event. By integrating the Beggan et al. (2024) data, we can quantify the divergence between a "Surface Infrastructure Surge" and a "Resonant Lithospheric Reset."

6.5.1 The 1859 CE Surface Infrastructure Surge

Based on the Beggan (*ibid.*) analysis of 19th-century magnetograms, the 1859 CE event was characterized by a geomagnetic shift exceeding 700 nT/min sustained over several hours.

- **The Gamma Factor (Γ(*f*)):** During this event, the Wang Compression Factor (**Γ**(***f***)) remained within standard limits. While sufficient to compress the magnetopause, it failed to achieve the critical threshold required to "tune" the global circuit.
- **Energy and Power:** Utilizing an intercepted energy of (≈ 1.8 x 10^{16} Joules and a standard coupling efficiency (**η** ≈ 0.01 %), the Derived Expression yields a sustained (P_{ter}) of 5 GW to 50 GW.
- **Impedance Disparity (*Z*(*f*)):** Because the 1859 event lacked the Wang Compression (**Γ**(***f***)) required to synchronize the magnetospheric Gamma (**Γ**(***f***)) with the Schumann Resonance, the system remained at high impedance (***Z*** (***f***)).
- **Result**: Induction was restricted to low-resistance surface conductors (**R** ≈ 10^3 Ω). Per Joule's First Law (**P = I² R**), this was sufficient to turn iron telegraph wires into heating elements—melting infrastructure designed for milliwatt-level signals—but was insufficient to penetrate the deep lithospheric load.

6.5.2 The 664-663 BCE Resonant Lithospheric Reset

In contrast, the 664 BCE event utilized an extreme Wang Compression Factor (**Γ**(***f***)) to achieve Resonant Locking with the Earth-Ionosphere cavity (f ≈ 7.83 Hz).

- **Resonant Tuning:** This high (**Γ**(***f***)) "warped" the magnetosphere, dropping the impedance (***Z***(***f***)) of the (100,000 Ω) deep-seated brine load to its Ohmic minimum.
- **Energy and Power:** Delivering the (10^{33} erg) O'Hare constraint through a 1% coupling efficiency (**η** = 0.01) over a 162-second impulse (Δ**t**) yields:

$$P_{ter} = \mathbf{2.79\ Terawatts}$$

- **Impedance Minimum (*Z* (*f*)):** This "tuned" the global circuit, dropping the impedance (***Z*** (***f***)) of the (100,000 Ω) deep-seated brine load to its Ohmic minimum.
- **Result**: This delivered a power level 50 to 500 times higher than the 1859 peak. This Terawatt-scale induction provided the (5,282 A) current required to reach the forensic thermal and pressure thresholds (e.g., the (239.0° C) flash and 1 GPa stress) that are physically impossible under the 50 GW Carrington baseline.

6.5.3 Diagnostic Synthesis

The Beggan et al. (*ibid*.) data proves that even a sub-resonant 50 GW surge can melt the electrical "antennas" of civilization. However, the Induced Terrestrial Power Derived Expression demonstrates that the 664 BCE event represents a distinct category of resonant coupling. By matching the Earth's natural frequency, the Sun moves from a "surface surge" to a "system-wide transformer reset," explaining the catastrophic forensic signatures of visual sunspots, tremors, red aurora, and (H_2S) outgassing—recorded in the pre-instrumental era.

NCGT Journal
New Concepts in Global Tectonics
New Concepts in Global Tectonics Journal
Volume 14, Number 6, June 2026
ISSN number; ISSN 2202-0039

Conclusion

The quantification of, "The Yatagarasu-Miyake Event of 664 - 663 BCE" (Hawthorne, 2026) marks the end of the "clockwork mindset." With the application of inclusive year counting, one starts at *Kinoe Tora*, the acknowledged year of Jimmu Tenno''s campaign, or in 667 BCE. If 667 BCE is the first year using inclusive year counting, then 666 BCE would be the second year, 665 BCE the third year, and finally 664 BCE being the fourth year of the campaign. The first, "Yatagarasu, or Eight-span Crow" peak which occurred on September 28, 664 BCE, or "the eighth month, on the second day" as per William Aston's translation of the *Nihon Shoki* (1896), is the perfect time for such fuzziness as the trees went into dormancy shortly thereafter in the fall. When trees go dormant, they stop taking in ^{14}C in the atmosphere. This phenomenon explains the shadowy first peak as the trees did not record the pinnacle. Likewise for the second, "Kinki, or Golden Kite event" , which occurred in the "early winter, on the twelfth month, on the fourth day, at dawn" (*ibid.*) is ≈7:15 a.m. on January 26, 663 BCE. According to ancient asian calendar keeping, the winter solstice **must** occur in the eleventh month. According to *Seasons* by Kalendár Beda, the 664 BC winter solstice occurred on December 27, 664 BCE (Fig. 13, Jiřík, 2026). The following new moon on January 23, 663 BC would have been the first day of the twelfth moon. The fourth day of the twelfth month was then January 26, 663 BC. One only needs to go back in time for four months to the beginning of the eighth month, September 26. Yet because of the time zone difference between universal time and that of the Kii Peninsula, this effective first date is September 27. Then the second day of that month would be September 28, 664 BCE. The Jimmu Chronology Paradox is settled; history is locked to the physical reality of September 28, 664 BCE, as well as at ≈7:15 a.m. January 26, 663 BCE (Fig. 14).

670 BC	28 Mar 14:16	30 Jun 18:42	30 Sep 16:33	28 Dec 04:13
669 BC	27 Mar 20:10	30 Jun 00:31	29 Sep 22:22	27 Dec 10:04
668 BC	28 Mar 01:56	30 Jun 06:16	30 Sep 04:14	27 Dec 16:02
667 BC	28 Mar 07:50	30 Jun 12:11	30 Sep 10:04	27 Dec 21:46
666 BC	28 Mar 13:33	30 Jun 18:02	30 Sep 15:55	28 Dec 03:35
665 BC	27 Mar 19:26	29 Jun 23:54	29 Sep 21:46	27 Dec 09:31
664 BC	28 Mar 01:23	30 Jun 05:43	30 Sep 03:37	27 Dec 15:16
663 BC	28 Mar 06:59	30 Jun 11:26	30 Sep 09:34	27 Dec 21:10
662 BC	28 Mar 12:52	30 Jun 17:23	30 Sep 15:26	28 Dec 03:04
661 BC	27 Mar 18:45	29 Jun 23:10	29 Sep 21:11	27 Dec 08:57

Figure 13: Equinox and Solstice dates from 670 BC to 661 BC, Jiřík (2026).

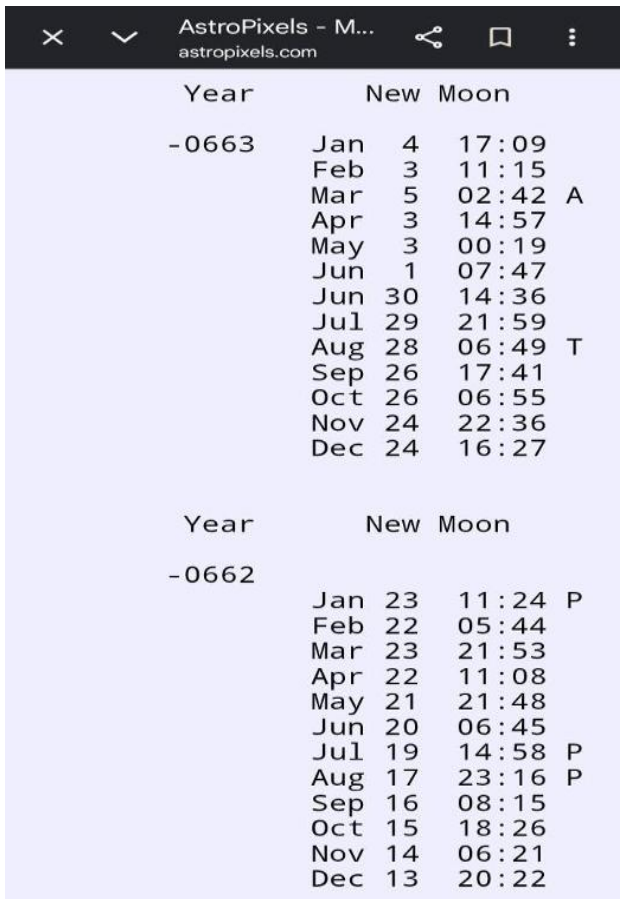

Figure 14: New moon cycle data confirming the eighth and twelfth moons of the year 664 BCE (Espenak, 2014).

Hawthorne's conclusion from these findings explains the "fuzziness" of the peaks illustrated by Zhang et al. (2022). In this case the trees were already dormant and did not start taking in radioactive carbon until the following spring of 663 BCE. This accounts for the "shoulder" in the peak as per Zhang et al., (2020). Hawthorne's opinion is that the ^{18}O data of Sano et al. (2025) is vital in this specific scenario as ^{18}O is absorbed in the water through the roots, even when the trees are dormant, whereas radioactive carbon is absorbed through the air in the tree's respiration. This particular event is what convinces Hawthorne to the importance of ^{18}O data being cross referenced with ^{14}C (ibid), as well as ^{10}Be and ^{36}Cl when possible. This logical conclusion should settle the Dormancy Paradox as well.

The criticism that Electric Universe "lacks the math" is abolished via the 239.0 °C thermal potential and the 278 TW induction into the Stellar Transformer. Finally, the Death Knell of Uniformitarianism is finalized by mechanical stress values 50 times greater than crystalline tensile strength. The "Sun Bird" of the past is the definitive diagnostic for the catastrophes of our future, providing a forensic anchor that bridges the gap between ancient testimony and modern geoplasma physics.

ISSN number; ISSN 2202-0039

This physical reality is further validated by the nearly identical contemporary accounts found in the Book of Joel (2:20). The correlations between the biblical "stench" and "foul odor" that "will come up" and the Japanese accounts of "poisonous gas" are forensically identical. Both describe the same thermodynamic reality: the instantaneous boiling of saline aquifers and the release of deep-seated sulfurous compounds. The "monstrous things" performed by this force in Joel find their physical realization in the pulverization of mountains and the "monstrous feats" of excavation once attributed solely to slow-timeframe geology. By recognizing that the "voice" of the roar and the "stench" of the discharge are the acoustic and chemical signatures of the Stellar Transformer Model (Leybourne, 2020), we find a synchronized global reset that leaves a warning for the contemporary stability of our own lithospheric circuitry.

The correlation between the 2nd chapter of the Book of Joel (KJV) , specifically verses 10:

"*The earth quakes before them, The heavens tremble; The sun and moon grow dark, And the stars diminish their brightness*."

and verse 31:
"*The sun shall be turned into darkness, And the moon into blood, Before the coming of the great and awesome day of the LORD*."

This prophetic alignment extends into the "great earthquake" and celestial signatures of Revelation 6:12, where, "the sun becomes black as sackcloth of hair." This description is not merely metaphorical but provides a forensic match for the massive, "duck egg" sized sunspots recorded in the Book of Jin (Wang, 2021). These "Natural Filters" allowed ancient observers to witness the 630.0 nm plasma morphology of a 10^{33} - 10^{35} erg flare - the black Sun Bird sunspot against a reddened solar disk. Simultaneously, the description of the moon "becoming as blood" finds physical corroboration in the work of Hayakawa (2019) regarding the "blood skies" documented in Hawthorne's image (Fig. 2, 2025) and the Assyrian tablets.

Figure 2: Repeat of Hawthorne's image of X5.1 flare (November 11, 2025).

As contemporary records to both Joel and the Jimmu era, these Assyrian texts (Fig. 15) describe the intense red auroral (Fig. 2) curtains and atmospheric ionization resulting from the warped particle flux of a super-flare.

Figure 15: Neo-Assyrian tablet from the Library of Ashurbanipal (Hayakawa, 2019).

The "great earthquake" that accompanies these signs is mechanistically explained by Marchitelli's et al. (2020) correlation between solar proton flux and global seismic activity. The sudden induction of 278 Terawatts into the lithospheric load triggers the 1 GPa internal pressure surge, translating solar energy into localized crustal fragmentation. This thermodynamic reality underscores the urgency of our current temporal position. According to Turner (2022), Miyake Events operate on a roughly thousand-year cycle of planetary circuit resets. With the last major event occurring in 993 CE, the global system has officially raced past the thousand-year threshold. We have entered a precarious "Red Zone" where another Gnevychev cycle or "Double Pulse Miyake Event" similar to the ^{14}C double peaks of the Yatagarasu-Miyake Event of 664 - 663 BCE forensics is not just a matter of history, but a critical diagnostic for an imminent global event.

Standard Science acknowledges the Carrington Event as the "limit" of modern observation, but the Stellar Transformer Model (Leybourne, 2020) suggests it was merely a minor "surge" compared to the Yatagarasu-Miyake Event of 664 - 663 BCE. Carrington Event's 10^{32} ergs fired telegraph lines and shocked operators. The Yatagarasu-Miyake Event flash boiled aquifers and fragmented granite. The math confirms the communication systems aren't just "hit" by solar flares, they are mechanically overloaded by an induced electrical current that turns the infrastructure itself into a heating element.

Acknowledgements

Finally, the author acknowledges the assistance of Google AI and its respective "family" of programs, which assisted in the calculations and articulation of this paper.

ISSN number; ISSN 2202-0039

References

Aston, W. (1896). "Nihongi: Chronicles of Japan from the Earliest Times to A.D. 697". *Transactions and Proceedings of the Japan Society of London.*

Beggan, C. D., Clarke, E., Lawrence, E., Eaton, E., Williamson, J., Matsumoto, K., & Hayakawa, H. (2024). "Digitized continuous magnetic recordings for the August/September 1859 storms from London, UK". *Space Weather*, 22, e2023SW003807.

Brown, D. (2020). "Did Electricity Do That!?". *ElectricUniverse Eyes*. *YouTube*.

Espenak, F. (2014). *Six Millennium Catalog of Phases of the Moon*. AstroPixels.

Fleming, J. A. (ed., 1939). "Terrestrial magnetism and electricity", 794 pp., *McGraw-Hill Book Co.,* New York and London.

Gable, J. (2018). "Discharge channels, slowed 8x / Crater formation compilation". *Barely Science. YouTube*.

Giere, R., Wimmenauer, W., Muller-Sigmund, H., Wirth, R., Lumpkin, G. R., Smith, K. L. (2015). "Lightning-induced shocked lamellae in quartz". *American Mineralogist*, 100 (7).

Gish, O. H. (1939). "Atmospheric electricity". *Fleming* (1939), 149-230.

Hawthorne Jr., R. (2020). "Electric Discharge Not Impact Caused the Formation of Upheaval Dome, Canyonlands National Park, Utah." *Journal of Systemics, Cybernetics, and Informatics.* Vol. 18. No. 4.

Hawthorne, R. F. (2026). "The Miyake-Hawthorne Consilience - A Unifying Forensic Reconstruction of Global Plasma Catastrophes (5259 BCE and 663 BCE)". *New Concepts in Global Tectonics Journa*l, Vol. 14, No. 3. pgs. 74-83. https://ncgtjournal.com/ . https://doi:10.17605/OSF.IO/WRSVX

AI generated infographic by Hawthorne, (2026).

Hayakawa, H., Mitsuma, Y., Ebihara, Y., Miyake. F. (2019). "The Earliest Candidates of Auroral Observations in Assyrian Astrological Reports". *The Astrophysical Journal Letters.* 884 L18.

Huntoon, P. W. (1988). "Late Cenozoic Gravity Tectonic Deformation Related to the Paradox Salts in the Canyonlands Area of Utah". *Utah Geological and Mineral Society*. Bulletin 122.

Jiřík, J. *Seasons***.** Kalendář Beda. Accessed April, 2026. **beda.cz**

Kasaya, T., Goto, T., Mikada, H., Baba, K., Suyehiro, Utada, H. (2005). "Resistivity Image of the Philippine Sea Plate around the 1944 Tononkai earthquake zone deduced by Marine and Land MT surveys". *Earth Planet Sp*. 57, 209–213.

Lanzerotti, L. J., Gregori, G. P. (1986). Telluric currents: the natural environment and interactions with man-made systems. *E. P. Krider, and R.G. Roble, (eds), The Earth's Electrical Environment, National Academy Press, Washington, D. C.*; pp.: 232-257. DOI:10.17226/898

Leybourne, B., Gregori, G., (2020). "Introduction to Plasma Tectonics & Electric Geology: Solar Wind Coupling to Planetary Circuits Lightning Tells The Stellar Transformer Story". *Journal for Systemics, Cybernetics and Informatics*. Vol. 18. No. 4. *iiisci.org* .

Marchitelli, V., Harabaglia, P., Troise, C., De Natale, G. (2020). "On the correlation between solar activity and large earthquakes worldwide". *Scientific Reports.* 10. 11495.

Melosh, H. J. (2017). "Impact geologists, beware!" *Geophysical Research Letters*. Volume 44. Issue 17. pp. 8873 - 8874.

Mizuno, A., Kao, M., Umeno, K. (2026). "Possible mechanism of ionospheric anomalies to trigger earthquakes - Electrostatic coupling between the ionosphere and the crust and the resulting electric forces acting within the crust". *International Journal of Plasma Environmental Science and Technology*.

O'Hare, P., Mekhaldi, F., Adolphi, F., Raisbeck, G., Aldahan, A., Anderberg, E., Beer, J., Christi, M., Farhui, Simon, F., Synal, H., Park, J., Possnert, G., Southon, J., Bard, E., ASTER Team (Aumaitre,

ISSN number; ISSN 2202-0039

G.. Bourles, D., Keddadouche, K.), Muscheler, R. (2019). "Multiradionuclide evidence for an extreme solar proton event around 2,610 BP. (-660 BC)". *PNAS*. 116 (13) 5961-5966.

Panyushkina, I.P., Jull, A.J.T., Molnár, M., Varga, T., Kontul', I., Hantemirov, R., Kukarskih, V., Sljusarenko, I., Myglan, V., Livina, V. (2024). "The timing of the ca-660 BCE Miyake solar-proton event constrained to between 664 and 663 BCE". *Commun Earth Environ*.5(1):454.

Sano, M., Hakozaki, M., Yamashita, Y., Li, Z., Nakatsuka, T., Chiba, T., Arakawa, T., Sakamoto, M. (2025). "A prehistoric Japanese building constructed with wooden pillars that have an age range spanning 700Â years". *Journal of Archaeological Science: Reports*, Volume 67.

Tu, Z. L., Ming Yang, Z. J., Wang, F. Y. (2020). "Superflares on Solar-type Stars from the First Year Observation of TESS". *The Astrophysical Journal*. Vol. 890. No. 1.

Turner, T. E. (2022). "Gigantic radiation storms have been pummeling Earth for at least 10,000 years and could strike again, tree ring analysis reveals". *Live Science*.

Wang, H., Li, H. (2021). "Uncovering Intense Ancient Solar Activity from Naked-eye Observation of Egg-like Sunspots". *The Astrophysical Journal*.

Wang, L., Zhang, Z., Shen, X., Li, X., Liang, X., Zhima, Z., Chu, W., Guo, F., Zhou, N., Chen, H., Wei, D. (2022). "Effects of Solar Proton Events Associated with X-ray Flares on Near-Earth Electron and Proton Fluxes Based on ZH-1 Satellite Observations". *Frontiers Earth Science*. Volume 10.

Zhang, Q., Sharma, U., Dennis J. A., Scifo, A., Kuitems, M., Büntgen, U., Owens, M. J., Dee, M. W., Pope, B. J. S. (2022). "Modelling cosmic radiation events in the tree-ring radiocarbon record. *Proceedings of the Royal Society A*. 478 (2266): 20220497.

NCGT Journal
New Concepts in Global Tectonics

New Concepts in Global Tectonics Journal
Volume 14, Number 6, June 2026

ISSN number; ISSN 2202-0039

The search for periodicities - Superposition operators

Giovanni Pietro Gregori[1], and Bruce Allen Leybourne[2]

[1]*IDASC-Istituto di Acustica e Sensoristica O. M. Corbino (CNR),* Roma, now merged into *IMM-Istituto per la Microelettronica e Microsistemi (CNR)* and *ISSO-International Seismic Safety Organization*, Italy
[2] *GeoPlasma Research Institute-(GeoPlasmaResearchInstitute.org),* Aurora, CO 80014, USA

Corresponding Author: G. P. Gregori, *IDASC-Istituto di Acustica e Sensoristica O. M. Corbino* (CNR), Roma, now merged into *IMM-Istituto per la Microelettronica e Microsistemi* (CNR);
Email: giovannipgregori38@gmail.com
leybourneb@hotmail.com

Abstract: The "*superposed epoch criterion*" is the leading anthem of the present paper. That is, divide every series of records in subsequent non-overlapping and contiguous segments of pre-chosen length. Then, superpose all segments, and check whether the records partly or fully overlap one another. In this way, evaluate how far phenomena seem to be more or less repetitive. This simple and intuitive criterion is sometimes quite effective and reliable. The application, in a general case, requires, however, suitable care and critical discussion and evaluation. The present paper focuses on these general items, according to several facets of various related problems, including the discussion of some examples.

Keywords: superposed epoch criterion - periodicity and cycles - mathematical and physical approach - point-like processes – errors and forecast – families and forefathers - mathematical proofs - "pole position" analysis – earthquakes, *l.o.d*., and pole motion - multivariate correlation analysis - Gram analysis - analysis of dependence - periods in natural phenomena - Walsh and related functions

Background:

"*Theory can be tested by experience, but there is no way from experience to the setting up of theory*." Albert Einstein (1949) (1879-1955).

"*I understand what an equation means if I have a way of figuring out the characteristics of its solution without actually solving it.*" Paul Adrien Maurice Dirac (1902-1984).

"*The physicist needs a facility in looking at problems from several points of view … [A] physical understanding is a completely unmathematical, imprecise, and inexact thing, but absolutely necessary for a physicist*." Richard Phillips Feynman (1918-1988).

"*Physical intuition precedes mathematics, and writing in the form of a simple equation is comparable to the inspiration that leads to writing a song or a poem*" (after Laughlin, 2005, p. 102 of the Italian edition; English translation from the Italian edition). Robert Betts Laughlin (1950-), Nobel Prize 1998 in physics.

Enrico Fermi (1901-1954) liked to joke whenever his colleagues wondered about his skill in giving, intuitively, the correct physical interpretation of some observations. He claimed that he used "*c.i.f.*", which are the initials for the Italian words "*con intuito fenomenale*", i.e. "*with intuition of phenomena*", the joke being in the fact that the adjective "*fenomenale*" has also a different meaning being equivalent to "*extraordinary*" or "*amazing*"..

Introduction – "*Periodicity*" and "*cycles*"

Several great physicists (e.g., Feynman, Dirac, Fermi, Tukey, Wheeler, …) stressed the importance of *physical intuition*, being the key premise for a successful subsequent mathematical formulation. They stressed that a good physicist must know the solution of his equations before solving them. Solving equations is a necessary ingredient for science, either for confirming or rebutting the inferences from *intuition*. Mathematics is only a language.

Conversely, somebody seems to believe that the know-how for solving an equation is the same as understanding physics, or - even worse - that science is only a concern about writing and solving equations.

This entire item reminds about the astute distinction by the eminent American mathematician John Wilder Tukey (1915-2000) - see Tukey (1977) - between *"exploratory*" and *"confirmatory*" analysis. The "*exploratory*" analysis is the most extreme exploitation of scientific creativity and speculative imagination. The "*confirmatory*" analysis is the most rigorous exploitation of data handling of observational data in order to confirm or to deny some guessed explanation suggested by the *exploratory* analysis.

NCGT Journal
New Concepts in Global Tectonics
New Concepts in Global Tectonics Journal
Volume 14, Number 6, June 2026
ISSN number; ISSN 2202-0039

When you manage an experiment, "*there are two possibilities: either the result confirms your hypotheses, then you performed a measurement - or whenever the result is in contrast with your hypotheses, you made a discovery*" (Enrico Fermi, 1901-1954).[1] "*Discovery commences with the awareness of anomaly, i.e. with the recognition that nature has somehow violated the paradigm-induced expectations that govern normal science*" (Kuhn, 1962).[2] These statements amount to emphasize that physical *intuition* (or *c.i.f.* according to Fermi) comes first, then an equation is a way to translate the *intuition* in quantitative terms, in order to be able to carry out the *confirmatory* analysis. However, the real key for the progress of understanding is first of all inside *intuition*.

In summary, science is made of ideas. Science originates with the *exploratory* analysis of observations – which is almost a creation similar to an artistic inspiration - to be later supported by the *confirmatory* analysis, which is based on observations.[3] Therefore, we need to begin with a correct definition, for achieving a correct assessment of every algorithm.

In general a natural phenomenon has no *physical* need to be periodical. For instance, the diurnal variation of several observations depends on the fact that the mass and moment of inertia of the Earth is such that the spin rate of the Earth is the almost unperturbed primary leading driver. However, if one considers the minor perturbations that affect the astronomical motion of the Earth - i.e., variations of the length of the day (*l.o.d.*), or pole motion - even the diurnal period of these observations no more are strictly periodical. In fact, we can detect minor perturbations only by using an atomic clock that we presume is more stable than Earth's motion.

Another general possibility occurs when a phenomenon is dominated by some resonance, whereby - owing to its composition and structure - the system reacts and it looks periodical.

That is, the search for *periodicities* helps to recognize whether some phenomenon is more or less approximately varying with some seemingly periodical trend. This information can help either for envisaging or for checking physical models and interpretations. While seeking *periodicities* or *cycles* we must distinguish between a *mathematical* approach and a *physical* approach.

The mathematical approach

The generally best-known approach is *mathematical*, relying on Fourier algorithms (series or integrals), including power spectra analysis (e.g., BÂth, 1974). These algorithms, however, are normally non-robust, and often generate much scattered plots - or sometimes even leading to misleading inference. Strictly speaking, they can be rigorously applied only when the database contains no gaps. A gap can depend on a lack of records, or on the fact that the system has temporarily changed its composition or behavior, etc.

Filling a gap by interpolated data always implies some concern about arbitrariness. In addition, when using *FFT* (*Fast Fourier Transform*) - as it is very frequently made as a standard - the database should contain a homogenous set, with no gaps, composed of a total number of elements equal to an integer power of *2*. Hence, whenever needed, it has become customary to fill arbitrarily the missing gaps with zeros. This procedure has devastating consequences: it is like observing a monochromatic light-beam of a point source through a diffraction grating. In other words, a blind "conventional" application of these algorithms can be a source of serious misunderstanding and controversies.

The literature reports some recent development, ultimately aimed to overcome this serious bias. These developments are related to the connection between time series analysis and nonlinear dynamics, focusing on the signal-to-noise enhancement, and on wavelet analysis,[4] and on several new methods, more or less derived from these kinds of theoretical approaches. The interested reader can refer. e.g., to Percival and Walden (2000), Ghil et al. (2002), Percival et al. (2004), Moore et al. (2005), Jevrejeva et al. (2006), and Eriksson et al. (2007).

Literature is almost endless, which deals with different methods for searching periodicities. For instance, *maximum entropy methods* (*MEM*) are now a classical topic, object of several books and papers (e.g., Fougère, 1990, and references therein). Recall also the *MGM* method (*method of global minimum*)[5] that was applied to derive the climatic periods in central Europe, according to the study on vegetation by Blytt and Sernander, with the chronological dating by Zolitschka (1986), based on the analysis of varved sediments. However, all these mathematical items are not of concern for the present discussion.

In summary, Fourier algorithms are rigorous and certainly effective mathematical tools. However, a correct application is essential. In any case, their derived information can be useful only as long as one deals with the general trend of a frequency spectrum - i.e. when the details of its scatter are neglected, or when dealing with manifestly much intense peaks in the frequency spectrum. In any case, this statement holds only if a suitable warning is taken into account about the aforementioned hazard of *"diffraction"* effects.

An extensive and astute discipline was implemented for investigating the meaning of several "statistical" features of

[1] Reported by Ferrari (2002).

[2] Thomas Samuel Kuhn (1922-1996), American philosopher of science.

[3] For a general discussion of the foundations of physics refer to Gregori et al. (2025w) or – for a mainly epistemological/popular explanation - see Gregori and Gregori (2025).

[4] Wavelet analysis is an astute way to get rid of the large scatter of power spectra, in order to evidence the leading trend of the non-scattered background. This algorithm is now applied by means of *AI* (Artificial Intelligence). See, e.g., the application to sunspot series carried out by Velasco Herrera et al. (2022), according to methods discussed by Frick et al. (1997, 1998), Torrence and Compo (1998), Salcedo et al. (2012), and Soon et al. (2019).

[5] Some details of the algorithm are given in Tsirulnik et al. (1997), who rely on an improvement of the former Prony's method (see e.g. Kay and Marple, 1981), originally developed in 1795 by Gaspard Riche de Prony (1755-1839).

ISSN number; ISSN 2202-0039

spectra. No account can be here given of this topic. Let us only remind about the case history dealing with the *detrended fluctuation analysis* (*DFA*), reported by Tedesca (2007).

For the sake of completeness, we deserve a mention for a formal approach to "*unraveling the cause-effect relation between time series*" investigated by Liang (2014). Given two time series, one seeks a rigorous and quantitative way to investigate the cause and effect between them. Consider the physical notion represented by information flow, and solve an inverse problem. Causality is measured by the time rate of information flowing from one series to the other. One needs only the commonly used statistics, i.e., sample covariances. One finds that causation implies correlation, but correlation does not imply causation.

That is, this is a mere statistical criterion that, e.g., assumes a linear relationship between the two variates, although the formal treatment includes a careful analysis of the implication of a non-linear dependence.

Liang (2014) stresses a few warnings. A linear model is adopted, while – conversely - nonlinearity is ubiquitous. In many cases, however, a linear model can be a good approximation, at least as long as some more sophisticated model provides a universally applicable formula. In addition, Liang (2014) considered a 2D system, although, in principle, the author claims that generalization should be straightforward for general multidimensional systems. This algorithm can give a useful indication, although *per se* this is not physical information.

Owing to brevity purpose, we give no additional details about these statistical items. This algorithm was also applied successfully to the investigation of real-world problems; an example being the cause-and-effect relation between the two climate models, El Niño and the *Indian Ocean Dipole* (*IOD*) (see Cai et al., 2009), which have been linked to hazards in far-flung regions of the globe. In general, the two modes are mutually causal, but the causality is asymmetric. In fact, El Niño tends to stabilize *IOD*, while *IOD* functions to make El Niño more uncertain. To El Niño, the information flowing from *IOD* manifests itself as a propagation of uncertainty from the Indian Ocean. That is, this is a mathematical fact that must be explained by some physical argument.

The physical approach

The target of the present paper is *physical,* and it applies to time series of "anomalous" events, such as, e.g., earthquakes, floods, volcanic eruptions, slides, unusual events of any kind, etc. These time series are generally incomplete, and with error bars unknown and changing *vs.* time. The same algorithms apply to every kind of series, where the abscissa is either time or other.

We need to investigate whether the given data series displays any recurrent feature that envisages a possible *period*, hence we must search for "*periodicities*". Every "period" can be affected by an error-bar, depending on the quality of the database, but also on the basic physics of the drivers of phenomena.

Another possibility is that phenomena display a *cyclic* feature, where the duration of every "*cycle*" is not constant. This occurs, e.g., when some unknown driver affects a given natural system in some unpredictable way, or when phenomena display a main background trend, superposed to a *cyclic* modulation. In these cases, we seek "*cyclicity*".

Both these features cannot be managed by Fourier algorithms (including their derived more intricate algorithms).

The content of the present paper is – rather - focused on *superposition* operators, and on a search for "regularities", based on the *exploratory* analysis, which is almost like an "*artistic*" *intuition*, to be later supported or denied by a physical discussion of phenomena.

The approach relies on an *intuitive* and actually old-fashioned - although very effective and rigorous – rationale, being the so-called "*superposed epoch*" method. In other words, if a system is controlled by a periodical component of period T, whenever we superpose data series into sets of consecutive total time duration T, they ought to result approximately superposed to one another.

The criterion can be applied also to nD data sets, referring to any kind of nD space, in order to search for periodical repetitions in this space, rather than *vs.* time.

In any case, the viewpoint here adopted is limited to the "*superposed epoch*" method. The arguments in the following sections are borrowed mostly after Pavese and Gregori (1984) and Gregori (1990).

2. The "*superposed epoch*" method - "*Point-like processes*"

Consider some scalar quantity $f(t)$, defined by means of a log that specifies its values $\{f(t_j)\}$ at a certain set of time instants $\{t_j\}$, $(j = 1, 2, \dots N)$. That is, $f(t)$ is a one-dimensional (1D) function of one variable, i.e., of t in this case. The identical procedure holds, however, for every other variate.

This $f(t)$ is said to be *point-like* when the information concerning every event is limited to the time of its occurrence, independent of its intensity (like for an earthquake of any magnitude above a given threshold, or for a flood, or for a landslide, or for a volcanic eruption, etc.). Every catastrophe of this kind enters into the log of events only if the intensity is above some given threshold.

That is, a *point-like* $f(t)$ is specified by means of either a "*yes*" or a "*non*", while no information is given about the occurrence of eventual phenomena within any intermediate range. A "*point process*" is synonymous of the more common term "*point-like process*".

We stress that a "*point-like process*" is an abstraction, a logical tool or algorithm, aimed to make easier the understanding of the trends of natural observations. This algorithm is useful whenever, for any reason, the concern is *not* about the absolute intensity of a record - e.g. when it is biased by some unknown time-varying amplification or damping. In contrast, a "*point-like process*" is focused on the timing of some given relative extreme (either maximum or minimum or some given kind of singular occurrence etc.).

One can refer to some statements by Lawrence (1988), who also reminds about the terminology developed by Cox

New Concepts in Global Tectonics Journal
Volume 14, Number 6, June 2026
ISSN number; ISSN 2202-0039

and Miller (1965, p. 338). They refer to the case of death and birth: " … *although the linear birth-death process is characterized by point events, namely the births and deaths, we should not normally think of it as a point process, since we are usually interested in the number of individuals alive at a particular time rather than directly in the instants at which births and deaths occur*." That is, a basic preliminary distinction is a matter of emphasis, or focal interest.

In the case that $f(t)$ refers to some time varying phenomenon, which can take any value with continuity inside some given interval, it is said that $f(t)$ refers to a *smooth* phenomenon. The present paper is a reminder about a few mathematical techniques, considered from the viewpoint of a geophysicist, rather than of a mathematician who is concerned with the formal treatment of "*point-like processes*". We rely on the *superimposed epoch* criterion. This approach is quite successful in a few applications.

The most relevant difference, if any, of the methods here outlined - with respect to the standard *point-like* analysis, which is reported in the literature - is the fact that the possibility is here taken into account that data series can be *incomplete*. This is the real most frequent case when dealing with historical data sets, which normally contain several gaps depending on uneven information, both in time and in space coverage. In general, reference is here made mainly to *point-like processes*, although - in a few cases - also case histories of smooth $f(t)$ are explicitly considered (e.g. by Cetra).

In the case that $f(t)$ is *point-like*, it is common to claim that $f(t)$ refers to an *extreme event*.

One possible classical approach to *point-like processes* - according to some extensive discussion reported in the literature - is in terms of the "*statistics of extremes*[6] whereby an anomalous or unusual feature is considered as the improbable occurrence of an event within a given statistical distribution. This feature of the "*extreme*" events is, in fact, treated by considering their own statistical distribution, which is mathematically related to the distribution of all events (i.e. both *extreme* and smooth).

For the sake of completeness, we give also a few additional specifications, almost like a warning, because - while referring to a given data handling – every algorithm can be well suited only whenever its implicit assumptions can be satisfied, both by the physical system of concern, and by the completeness of the database. In fact, under suitable circumstances, floods, anomalous climatic events, earthquakes, or all kinds of unusual events, can be treated in this way.

Let us first suppose that we deal with time series of data that refer to a quantitative measure of a given physical quantity (e.g., the total water flux per unit time in a river). The time series is supposed to be complete and reliable. That is, the gaps (which often certainly exist in historical data series) are neglected, when they have an unknown location in time. Conversely, we know that some given, well-known, and temporally well-defined gaps can be eventually known. In any case, the distribution is known of the available measurements or records.

Split the total time-span of the data into equal-time intervals of a given duration, e.g. into intervals of $1\ year$. Search for the maximum and minimum values of the water flux per unit time within every interval. All these maxima, and all these minima, i.e. both kinds of *extremes*, accordingly satisfy a given distribution. Whenever the distribution of the original data sequence is known, the distribution of the *extremes* can be evaluated, which in general will depend on the duration ($1\ year$) of the chosen elementary interval. The theory can estimate the expected return time of a given event of some given severity, etc.

Consider the case of a time sequence - strictly with no gap - of the dates (e.g.) at which the surface of a given lake is exceptionally freezing. This datum is not *per se* an extreme, as it states that air temperature was below zero, although one cannot know how low it was. In any case, we know the return-time of the event, and this datum alone can be treated in terms of the statistics of *extremes*. A similar situation applies, in some respect, to earthquake series with magnitude above some threshold, and epicenter in some given area. However, whenever the dates of frozen lake contain gaps, the statistics of *extremes* cannot be applied – e.g. when we know when the surface of the lake froze, but, otherwise, in general we don't know whether the lake surface did not freeze, or whether, perhaps, it actually froze while this information is missing.

Similar comments apply to incomplete - or presumably incomplete – earthquake series. As far as floods and anomalous climatic events are concerned, the historical information is *per se* qualitative, and it is similar to the frozen lake information. In fact, even a hydrometric information is biased - because the water flux per unit time in the river depends on the state the river bed, which changes in time due to sediment deposition and to anthropic action (industrial settlements, building of bridges, banks, dykes or dams, different kind of cultivation, i.e. either tall trees, or corn, or grass, etc. inside the banks, cutting or replanting of trees on the slopes of the whole catchment basin, etc.). All these factors - under unusual heavy rain conditions - can significantly change the speed of the water flow.

In summary, the application of the theory of *extremes* - similarly to every other algorithm - makes sense only whenever one is conscious of the primary physical requirements and undeclared implications that are unavoidably introduced by mathematics. The physical "feeling" of phenomena by the researcher must always prevail.

A second approach is to identify every "anomalous" event with a Dirac δ-function in time, as its time duration is much shorter than the typical time scale of the repetition of the phenomenon of leading concern. From a mathematical viewpoint, the actual non-infinitesimal time duration of every event will actually be of no concern in the analysis of

[6] Refer to Gumbel (1958), Jenkinson (1969), Galambos (1978), Prescott and Walden (1980), West (1982), Castillo (1988), Liao and Shimokawa (1999), ...

NCGT Journal
New Concepts in Global Tectonics
New Concepts in Global Tectonics Journal
Volume 14, Number 6, June 2026
ISSN number; ISSN 2202-0039

the occurrence *per se* of the *extreme* event. When choosing this viewpoint, the data series is thus substituted by a sequence of values "0" or "+1". This kind of series could be treated in terms of an expansion of Walsh (or related) functions (see the Appendix). Then, a correlation, or convolution, analysis can be carried out in order to search for a *sequency* spectrum (see e.g. Beauchamp, 1984, Ch. 3). This procedure, however, requires that the original data series is *complete* and *homogeneous*, a feature that only seldom occurs in real historical data series.

All these basic warnings can be avoided by means of the approach here considered. The discussion is here concerned with *point-like processes* considered from the aforementioned Dirac δ-function viewpoint. Three main items are discussed:

(i) presentation of a few previous case histories of data handling in 1D;

(ii) discussion of some formal generalizations still referring to the 1D case; and

(iii) generalization of the procedure to the nD case.

Let us point out that we must suppose that the database has been preliminarily suitably checked and "cleaned" for possible errors, and also prepared by some eventual *physical* selection. That is, eventual physical distinctions (like distinguishing spates from floods, or the rejection of the aftershocks, or of earthquakes with magnitude below some threshold, etc.) must precede the statistical procedures that is here considered. This separation can often be effectively carried out by the procedures for the *rejection of the outliers* (see Gregori et al., 2026e).

The algorithms here considered are basically robust – unlike, e.g.,. the aforementioned Fourier algorithms. Hence, some reasonable amount of spurious data – that often refer to physically different phenomena - in general has no relevant influence on the conclusion. However, if the percent of spurious information is exceedingly large, even the most robust algorithm will give erroneous inferences.[7]

3. The 1D case.

Refer to[8] Table 1.

Defining $\mathfrak{H}$ - Here $\mathfrak{H}$ means "*historical data series*". We first assume that this series is lD, and subsequently, whenever needed, it is generalized to the nD case history.

Defining $\mathfrak{D}$ - It implies to substitute every "*point*" with a "*discrete*" non-infinitesimal "*elementary square*" of unit side. $\mathfrak{D} \otimes \mathfrak{H}$ means that the operator $\mathfrak{D}$ is applied to $\mathfrak{H}$. By $\mathfrak{D}$ we mean that the time duration of every event is arbitrarily chosen *a priori* and considered equal to some discrete value (in contrast to the infinitesimal duration of a Dirac δ-function). That is, every point-like Dirac δ-function is changed by $\mathfrak{D}$ into an elementary square of unit side (where the unit has been arbitrarily prechosen). This $\mathfrak{D}$ operator is optional in the procedure here proposed, i.e. with no loss of generality this $\mathfrak{D}$ operator can be either applied to $\mathfrak{H}$ or not, depending on the needs of the specific database and analysis, which is carried out in the following.

Table 1. Logical sequence of the $\mathfrak{Urp}$ analysis for the 1D case

$$\mathfrak{H}$$
$$\mathfrak{D} \otimes \mathfrak{H}$$
$$\mathfrak{Urp} \otimes \mathfrak{D} \otimes \mathfrak{H} \pm \sqrt{\mathfrak{Urp} \otimes \mathfrak{D} \otimes \mathfrak{H}}$$
$$\sqrt{\mathfrak{Urp} \otimes \mathfrak{D} \otimes \mathfrak{H}} \pm 1/2$$
$$\mathfrak{R}_{ES} \otimes \mathfrak{D} \otimes \mathfrak{H} \equiv (1 - \Lambda) \otimes \sqrt{\mathfrak{Urp} \otimes \mathfrak{D} \otimes \mathfrak{H}} \pm 1/2$$
$$\mathfrak{Cetra} \otimes \mathfrak{R}_{ES} \otimes \mathfrak{D} \otimes \mathfrak{H}$$

Defining $\mathfrak{Urp}$ - A given *point-like process* has a recurrence in time of period T whenever, statistically, the probability of its occurrence is greater - than the background - at time intervals of duration T. A perfectly periodic phenomenon has 100% probability to occur at the exact time (e.g., an eclipse, although always within a suitable error-bar). However, other phenomena may have only a minor periodical component, while a non-periodic trend plays a more or less relevant role. Therefore, the concern is about recognizing whether there is - or not - any periodic component, and what is its percent relevance.

The definition of the operator $\mathfrak{Urp}$ (*Automatic Research for Periodicities*) is exemplified in Fig. 1. The leading idea is that, if one puts the time origin (or if we "restart the stopwatch" every time) immediately after the occurrence of one event of the data series - and whenever there is an eventual probable recurrence of the phenomenon after a time lag T - one must find, statistically, the occurrence of another event at time T .This holds no matter how incomplete the database is.

The result can show either a regular superposition of periodic events, or a random distribution, or a mixture of the two possibilities (as it has been discussed up to some extent by Pavese and Gregori, 1984).

For future reference, let us associate a specific name to the time origin on every partial data series. Briefly call "*strip*" every partial data series of this kind, and call "*time of pole position*" the respective time origin of every given strip.

Pavese and Gregori (1984) discuss the analogies of this $\mathfrak{Urp}$ operator with the formal standard procedures used by statisticians when dealing with *point-like processes*. It can be shown (see section 5) that the final histogram – henceforward to be briefly called $\mathfrak{arp}$ (in the aforementioned papers the symbol "$\mathfrak{U}$" was used) - has a value that has a Poisson distribution with standard deviation $\pm\sqrt{n(T)}$, where $n(T)$ is the ordinate of $\mathfrak{arp}$ at T.

[7] Specific examples are given, e.g, in Pavese and Gregori (1984), Alessandrini et al. (1987), Fiorentino et al. (1988), Gregori et al. (1988), and Pavese et al. (1992).

[8] After Gregori (1990). With kind permission of the late Wilfried Schrˆ der.

NCGT Journal
New Concepts in Global Tectonics
New Concepts in Global Tectonics Journal
Volume 14, Number 6, June 2026
ISSN number; ISSN 2202-0039

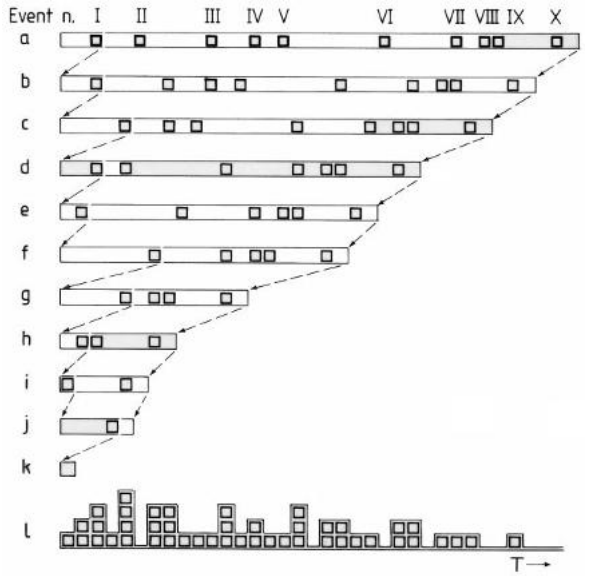

Fig. 1. Definition of $\mathfrak{Urp}$. Refer to an arbitrary data series $\mathfrak{H}$ (e.g. *vs.* time) of, say *10* point-like events [row *a*, defined by arbitrary choice]. For simplicity, all events are here supposed to have an equal time duration (although this assumption can be dropped, see text). Change the origin on the time axis, and put it immediately after the occurrence of the 1st event (or state that you "*restart the stopwatch*" immediately after the occurrence of the 1st event) and get *strip b*. Similarly, restart the stopwatch after the 2nd event, and get *strip c*, ... restart the stopwatch after the 10th event and get *strip k*. Sum up all these *strips b,c, ... ,k* (but not *strip a*) and get the histogram *l*, which is called $\mathfrak{arp}$. This operation is said to be carried out by the operator $\mathfrak{Urp}$, and it is indicated by $\mathfrak{Urp} \otimes \mathfrak{H}$. In the case of a random distribution of the *10* events within $\mathfrak{H}$, the result, i.e. $\mathfrak{arp}$, approximately looks like a right-angled triangle with right angle in the origin. After Gregori et al. (1988) and Gregori (1990). With kind permission of the late Wilfried Schrˆ der.

When the events are randomly distributed, $\mathfrak{arp}$ must display an approximately linear decreasing trend. It looks like a right-angled triangle with right angle at the origin. This is a consequence of the progressive shortening of the *strips* as suggested by Fig. 1. Henceforward, this trend will be here called the "*triangle effect*".

Defining $\sqrt{\mathfrak{Urp}}$ - Evaluate $\mathfrak{Urp} \otimes \mathfrak{D} \otimes \mathfrak{H}$ and get $\mathfrak{arp}$, or, say, a hystogram $n(T)$ *vs.* T. Then, plot a new histogram defined by $\sqrt{n(T)}$ *vs.* T, and call it $\sqrt{\mathfrak{arp}}$. It can be shown (see section 5) that $\sqrt{n(T)}$ has a normal distribution with standard deviation $\pm 1/2$. [9] By this, the *important achievement* is obtained that (unlike it occurs for $\mathfrak{arp}$) the error-bar in the final histogram $\sqrt{\mathfrak{arp}}$ is *independent* of T.

Let us, rather, reconsider the same argument that deals with the physically sound criterion that is the basis for the parameter expressed by (34) [compared to (33)] of Gregori et al., 2026e). Call $a(T) \equiv n(T)$ the ordinate of $\mathfrak{arp}$ corresponding to abscissa T. Hence, $\mathfrak{arp}$ is defined by

$$a(T) \pm \Delta a(T) \equiv a(T) \pm \sqrt{a(T)} \tag{1}$$

Owing to the aforementioned property (see section 5) Gregori et al. (2026e) the error-bar of $\sqrt{\mathfrak{arp}}$ is

$$\sqrt{a(T)} \pm \Delta\sqrt{a(T)} \equiv \sqrt{a(T)} \pm \frac{1}{2} \tag{2}$$

that is, if $\mathfrak{Urp}$ has an error bar $\sqrt{a(T)}$, then $\sqrt{\mathfrak{arp}}$ has an error bar $[1/2]$.

The choice of the elementary interval when constructing the $\mathfrak{arp}$ - When we must draw a given histogram, the first step is to choose the elementary interval Δx to be used on the x-axis (which is also called the *abscissa axis*). If Δx is exceedingly small, the histogram looks like a scattered sequence of isolated boxes. If it is exceedingly large, we miss several details of the histogram.

When drawing an $\mathfrak{arp}$ the following criterion can be used. Concerning the following computation, for simplicity let us assume that the available database is given by means of data, where every datum has a duration of a unit time interval.[10] The database is composed of N elements spread on a total time lag of duration L. Call x and y, respectively, the abscissa and ordinate of $\mathfrak{arp}$. One event occurs at a mean time-delay of $\Delta x_a = L/N$. Let us compute the total integral of the $\mathfrak{arp}$ between $x = 0$ and $x = L$, which is the surface S contained between the ordinate of $\mathfrak{arp}$ and the abscissa axis or x-axis.

The first *strip* used for constructing the $\mathfrak{arp}$ has a total area N . Consider a *strip* where the N elements are uniformly spread all over the entire time span L. A strip of total length L and of total area N has a vertical width $w = N/L$.

The second *strip* adds an additional area that can be estimated as a *strip* of the same width w but of length $L - L/N$, i.e. it adds $w(L - L/N) = (N/L)(L - L/N)$.

The third strip adds an additional area $w(L - 2L/N) = (N/L)(L - 2L/N)$. Etc.

The result is therefore

$$S = \sum_{p=0}^{N} (N/L)\,(L - pL/N) = N(N+1)/2 \tag{3}$$

Owing to the triangle effect, the $\mathfrak{arp}$ has the approximate figure of a right-angled triangle with cathetus along the x-axis of length L, hence with cathetus along the y-axis of length $H = 2S/L$. The hypotenuse is a segment of the line $y(x) = -(H/L)x + H$.

Call Δx the elementary interval chosen for constructing the $\mathfrak{arp}$ histogram. The number $n(x)$ of boxes piled up at the abscissa x is therefore such that

$$n(x)\Delta x = -(H/L)x + H \tag{4}$$

Let us require that it should be, say, $n(0) \sim 100$. This is convenient, as for $x = 0$ it would be $\sqrt{\mathfrak{arp}} \sim 10 \pm 1/2$. Hence, the $\sqrt{\mathfrak{arp}}$ peaks can be easily recognized, and no excessive loss in precision is attained in the definition of a period. Hence, from (4) it is found

[9] Guivanni P. Gregori is indebted to the late Professor John Wilder Tukey (1915-2000) for this suggestion.

[10] This assumption implies no loss of generality, as the present estimate is only aimed to give and indication of the order of magnitude of the elementary interval Δx to be used for constructing $\mathfrak{arp}$.

NCGT Journal
New Concepts in Global Tectonics
New Concepts in Global Tectonics Journal
Volume 14, Number 6, June 2026
ISSN number; ISSN 2202-0039

$$\Delta x \sim \frac{H}{100} = \frac{N(N+1)}{L \cdot 100} \qquad (5)$$

This is a reasonable and maybe "optimum" choice for constructing an $\mathfrak{arp}$ on a given data set.

Defining Λ - The operator Λ gives a weighted-running-average, computed according to the definition of Fig. 2b. The operator Λ should be distinguished from the operator Π that gives a simple (i.e. non-weighted) running-average (as shown by Fig. 2a). When exploiting some practical example - as it can be readily verified - the operator Λ gives a much more effective filtering than Π, as it is evident when comparing the system functions of the two filters, as shown by the right plots in Fig. 2 (see, e.g., BÂth, 1974, p. 54).

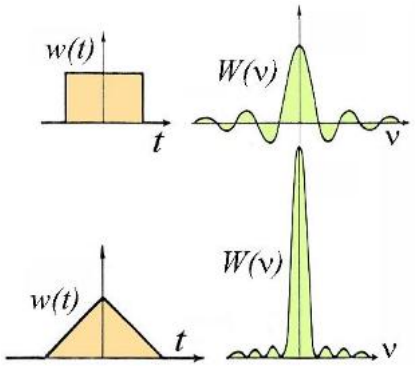

Fig. 2. *(a)* Definition of Π, i.e. of a filter that evaluates a running average over $2k+1$ units. *(b)* Definition of Λ, i.e. a filter that evaluates a weighted-running-average, giving to every datum a weight that is linearly proportional to its distance from the central value of Λ. Other filters can be easily imagined, e.g. having a weight defined by a Gaussian function, etc. After Gregori et al. (1988) and Gregori (1990). With kind permission of the late Wilfried Schrˆder.

This Λ filter is systematically used in the following. However, if the reader prefers any other suitable filter, no change is required for the rationale of the present approach. Henceforward, Λ can be considered as denoting any kind of suitable and quite general filter that selects only some given frequency band (see, e.g., BÂth, 1974 or Kulhanek, 1976).

For a *point-like process*, it is[11]

$$\Pi^2(\pm k) = \Lambda(\pm 2k) \qquad (6)$$

Defining $\mathfrak{R}_{ES}$ - The operator $\mathfrak{R}_{ES}$ evaluates a residual by means of suitable data handing on any given input histogram $\mathfrak{H}$. Here it is applied either to $\mathfrak{arp}$ or to $\sqrt{\mathfrak{arp}}$. That is, evaluate $\Lambda \otimes \mathfrak{G}$, and subtract $\Lambda \otimes \mathfrak{G}$ from the original $\mathfrak{H}$, i.e. evaluate $(1-\Lambda) \otimes \mathfrak{H} \equiv \mathfrak{R}_{ES} \otimes \mathfrak{H}$. It should be noted that $\mathfrak{R}_{ES}$ must apply $(1-\Lambda)$ to $\sqrt{\mathfrak{Arp} \otimes \mathfrak{D} \otimes \mathfrak{H}}$, while it should *not* evaluate the quantity $\sqrt{1-\Lambda} \otimes \mathfrak{Arp} \otimes \mathfrak{D} \otimes \mathfrak{H}$, as the second procedure would imply computing a weighted running average over data having an uneven error bar.

Defining $\mathfrak{Cetra}$ - The operator $\mathfrak{Cetra}$ (*Computing Errors, Trends, and Associated parameters*) [12] relies on the *superimposed epoch criterion* and it works as follows.

The data series $f(t)$ can be *either point-like* or a smooth function - and in such a second case it can be either a continuous analytic function, or a function tabulated in a log and defined at a discrete set of points $\{t_j\}$, i.e. $\{f(t_j)\}$, with $(j = 1, 2, \ldots, n)$. Plot this $f(t)$ over a transparent sheet. Arbitrarily choose a trial "*segment*" (or "*period*", e.g., when the independent variable is time t) and call T the "*period*". Cut the transparent sheet into several contiguous *segments*[13] of total length T (as in Fig. 3). Superpose all these *segments*. In the literature, this is called *cycle diagram* of modulo T of $f(t)$. This *cycle diagram* of modulo T will be here symbolized as an operator $\mathfrak{Cydia}$, i.e. a *cycle diagram* is represented by $\mathfrak{Cydia} \otimes f(t)$, where $\mathfrak{Cydia} = Cydia$ is the acronym for *cycle diagram*.

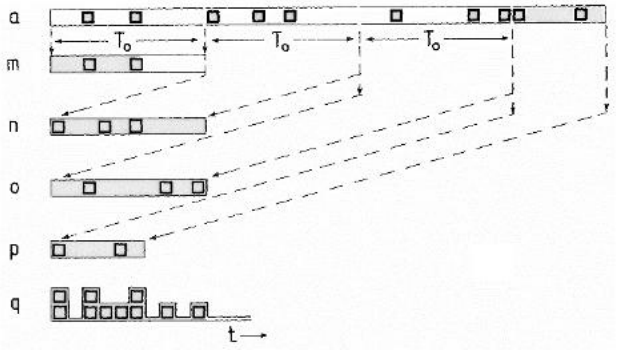

Fig. 3. Definition of "*cycle diagram of* $\mathfrak{H}$ *modulo* T_0". Consider the same data series $\mathfrak{H}$ of *10* events considered in Fig. 1. Pre-choose a given trial period T_0. Cut $\mathfrak{H}$ into the segments *m, n, o, p*, every one being of duration T_0. Sum up all these segments and get the final histogram $\mathfrak{q}$. This procedure is performed by the operator $\mathfrak{Cydia}$ and it is indicated by $\mathfrak{Cydia} \otimes f(t)$. After Gregori (1990). With kind permission of the late Wilfried Schrˆder.

Finally, apply some specific statistical analysis - to be specified in a moment - and evaluate a statistical parameter (generally called $\mathfrak{p}$) that gives a quantitative indication of how well the different superimposed segments plotted in the *cycle diagram* match with one another. $\mathfrak{Cetra}$ carries out this operation and evaluates this parameter $\mathfrak{p}$.

The definition of $\mathfrak{p}$ can be given in different ways. This is the object of Gregori et al. (2026e). For every specific application it is eventually convenient to carry out a few attempts, by means of different definitions of $\mathfrak{p}$, and to compare the different results for pointing out the comparatively intuitively clearer inferences.

[11] G. P. Gregori is indebted to Dario Camuffo for this remark.

[12] "*Cetra*" in Italian means a special kind of lyre, from the Latin "*cythara*". See Alessandrini et al. (1987), Fiorentino et al. (1988), and Gregori et al. (1988).

[13] Notice the following distinction. We call "*strip*" a fraction of the original data series beginning from the *pole position* – and every *strip* is chosen with origin of at a different chosen "*pole position*". The *strip* continues until the very end of the data series. In contrast, a "*segment*" is a fraction of the original data series having a total duration T, independent of the choice of the *pole position*. The length of the very last "*segment*" can even be $< T$.

NCGT Journal
New Concepts in Global Tectonics
New Concepts in Global Tectonics Journal
Volume 14, Number 6, June 2026
ISSN number; ISSN 2202-0039

Let such a $\mathfrak{p}$ to be evaluated for several trial values of T, i.e. one actually evaluates a function $\mathfrak{p}(T)$. Finally, plot $\mathfrak{p}(T)$ vs. T, and call " $\mathfrak{Cetra}$" this plot. In general, one can define the sign of $\mathfrak{p}(T)$ in such a way that a relative maximum of $\mathfrak{p}(T)$ vs. T results to be associated with a better matching of the segments of $f(t)$ in the *cycle diagram* $\mathfrak{Cydia}$.

A practically important operational advantage of $\mathfrak{Cetra}$ is the fact that, if there is one apparent recurrence period - or briefly one "*periodicity*" - say at T_0, one finds evidence for *periodicities* also at $k\,T_0$ for every $k = 2, 3, \ldots$.

Therefore, one can apply $\mathfrak{Cetra}$ in an iterative way, i.e. evaluate $(\mathfrak{Cetra})_j \otimes \mathfrak{R}_{ES} \otimes \mathfrak{D} \otimes \mathfrak{H}$ (for $j = 2, 3, \ldots$), and always find evidence for the same recurrence time T_0.

Errors while applying $\mathfrak{Cetra}$ - Every definition of $\mathfrak{p}$ must start from a *cycle diagram* $\mathfrak{Cydia}$. Consider - for every given abscissa x on this *cycle diagram* $\mathfrak{Cydia}$ - a moving average computed over all points that fall inside a pre-chosen, moving, elementary interval Δx centered around x.

For every given elementary moving interval along x and of amplitude Δx, consider the distribution of all points that enter into the definition of the moving mean value.

Intuitively, this concept reminds about a conditional distribution of a multivariate point distribution, although the present concept is *per se* different, as it deals with a non-vanishing interval Δx. Conversely, in the definition of *cycle diagram* Δx can be supposed to be vanishing.

Then, let us draw a continuous interpolating line - let us call it $y(T)$ – through all these *point-like* estimates of a moving average on the given cycle diagram. Note that, henceforward, $y(T)$ is a continuous function, although it was computed by interpolation at some discrete and pre-chosen set of points on abscissæ.

Finally, refer to every actually observed datum - call it $z_k(t)$ (for $k = 1, 2, \ldots$) - which is represented by one given point on the cycle diagram. Consider its respective distance, either positive or negative, with respect to this $y(T)$. Call "k-th residual" this distance $z_k(t) - y(T)$. The distribution of the ensemble of all these $z_k(t) - y(T)$ (and for brevity purposes let us call it "*distribution of residuals associated to T*") is finally to be tested, by analyzing its Gaussianicity, by means of a suitable parameter $\mathfrak{p}$, as per Gregori et al. (2026e).

However, there is a concern about error-bars. When comparing this "*distributions of residuals*" associated to T_1 and T_2 (with $T_1 \neq T_2$), the total number of points that enter into every respective cycle diagram $\mathfrak{Cydia}$ is always the same. However, the number of points that drop into every elementary interval Δx gets smaller the longer is T. In the extreme case history when T equals almost the entire time span of the given original observational database, only one observational point (or almost only one point) will fall inside the almost unique elementary interval Δx. In this case, the "*distribution of residuals*" will shrink into a Dirac's δ-function centered around the origin. Hence, all Gaussianicity tests miss every significance.

Even avoiding this extreme condition - that in every practical application will never be attained - it is certainly incorrect from a strict point of statistical rigor to compare *sic et simpliciter* the "*distributions of residuals*" associated to T_1 and T_2 (with $T_1 \neq T_2$). We must introduce suitable corrections. It is sure that a bias exists, which is more amplified the longer is the pre-chosen trial period T of the cycle diagram. From a practical viewpoint, however, in the case of a sufficiently large original database, this bias will be almost negligible.

Consider the statistical process of the evaluation of the aforementioned moving average inside only one given elementary interval Δx. The plotted points display a distribution that is supposed to be approximately Gaussian, and its standard deviation $\sigma(T)$ is formally estimated by means of its rms deviation. It is well-known, however, that this estimate ought to be corrected by a suitable coefficient derived from the Student-t distribution. On the other hand, when the total number of elements of the distribution is larger than, say, a few tens, this correction is almost negligible.

This entire criterion, however, is of little practical help for the present case history, as it deals with a correction to be applied to every single Δx interval displayed in the final "*distribution of residuals*".

In contrast, for such a purpose, it is quite effective the same criterion applied for the argument dealing with (2). In fact, we can reasonably guess - on sound physical arguments - that the deviation (or residual) $z_k(t) - y(T)$ of every given point $z_k(t)$, with respect to its corresponding moving average $y(T)$ in the *cycle-diagram*, partakes into an ideal distribution having standard deviation $\sim \sqrt{y(T)}$. This ideal distribution is already semi-standardized (see Gregori et al 2026e), because, owing to definition, its average μ is $\mu = 0$.

Let us transform this already semi-standardized distribution into a totally standardized distribution. That is, instead of $z_k(t) - y(T)$, consider the "corrected" residual $[z_k(t) - y(T)]/\sqrt{y(T)}$. Hence, the distribution inside every elementary Δx interval has a unit standard deviation. Hence, the ensemble of all these "corrected residuals" defines the "*corrected distribution of residuals*", over which the aforementioned chosen test for Gaussianicity can be safely applied.

This shrewdness fully solves the concern about error-bars, and their amplification while increasing the trial period T of the *cycle diagram*.

Forecast - Refer to [14] Table 2, fully explained in the following. Forecasts can be made, whenever physically feasible, by means of the aforementioned operator $\mathfrak{Cydia}$. In fact, when one knows that the phenomenon has some apparent *periodicity* T, let us construct the *cycle diagram* of modulo T, and let us evaluate (much like $\mathfrak{Cetra}$) a running average over it, and its rms deviation as well. Plot and superpose this running average with its standard deviation

[14] After Gregori (1990). With kind permission of the late Wilfried Schr^ der.

NCGT Journal
New Concepts in Global Tectonics
New Concepts in Global Tectonics Journal
Volume 14, Number 6, June 2026
ISSN number; ISSN 2202-0039

over the original plot of the observational database, and extrapolate it into the future.

Table 2. Additional logical steps for completing the 1D $\mathfrak{Arp}$ analysis and apply to the ND case

Forecasting

$$\mathfrak{Cydia}(T) \otimes \mathfrak{H} \pm \sigma(CY, T)$$

Interpretation

Filtering
Period family and *forefather* period
Induced and deduced forefathers
Family relations between *forefathers*

Cross-dependence

$\mathfrak{xArp}$	(or $\mathfrak{xbArp}$)
$\mathfrak{cArp}$	(or $\mathfrak{edArp}$)
$\mathfrak{nArp}$	(or $\mathfrak{nbArp}$)
$\mathfrak{nxArp}$	(or $\mathfrak{uxbArp}$)
$\mathfrak{ncArp}$	(or $\mathfrak{ncdArp}$)

The result gives the eventual evidence either *(i)* that we achieved some statistically reliable forecast, or *(ii)* that the apparent *periodicity* T is due to some minor component in the data series that has no strong influence on its occurrence. In this case, no forecast can be realistically made by means of this algorithm and extrapolation, as the phenomenon displays no sufficient regularity - and no physically significant extrapolation can be made.

Hunting *period families*, and their "*induced*" and "*deduced*" forefathers. "*Fine*" structure - Suppose that after applying $\mathfrak{Cetra}$ [or $(\mathfrak{Cetra})_j$ (i.e. applied iteratively on residuals] one finds the *periodicities* kT_1, kT_2, kT_3, ... ($k = 1, 2, \ldots$). One can apply Λ, whereby some given frequency band is selected close either to $1/T_1$, or to $1/T_2$, or to $1/T_3$, ... Then, apply $\mathfrak{Cydia}$ and evaluate the expected component $\mathfrak{H}(j)$ of $\mathfrak{H}$ that is most probable to occur with a given recurrence *period* of time T_j, ($j = 1, 2, \ldots$).

The concern is about deciding how many different T_i ($i = 1, 2, \ldots$) ought to be physically considered, and what is their relative relevance for the observed phenomenon.

Concerning the order of the $\{T_i\}$ ensemble, let us state for a moment that a T_j comes first when it appears "more evident" (on an intuitive basis) than the subsequent ones. However, another decision is by assessing whether one given period T_j is fundamental (i.e. it is of the form $T_j = kT_h$, with $k = 1$), or it is the k-th multiple of some other T_h (i.e. it a $T_j = k\,T_h$ with $k > 1$), or whether it is a higher harmonic of some other period T_h (i.e., it is of the form $T_j = T_h/m$, where $m > 1$ is an integer).

Introduce the following definitions. A *forefather period* (or briefly a *forefather*) is any period T such that two conditions are fulfilled:
it is not an integer multiple of another period; and
it is not a higher harmonic of some other period (i.e. no T must exist such that $T_j = T/m$, being $m > 1$ integer).

Thus, every forefather T_j is in general associated to some suitably large set of other periods T given by

$$T = kT_j/m \ (k, m > 1; \text{integers}) \qquad (7)$$

The set $\{kT_j/m\}$ ($k, m \geq 1$ integers) is said to be a *period family*, or briefly a *family*, having *forefather* T_j, and it will be briefly indicated by $\mathfrak{F}(T_j)$.

If all *periodicities* are known with no error-bar, it is easy to recognize a *forefather* from the set of all other envisaged *periodicities*. In reality, however, this never occurs.

Hence, the best way to distinguish a forefather (say T_1) from an integer multiple of another period T_2 (where $T_2 < T_1$), is to apply preliminarily a filter (Λ or some other filter) to $\mathfrak{H}$ in order to remove all frequencies $\geq 1/T_1$. In the case that it is $T_1 = kT_2$, when we evaluate on the pre-filtered data series $\mathfrak{Cetra} \otimes \mathfrak{R}_{ES} \otimes \Lambda \otimes \mathfrak{D} \otimes \mathfrak{H}$ and we no more find the signal at $T = T_1$. In the case that, physically, within $\mathfrak{H}$ there is this period T_1, one finds evidence for T_1 even after applying this pre-filtering. Thus, after a check and trial procedure, one is left with a sequence $\{T_i\}$, (with $i = 1, 2, \ldots$) that can be tentatively presumed to be a set of possible *forefathers*.

When this selection has been made, a temporary hierarchy of *forefathers* can be envisaged, depending on the apparent (intuitively speaking) importance of their respective role played within $\mathfrak{H}$. Then, reorder by decreasing importance the periods T_j according to this hierarchy, and evaluate $\mathfrak{H}(1) = \mathfrak{Cydia}(T_1) \otimes \mathfrak{H} \pm \sigma(CY, T_1)$ (where the symbol for the error bar is self-explanatory). Then, evaluate $\mathfrak{H}_1 = \mathfrak{H} - [\mathfrak{Cydia}(T_1) \otimes \mathfrak{H}] \equiv \mathfrak{H} - \mathfrak{H}(1)$ and apply anew the same procedure as above and evaluate $\mathfrak{Cetra} \otimes \mathfrak{R}_{ES} \otimes \mathfrak{D} \otimes \mathfrak{H}_1$ in order to search for the next seemingly most important period T_2. Evaluate $\mathfrak{H}(2) = \mathfrak{Cydia}(T_2) \otimes \mathfrak{H}(1) \pm \sigma(CY, T_2)$ and $\mathfrak{H}_2 = \mathfrak{H}(1) - [\mathfrak{Cydia}(T_2) \otimes \mathfrak{H}(1)] \equiv \mathfrak{H}(1) - \mathfrak{H}(2)$, etc.

The result is that $\mathfrak{H}$ has been - although, only temporarily, see below - decomposed into a sum

$$\mathfrak{H} = \mathfrak{H}(1) + \mathfrak{H}(2) + \ldots \qquad (8)$$

where $\mathfrak{H}(j)$ is the component of $\mathfrak{H}$ having *periodicity* T_j.

However, this procedure is arbitrary in several respects.

- *First*, the choice of the T_j hierarchy relies on an intuitive and subjective decision.
- *Second*, another arbitrary choice is the decomposition (8), which assumes that $\mathfrak{H}(1)$, $\mathfrak{H}(2)$, ... are combined with one another according to an *additive* law. Differently stated, what are the true *family relations* (see below) among different *forefathers*?
- *Third*, some decision had to be implicitly taken when assessing whether a given period is a *forefather* or not, concerning the actual expected role of the errors in the determination of the several T_j.

Common sense, and mostly the fundamental physical "intuition", plays a basic role in all this scheme and in the decisions to be taken. However, no matter how good this simple criterion may appear, there is need for some quantitative rigor for the assessment of a heuristically most appropriate methodology.

Hence, let us define as follows the "*induced*" and the "*deduced*" periods.

Logical induction - as used by Aristotle and Galileo - means a logical process whereby one starts from experimental evidence and gets its intrinsic regularities or apparent correlations, or empirical "physical laws". That is,

ISSN number; ISSN 2202-0039

nothing is left to the subjectivity or speculation of the researcher, and everything is decided by the experimental data log *per se* and by a suitable statistical analysis. Such an inductive approach, however, practically gives effective and reliable results (within the experimental error-bars) as far as it does not require unrealistic and very large data sets.

Conversely, *logical deduction* is a different logical step. That is, one imagines a trial model, and implements it by logics and mathematics. Then, one feels confident, and takes for granted this model, as long as it succeeds to explain the available observations. Whenever the envisaged mode fails to explain - or it appears to be in contradiction with - some experimental evidence, the researcher will search for an explanation by means of a different or improved model, etc. The "*deductive*" - unlike the "*inductive*" - science can normally raise debates among supporters of different viewpoints, models, or approaches.

Differently stated, the Aristotle's and Galileo's "*induction*" is somewhat related to Tukey's "*exploratory analysis*", while Aristotle's and Galileo's "*deduction*" is more akin to Tuckey's "*confirmatory analysis*". See section 1.

The periods T_j evaluated as above are therefore *induced* periods. However, sometimes, one knows that some periods are physically known from other evidence. For instance, the annual variation affects several phenomena, but it appears nonsensical to measure the length of the year by means of a temperature data series at a given site. In fact, astronomers do it much better by means of their observations. Hence, one can just state that every *induced* T_j close to 1 $year$ is the annual variation. In this case, T_j is known with a high accuracy, as its value is known on the basis of evidences other than the data series of concern. Hence, it is a *deduced* value (when dealing with the present data series alone), and this *deduced* value is much more accurate than its corresponding *induced* value.

Similarly, all tidal periods are much better known[15] on the basis of the formal theory of tides than on the basis of climatological evidence.

Another example is the *QBO* (*Quasi Biannual Oscillation*), which is one of the best evidenced climatological *periodicities*, and it appears to be best measured by making reference to the equatorial stratosphere (e.g., Lamb, 1972), although it can be observed also at high latitudes (e.g., Ford et al., 2009 concerning the Antarctic mesospheric winds and polar vortex dynamics).

As well, the period of the solar cycle variation can be best estimated by solar astronomy.[16] On the other hand, the large amount of arbitrariness ought to be taken into account, which is well-known to be behind the definition of sunspot number (see section 11), by which tree rings (e.g.) are a more objective sensor, even upon considering all "disturbances" originated by the local environmental conditions at the site where the tree growth. Etc.

In summary, the substitution - whenever possible - of every *induced* period by its corresponding *deduced* value – as far as possible - will help in getting rid of some numerical errors in the definition of the periods. In addition, this approach often is an indirect help to decide what are the *forefathers* etc.

Suppose now that $\mathfrak{H}$ displays only two periods T_1 and T_2 - having components evaluated as above and given by $\mathfrak{H}(1)$ and $\mathfrak{H}(2)$, respectively. The concern is about choosing between the existence either of an *additive* - or rather of a *multiplicative* - *family relation*, namely between the two following possibilities

$$\mathfrak{H} = \mathfrak{H}(1) + \mathfrak{H}(2) \qquad (9)$$

$$\mathfrak{H} = \mathfrak{H}(1) \times \mathfrak{H}(2) \qquad (10)$$

(where "$\times$" means multiplication). The reply must be inferred from $\mathfrak{H}$ itself, which is, in fact, the only available source in our analysis. That is, $\mathfrak{H}(1)$ and $\mathfrak{H}(2)$ imply the existence - which was already recognized by the preceding analysis as above - of the two sets of *period families*

$$\mathfrak{F}_1 \equiv \{kT_1/m\}\ (k, m \geq 1, \text{integers}) \qquad (11)$$

$$\mathfrak{F}_2 \equiv \{hT_2/n\}\ (h, n \geq 1, \text{integers}) \qquad (12)$$

In general, eventually not all elements of every set are observed. In fact, the physical system might resonate at some given frequency better than at others. For instance, the physical tidal input is the same, but different physical systems react differently, depending on their specific resonance periods.

Suppose that the multiplicative relation (10) holds among the families $\mathfrak{F}(T_1)$ and $\mathfrak{F}(T_2)$. In this case, their respective set of beats must exist

$$\mathfrak{B}(T_r, T_s) = \{(k_r T_r/m_r)\} \pm \{(k_s T_s/m_s)\} \qquad (13)$$

$$(k_r T_r/m_r) > (k_s T_s/m_s) \qquad (k_r, m_r, k_s, m_s \text{ integer})$$

where, for a matter of strict mathematics, only the beats have to be expected that are related to the addition or subtraction of actually observed members of the families (11) and (12).

We stress that $\mathfrak{B}(T_r, T_s)$ should not be considered a *family* (even though it appears just like a *family*, because it satisfies the formal requirements of a *family*), because, when a beat-set exists, in addition to the two sets $\{kT_r/m\}$ and $\{kT_s/m\}$ with $(k, m = 1, 2, \ldots)$, also the two sets $\{k\,[T_r \pm T_s]/m\}$ are observed.

Moreover, define

$$T_u = T_r + T_s \qquad T_v = |T_r - T_s| \qquad (14)$$

and call (T_u, T_v) the *conjugate pair* of the pair (T_r, T_s). Hence, reciprocally, also (T_r, T_s) is the conjugate pair of (T_u, T_v).

There are therefore two possibilities, and there is need to decide what the couple is of real *forefathers*, and what its *conjugate pair*. That is, either T_r and T_s are the actual *forefathers* of two *families*, and therefore T_u and T_v (and their apparent *families*) are their beat set, or vice versa. The distinction between the two possibilities depends on whether one *pair* is better evidenced than its *conjugate pair* (see, e.g., the Tiber case here below). An obvious physical criterion, whenever applicable, occurs when either one or several periods T_r, T_s, T_u, T_v are known to be *deductive*.

[15] See, e.g., Chapman and Lindzen (1970), Godin (1972), Lisitzin (1974), and Melchior (1978).

[16] For instance, see Whyte (1977), Eddy (1978), Schove (1983), Christensen-Dalsgaard and Frandsen (1988), and several references mentioned in section 11.

NCGT Journal
New Concepts in Global Tectonics
New Concepts in Global Tectonics Journal
Volume 14, Number 6, June 2026
ISSN number; ISSN 2202-0039

Whenever a given period has a specific physical meaning and driver, the observed phenomenon appears periodic, although not necessarily displaying a perfect sinusoidal trend. The deviation from a sinusoid is represented by several terms of higher harmonics. In addition, if the algorithm relies on the *superposed epoch criterion*, one unavoidably finds also several integer components both of the *forefather*, and also of every higher harmonic term.

Therefore, note the different meaning: *(i)* of a *forefather*, *(ii)* of a member of a *family*, and *(iii)* of a member of a *beat set*.

A real *forefather* has a potentially relevant physical meaning. For instance, the solar day, or the lunar day, or the solar year, or the lunar synodic period, or the 18.6 $year$ Metonic lunar cycle, or the ~11 (or ~22) $year$ solar cycle, or, maybe, even the *QBO*, are all related to actual forcing factors in the environment, related either to the astronomical motion of the Earth or of the Moon, or to solar physics, or to some typical resonance period of the system, or to some other cause for *QBO*, etc. Hence, one must expect the *forefathers* to be related to these physically fundamental *periodicities*. In any case, we stress the fundamental role of *physical intuition*.

In contrast, every member of a *family* has a much more limited physical implication. In fact, if it is a higher harmonic of a *forefather*, its physical role is only to contribute to the definition of the actual shape of the non-strictly-sinusoidal phenomenon, being repeated with the *periodicity T* (i.e., it is just one term in the Fourier series expansion having as fundamental period the *forefather T*). When the member of the *family* is just a multiple of another member, it has no actual physical meaning *per se*, being just the result of a mathematical property of $\mathfrak{Arp}$.

Concerning the periods that are members of a *beat set*, they are only a matter of mathematics, not of physics, simply resulting from the *multiplicative* combination of two sinusoidal curves.

Hence, it is worthwhile to spend some effort in order to recognize the actual *forefathers* with respect to all other periods within either an $\mathfrak{arp}$ or $\sqrt{\mathfrak{arp}}$ etc., because, in fact, this is a real crucial point when attempting to envisage some *physical* interpretation.

In summary, whenever one has eventually recognized several period *families* $\{\mathfrak{F}(T_j)\}$ $(j = 1, 2, \ldots)$, one should search for their respective *beat sets* $\{\mathfrak{B}(T_i, T_j)\}$, with $(i, j = 1, 2, \ldots)$. If suitable evidence for the existence of *beat sets* is found, then the *multiplicative family* relation (10) holds. Otherwise the *additive* relation (9) should be preferred.

Whenever the number of *families* is greater than *2*, several possible combinations can occur. For instance, in the case of *3 families*, it could be either $\mathfrak{H} = \mathfrak{H}(1) + \mathfrak{H}(2) + \mathfrak{H}(3)$ [and no $\mathfrak{B}(T_1, T_2)$, $\mathfrak{B}(T_1, T_3)$, and $\mathfrak{B}(T_2, T_3)$ will be found], or $\mathfrak{H} = \mathfrak{H}(1) \cdot \mathfrak{H}(2) + \mathfrak{H}(3)$ [in which case only $\mathfrak{B}(T_1, T_2)$ exists], etc. In practical cases, one can expect that the resulting number of *families* ought to be a limited set. In any case, a mere mathematical approach can give no physical evidence. Differently stated, *physical intuition* comes first. Then, the search for *periodicities*, *forefathers*, etc. can confirm or not the guessed *physical* interpretation.

4. Hunting *forefathers* in the historical series of the Tiber floods

The specific case history is here discussed of the historical series of the Tiber floods. The purpose is only to show how intricate is this kind of analysis.

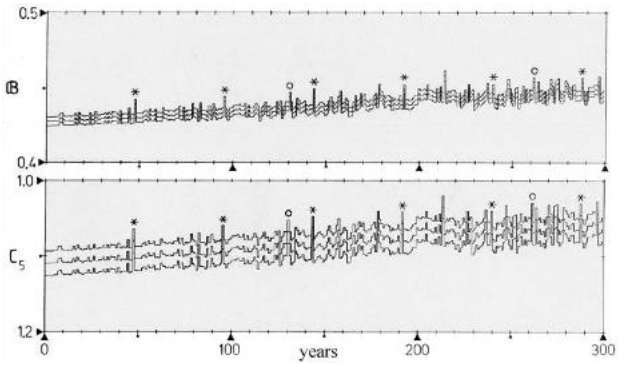

Fig. 4. Results of $\mathfrak{Cetra} \otimes \mathfrak{R}_{ES} \otimes \sqrt{\mathfrak{Arp} \otimes \mathfrak{D} \otimes \mathfrak{H}}$ applied to the 23 $century$ series of Tiber floods in Rome. The figure is taken from Gregori et al. (1988). The most relevant peaks are evidenced by special symbols (a different symbol for every different family). The upper plot shows p_2 [or $\mathfrak{A}$, see Gregori et al., 2026e] and the lower plot p_3 [or $\mathfrak{B}$, see Gregori et al. 2026e]. For discussion see text. With kind permission of the late Wilfried Schr^ der.

Begin by the $\mathfrak{Cetra}$ output shown in Fig. 4. Evidence is shown of the possible *families* $\mathfrak{F}(214)$, $\mathfrak{F}(48)$ and $\mathfrak{F}(131)$. There is a possibility, however, that one *family* of this kind is only the *beat set* of the other two *families*. For inspecting this, consider that in Fig. 4 actual evidence is given only for the periods

$$\begin{array}{ll} k \cdot 48 & (k = 1, 2, \ldots, 6) \\ k \cdot 131 & (k = 1, 2) \\ k \cdot 214 & (k = 1) \end{array} \qquad (15)$$

Refer to all these periods and evaluate[17] Table 3, where, for every entry T_r (rows) and T_s (columns), the value $|T_r - T_s|$ appears written above the main diagonal of this square matrix, and the value $T_r + T_s$ is written below it. *Beats* between periods of the same *family* obviously have not been explicitly indicated, as well as all beats with $T > 300$ years that fall outside the range of Fig. 4. Then, check whether any one of these *beats* can be recognized as being a member of one of the three proposed *families* (15). In this particular case, only two possibilities are found, namely

$$\begin{array}{l} 2 \cdot 131 - 1 \cdot 48 = 1 \cdot 214 \\ 2 \cdot 131 - 1 \cdot 214 = 1 \cdot 48 \end{array} \qquad (16)$$

The $\mathfrak{F}(214)$ seems to be well recognizable (as it is, maybe, the best-defined peak in Fig. 4). Therefore, a first possibility is that the relations (16) imply either that $\mathfrak{F}(214)$ and $\mathfrak{I}(48)$ are real *families*, and that the 131 and

[17] Reproduced with kind permission of the late Wilfried Schr^ der.

NCGT Journal
New Concepts in Global Tectonics

New Concepts in Global Tectonics Journal
Volume 14, Number 6, June 2026

ISSN number; ISSN 2202-0039

262 periods are members of $\mathfrak{B}(214,48)$ (in such a case $262 = 214 + 48$ and $131 = 214/2 + 48/2$), or that $\mathfrak{F}(214)$ and $\mathfrak{I}(131)$ are the *families* and the apparent $\mathfrak{F}(48)$ is composed of members of $\mathfrak{B}(214,131)$.

Table 3. Hunting *forefathers* in the Tiber flood series

	48	96	131	144	192	214	240	262	285	393
48			83			166		214		
96			35			118		166		297
131	179	227		13	61	83	109		157	
144			275			70		118		249
192						22		70		201
214	262						26	48	74	179
240								22		153
262									26	
288										105
393										

Another possibility is that $\mathfrak{F}(48)$ and $\mathfrak{I}(131)$ are the real *families*, and the apparent $\mathfrak{F}(214)$ is a part of $\mathfrak{B}(48,131)$.

Or, still another possibility is that there are three *families* (15), and that no *beats* exist, or that if the *beats* of all three couples of *families* exist, they are only minor structures in Fig. 4. Then, one could even hypothesize the existence of *beats* between a member of a *beat set* and a member of a *family*, etc.

As a matter of fact, such an example of the Tiber deals with a very limited database, and the results plotted in Fig. 4 appear statistically poor (e.g., even when compared with the Tanaro/Bormida case, see Gregori et al., 1988).

In any case, a tentative suggestion is that, maybe, the fine structure of Fig. 4 can be the key for providing some hint indicating what is likely to be the most reasonable choice among the different aforementioned possibilities.

In fact, if one lists, by increasing duration, the periods that appear inside the square matrix of Table 3, this list contains *22* different periods (excluding the 48 and 214 values that are in any case also members of a *family*). The fine structure of Fig. 4 contains ~ 70 additional minor peaks [in addition to the periods (15)].

It is questionable to assign any statistical significance to any kind of this minor structure. It ought to be emphasized, however, that the *beats* should be considered not as a physical fact, rather a mere mathematical consequence of the multiplicative relation (10). That is, a minor structure in Fig. 4 is not significant *per se*, while it can give some hunch when considered altogether in the frame of the entire set composing the fine structure.

In other words, one can try to list all the minor features shown in Fig. 4 (they are ~ 70 values of T). Then, compare them with the *22* values appearing in the square matrix in Table 3, and check whether there is any correspondence between the two lists. If, say, one finds that only some specific rows or columns in the matrix show this correspondence, then it is possible to envisage that, maybe, there are only some *families*, and/or a few *beat sets*, etc.

This has been done for the Tiber case, but $\mathfrak{B}(131,48)$ and $\mathfrak{B}(214,48)$ show half correspondence and half non-correspondence of the expected minor structures. Hence, there is no correspondence (the 50% apparent correspondence has to be generally expected just a matter of coincidence). On the contrary, the $\mathfrak{B}(131,214)$ is expected to show (in the range $0 < T < 300$) only 3 beats, namely: $262 - 214 = 48$, $214 - 131 = 83$, and $393 - 214 = 179$. In fact, Fig. 4 clearly shows well defined peaks at 48, 83, and 179. This appears encouraging. Hence, a tentative conclusion is that either the Tiber floods have three period *families* that behave like

$$\mathfrak{H} = \mathfrak{H}(131) \cdot \mathfrak{H}(124) + \mathfrak{H}(48) \qquad (17)$$

or, they have only two period *families* that behave like

$$\mathfrak{H} = \mathfrak{H}(131) \cdot \mathfrak{H}(124) \qquad (18)$$

Let us also remark that the conjugate pair of $(131,214)$ is $(83,345)$, and the 131 and 214 *families* in Fig. 4 appear better defined than the 83 family (the 345 peak is outside the range of Fig. 4). Hence, the actual *forefathers* seem to be 131 and 214 (and possibly also 48), with the *family relations* (17) and (18).

All this looks intriguing. However, when performing an additional check, it does not seem possible (as it has to be expected) to recognize any peak at $T = |k_1 \cdot 214 - k_2 \cdot 131|$ (with $k_1, k_2 > 1$, integers, and such that $T < 300$).

Just as a curiosity, note that the $\sim 48\ year$ *periodicity* seems to fit with the similar periods displayed by the historical Hungarian aurora record ($\sim 42.85\ year$; Scafetta and Willson, 2013) or by the Tanaro/Bormida climate anomalies ($\sim 42.7\ year$ Gregori et al., 1988), or by volcanic activity (Simkin and Siebert, 1994; Quinn, 2010, p. 52), or in the seismicity of Kamchatka, although Gusev (2008) found a $\sim 57\ years$ cycle. All this is, however, tentative and speculative.

Therefore, the search for the period *families*, for their respective *forefathers*, and for their *relations*, appears in any case physically important, but practically cumbersome or difficult. Unless the multi-period trend is very evident, clear inferences can be inferred only in the case that some physical model can be envisaged, and that the period analysis is carried out for testing it.

In any case, suppose that all *families* have been recognized, as well as the type of their respective *relations*. Thus, one knows a tentative algebraic relation, e.g. like (17) and (18), among the several *periodicities* $\mathfrak{H}(j)$. Then, it is possible to evaluate, by means of a perturbation procedure, some iterating improvement of the definition of all $\mathfrak{H}(j)$, and to drop in this way the temporary numerical definition as above of every component $\mathfrak{H}(j)$ and of their temporary hierarchy.

NCGT Journal
New Concepts in Global Tectonics
New Concepts in Global Tectonics Journal
Volume 14, Number 6, June 2026
ISSN number; ISSN 2202-0039

This would complete the analysis for the search for *periodicities*, for all their respective optimally estimated components $\mathfrak{H}(j)$, and for the type of *relationship* (i.e. either *additive* or *multiplicative*) that should be presumed for their reciprocal formal mathematical connections and for their relative hierarchy.

In any case, we must emphasize that absolute truth is beyond the realm of statistical analysis. Only a "probable" truth can be attained; the level of reliability being basically related to the extent being permitted by the available physical database. A poor database can hardly provide a probable truth having a high reliability, and no mathematical method can obviate to a physically scanty information.

However, since the historical evolution of the environment is an experiment that cannot be repeated, we must try to get out "all" possible "probable" truth, even when it is not highly reliable. It will be left to the responsibility of the geophysicist or climatologist to use - or not - the possible vague evidence inferred from the aforementioned "*inductive*" analysis and to insert it into his "*deductive*" model.

5. Some formal mathematical proofs

The present subsection is included for the sake of completeness. It deals with the formal proof of some properties used in the preceding sections. The reader who is not interested in these rigorous formal items can directly refer to the subsequent section. The arguments here reported are mostly borrowed after Pavese and Gregori (1984) and references therein.

Whenever - compared with the time resolution that is considered while investigating a given phenomenon - an event has such a short time duration that it can be treated as "instantaneous", i.e. it can be described in terms of a Dirac δ-function, the event is called "*point-like process*" (see section 2). Some interesting applications were formerly concerned with biology, such as heartbeats, electrical impulses from a nerve cell or neuron, correlation between electrical impulses from two given neurons named "synapse", etc. Refer to Bryant et al. (1973), Brillinger (1975, 1975a, 1976a, b) and Brillinger et al. (1976).

The following mathematical details are excerpts from the remarkably clear and simple treatment by Brillinger (1976b). For simplicity, according to the viewpoint here considered, a *point-like process* can be considered as isolated in time - i.e. two floods or two climatic events occurring during, say, the same year are treated like a unique event. A *point-like process* is said "*stationary*" whenever its statistical properties are independent of time origin. Let us change a little bit the symbols for conforming with Brillinger's (ibid.). Call N the given series of events. For the time being, let us suppose that N is a complete series, i.e. it is composed by the set of events $\{a_j\}$, with $j = 1, 2, \ldots N$).

Important parameters of N are the mean density, p_N, and the second-order product density p_{NN} given, respectively, by

$$p_N = \lim_{h\to 0} Prob\{\text{point in the interval } (t, t+h)\}/h \tag{19}$$

$$p_{NN}(u) = \lim_{h,h\prime\to 0} Prob\{\text{point in } (t+u-h, t+u+h) \text{ and in } (t-h', t+h')\}/(4, h\, h') \tag{20}$$

with $-\infty < u < \infty$, when the limits exist.

Whenever one needs to investigate the correlation between two different sequences of point processes, say M and N, define for M both p_M and $p_{MM}(u)$ (similarly to the definition of p_N and p_{NN} for N) and also define the cross-product density $p_{MN}(u)$, by

$$p_{MN}(u) = \lim_{h,h\prime\to 0} Prob\{M \text{ point in } (t+u-h, t+u+h) \text{ and } N \text{ point in } (t-h', t+h')\}/(4\, h\, h') \tag{21}$$

Note that p_M, p_N, $p_{MM}(u)$, $p_{NN}(u)$, and $p_{MN}(u)$ do not depend on the lime t because the process is *stationary*. The meaning of these parameters is intuitively clear by stating, e.g., that $[p_N\ h]$ is the probably of finding an N point (or event) within a time interval of duration h. Similarly

$$Prob\{M \text{ point in } (t+u-h, t+u+h) \text{ and } N \text{ point in } (t-h', t+h')\} \sim pMN(u)\ 4\ h\ h' \tag{22}$$

(where h and h' are non-negative and "*small*"), or, in terms of the definition of conditional probability,

$$Prob\{M \text{ point in } (t+u-h, t+u+h) \text{ with given } N \text{ point of coordinate } t\} \sim 2\ h\ p_{MN}(u)/p_N \tag{23}$$

Whenever the M and N point distributions are independent, (23) is just

$$Prob\{M \text{ point in } (t+u-h, t+u+h)\} \tag{24}$$

Therefore, in this case, it is

$$p_{MN}(u)/p_N = p_M \quad \text{or} \quad p_{MN}(u) = p_M\, p_N \tag{25}$$

Suppose that both M and N are observed in the time interval $(0, T)$ - where T is the total time span of the data, and it is not the trial period used for $\mathfrak{Arp}$ and $\mathfrak{Cetra}$.

Divide $(0, T)$ into intervals of duration h. There are T/h intervals h of this kind. Since two events, which occur within the same h interval, are treated as one and the same point, there are at most T/h points either in M or in N. Call $M(T)$ and $N(T)$ the real such a total number of given M and N points, respectively. Call $s_1 < s_2 < \ldots < s_{M(T)}$ the series of the time instants of occurrence of the $M(T)$ points of the M series, and $t_1 < t_2 < \ldots < t_{N(T)}$ the same for the N series.

This suggests estimating $p_M\ h$ by $M(T)/(T/h)$, i.e.

$$\hat{p}_M = M(T)/T \tag{26}$$

Similarly, it is $\hat{p}_N = N(T)/T$. In order to estimate $p_{MN}(u)$, let us start by defining

$$n(u,h) = \text{the number of } s_i \text{ such that } t_j + u - h < s_i < t_j + u + h \text{ for some } j \tag{27}$$

Then, (23) can be evaluated by $n(u,h)/N(T)$, which suggests the estimate

NCGT Journal
New Concepts in Global Tectonics
New Concepts in Global Tectonics Journal
Volume 14, Number 6, June 2026
ISSN number; ISSN 2202-0039

$$\hat{p}_{MN}(u) = \frac{n(u,h)\,\hat{p}_N}{N(T)\,2\,h} = \frac{n(u,h)}{2\,h\,T} \qquad (28)$$

These estimates, however, are only approximate, because - when repeating several times the experiment - one finds a different estimate per every experiment. This is called the "*sampling variation*". According to Brillinger (*ibid.*), the estimate (28) was proposed by Griffith and Horn (1963).

A fact, which is important in what follows, is proven by Brillinger (1976a), i.e.

$$n(u,h), \text{ for large } T, \qquad (29)$$
$$\text{is approximately Poisson distributed}$$
$$\text{with mean } [2\,h\,T\,p_{MN}(u)]$$

The relationship between $n(u,h)$ and the $\mathfrak{arp}$ is discussed below. A few interesting practical suggestions are given by Brillinger (1976b), which can result very useful for subsequent application.

Refer to (25) and consider the parameter $p_{MN}(u)/(p_M\,p_N)$. The supposed total reciprocal independence of M and N implies that this ratio is just 1. Evaluate it (by referring to some given real case history). In general, the ratio results other than 1. Since its distribution properties are known, it is possible to estimate, e.g., the 95% confidence interval within which it is either $= 1$ or $\neq 1$.

One can use directly the Poisson properties of $n(u,v)$. Or one can use a much simpler procedure. In fact, given a quantity P that is a Poisson variate with mean μ, it results (Kendall and Stuart, 1968) that P is approximately a normal variate with mean $\sqrt{\mu}$ and standard deviation $1/2$. Therefore $\sqrt{p_{MN}(u)/(p_M\,p_N)}$ is approximately normal with mean $\sqrt{\hat{p}_{MN}(u)/(\hat{p}_M\,\hat{p}_N)}$ and standard deviation evaluated as follows. From (28) and (29), and by calling $\sigma(A)$ the standard deviation of A, it is

$$\sigma\left[\frac{p_{MN}(u)}{p_M\,p_N}\right] \sim \sigma\left[\frac{p_{MN}(u)}{\hat{p}_M\,\hat{p}_N}\right] \sim \frac{\sigma[\,p_{MN}(u)]}{\hat{p}_M\,\hat{p}_N} \sim \qquad (30)$$
$$\sim \sigma\,[n(u,h)/(2\,h\,T)]/(\hat{p}_M\,\hat{p}_N)$$
$$\sim \sigma\,[n(u,h)]/(2\,h\,T\,\hat{p}_M\,\hat{p}_N) \sim$$
$$\sim \frac{\sqrt{2\,h\,T\,p_{MN}(u)}}{2\,h\,T\,\hat{p}_M\,\hat{p}_N} \sim$$
$$\sim \sqrt{2\,h\,T\,\hat{p}_{MN}(u)}/(2\,h\,T\,\hat{p}_M\,\hat{p}_N)$$

$$\sigma\left[\sqrt{\frac{p_{MN}(u)}{p_M\,p_N}}\right] \sim \frac{1}{2\frac{\hat{p}_{MN}(u)}{\hat{p}_M\,\hat{p}_N}}\,\sigma\left[\frac{p_{MN}(u)}{p_M\,p_N}\right] \sim \qquad (31)$$
$$\sim \text{by inserting (30)} \sim \frac{1}{(2\sqrt{2\,h\,T\hat{p}_M\,\hat{p}_N})}$$

Therefore, evaluate the 95% confidence intervals by adding $+1.96\left[1/(2\sqrt{2\,h\,T\hat{p}_M\,\hat{p}_N})\right]$ either to the 1 value, which is taken by $\sqrt{\hat{p}_{MN}(u)/(\hat{p}_M\,\hat{p}_N)}$ in the case of perfect reciprocal independence of M and N, or to the actual values of $\sqrt{\hat{p}_{MN}(u)/(\hat{p}_M\,\hat{p}_N)}$, or to some smoothed values of $\sqrt{\hat{p}_{MN}/(\hat{p}_M\,\hat{p}_N)}$ etc.

Let us consider the relation between the $\mathfrak{arp}$ and the second-order product density. The $\mathfrak{arp}$ is just $n(u,h)$ defined by (27) and evaluated over the actual available data sequence $\{e_j\}$ by choosing $h = 0.5\ years$ (when the given datum is one value per year). In this case, the M and N sequences are the same and coincide with $\{e_j\}$. That is, the cross-product density $p_{MN}(u)$ thus becomes the second order product density $p_{NN}(u)$. The parameter u is the trial period of the operators $\mathfrak{Arp}$ and $\mathfrak{Cetra}$. Instead, T is here the total time interval covered by the given data series. The trend to decrease of $\hat{p}_{NN}(u)$ vs. u means that the second-order product density of $\{e_j\}$ decreases as u increases.

Some doubt, however, can be raised about the correctness of this interpretation of $\mathfrak{arp}$, because $\{e_j\}$ is not complete and uniform like $\{a_j\}$. Rather, $\{e_j\}$ is only a subset of $\{a_j\}$, and it can be expected that the information was lost concerning a large fraction of $\{a_j\}$ events. Whenever some hunches are eventually available - which are suited to estimate in some way the amount of information missing in the data series - one should introduce some function that expresses a time-varying probability for the present availability of really occurred ancient events. This was made by Lee and Brillinger (1979), concerning a time sequence of earthquakes recorded in China during $1177\ BC - AD\ 1976$. They evaluated the data availability by considering several factors (population density, its "saturation" value, topography, extension of the Chinese empire along the centuries, probability of having the information recorded, probability of having kept until nowadays the relative records). All these estimates, however, necessarily rely on a large amount of subjectivity.

In any case, let us accept as a working hypothesis all these estimates of the probability of the present-day availability of a historical information. This treatment of historical data series permits us to conclude whether there appears to exist some *periodicity* within some given confidence limits (e.g. 95%) (Lee and Brillinger, *ibid.*). They propose an estimate of a *periodicity* of $300\ years$. Their data appear reasonably complete (they state that they are reliable only from the *16th century AD* onward), etc. This approach should be recommended whenever one wants to give reliable statements, within some well-defined confidence interval. This is the approach that every conscience-driven scientist should apply. Brillinger (1979) gives the formal rigorous support for this approach.

In addition, this is certainly the best viewpoint whenever one deals with a time sequence of observations that refer to an experiment that can be repeated as many times as needed. For instance, the heartbeats or some neurophysiological experiments can be repeated several times: consequently, the database is uniform, with no relevant gaps, and one therefore wants to infer definite statistical assessments from it.

In contrast, a historical data series (either climatological, or seismological, or volcanic, etc.) refers to an experiment that cannot be repeated. Consequently, in order to treat it, one must introduce some estimates of a probability of availability of the information.

On the other hand, one can look at the problem from a different viewpoint. Let us look at the data just as they are, and let us just search for some evidence for possible *periodicities*.

NCGT Journal
New Concepts in Global Tectonics

New Concepts in Global Tectonics Journal
Volume 14, Number 6, June 2026

ISSN number; ISSN 2202-0039

In this way, in principle there is no way to state whether an eventual *periodicity* has a physical origin, or it is just a casual result of the human historical vicissitudes that led to present-day availability of records. Even in this case, however, the information about *periodicity* is *per se* relevant. In fact, whenever, e.g., one finds the same *periodicity* for some affluent of the Po and for the Tiber, one must conclude that either the historical vicissitudes were similar in the Po valley and in Rome, or that there is some physics in that *periodicity*.

Therefore, if a given data series cannot be re-measured by an improved experiment, one must honestly attempt to extract every kind of possible information contained in the available data series. At the same time, according to this approach, every conscience-driven researcher must limit as much as possible every role of arbitrariness, such as while guessing probabilities of missing data, etc. That is, the concern is about extracting from the available historical information "all" the inferences that it can prove, but "no more than that", i.e. by avoiding every eventually false evidence deriving from any arbitrary decision. For instance, this is the same warning that applies to Fourier's algorithms, which are perfect and rigorous; but, when one adds arbitrary zeros or others to fill data gaps, etc., the inferred evidence can be eventually false and misleading (see section 1).

One example of an anthropic - and non-climatic - *periodicity* is given by the historical series of the Tiber floods in Rome (Fig. 5). Its information is detailed and reliable during two historical periods, i.e. *(i)* during the classical period of the Roman Republic and Imperial times, and *(ii)* since Renaissance time, with an almost total gap in between. Hence, the formal application of $\mathfrak{arp}$ leads to apparent evidence for a corresponding *periodicity*, which is in reality inside the data series, although the cause is clearly associated to the historical vicissitudes of the fall of the Roman Empire etc.

The $\mathfrak{arp}$ should be considered from a correct viewpoint, as it is a simple and intuitive way for seeking possible *periodicities* that are intrinsic inside the data sequence, independent of their origin.

An important warning deals with a bias that affects either $\mathfrak{arp}$ or $\mathfrak{Cetra}$. While constructing this histogram ($\mathfrak{arp}$ or $\mathfrak{Cetra}$), we must arbitrarily choose the time lag of a unit elementary interval. For instance, when dealing with a series of natural catastrophes, a frequent choice is to consider only the year of occurrence, as several ancient historical data often lack any additional information about the exact date of concurrence of phenomena. That is, the data handling proceeds just like in the case that every event paradoxically occurred on the same date of every given respective year, say, e.g. on January 1[st].

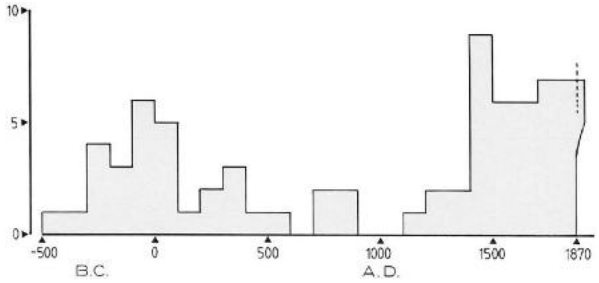

Fig. 5. Number of historical Tiber floods in Rome reported per century. The apparent *periodicity* of $\sim 16\ centuries$ depends on the historical anthropic events, not on natural phenomena. After Gregori et al. (1988). With kind permission of the late Wilfried Schrˆder.

Upon a detailed analysis[18] of the implications on the construction of the $\mathfrak{arp}$ or $\mathfrak{Cetra}$, it can be easily shown that this bias introduces some unwanted jumps in output that can eventually result perplexing or even misleading. This drawback can be easily - and rigourously - avoided by assigning an arbitrary and random date for every event of the observational data series. In fact, the physics of the result is independent of this arbitrariness, while the random variation of the arbitrarily given date permits to avoid the consequence of a purely mathematical and non-physical bias.[19]

Another concern deals with events for which even the year is uncertain. Suppose, e.g., that the datum of an ancient event has an error of say $\pm k\ years$. Hence, represent such a point-like event - instead of a unit square centered on its more probable year - by a rectangle of unit surface, having base equal to $2k + 1$.

This procedure can be eventually applied even to a data sequence where every point-like event is represented by a figure having any arbitrary shape. In any case, every figure must be supposed of equal area, if one wants to give equal weight to every point-event. The shape can be either a square, or a rectangle, or a triangle, or a quasi-Gaussian shape, etc.

Summarizing, the $\mathfrak{arp}$ coincides with $n(u,h)$, computed for $\{e_j\}$, but this does not mean that it can be used for estimating $p_{NN}(u)$. In fact, this computation should be needed for the $\mathfrak{arp}$ computed for $\{a_j\}$. Therefore, from this more limited viewpoint, one must deal with the $\mathfrak{arp}$ of $\{e_j\}$ *per se*, independent of the fact that the $\mathfrak{arp}$ of $\{a_j\}$ is related to $p_{NN}(u)$. Hence, since $n(u,h)$ is Poisson, the error of the $\mathfrak{arp}$ can be estimated by $\pm\sqrt{n(u,h)}$. Equivalently, one can rather plot directly $\sqrt{n(u,h)}$, instead than $n(u,h)$, and the error bar would be just $\pm 1/2$ (or, equivalently, one can plot $[2\sqrt{n(u,h)}]$ with error bar ± 1).

Several unanswered questions remain:

a) how "close" to each other any two *periodicities* can result, while they can be significantly distinguished;
b) how can one distinguish the multiplicity of every peak of *periodicity* in an $\mathfrak{arp}$ or $\mathfrak{Cetra}$;
c) how can one give a different weight to estimates of the same *periodicity* given by different multiplicities;

[18] This assessment was not immediate and required some thinking.

[19] Refer to Banzon et al. (1992) for details.

NCGT Journal
New Concepts in Global Tectonics
New Concepts in Global Tectonics Journal
Volume 14, Number 6, June 2026
ISSN number; ISSN 2202-0039

d) how can one deal with different, but close, *periodicities*;
e) how can one subtract a background from the $\mathfrak{arp}$ or $\mathfrak{Cetra}$ in order to get better evidence for the pattern of the peaks.

The first two questions *(a)* and *(b)* appear difficult. Indeed, owing to the mechanism whereby the $\mathfrak{arp}$ or $\mathfrak{Cetra}$ was constructed, it is very likely that all minor structures, all peaks, and all fluctuations, are related to one another. Therefore, concerning the low-value trial periods, the minor structures are not significant *per se*, unless they have some corresponding peaks at their respective higher multiples. No reply can be basically given to questions *(a)* and *(b)* above. See also the reply to the 5th question *(e)*.

Concerning the 3rd question *(c)*, one can use two simple arguments as follows. A peak of multiplicity 1 has an error $\sigma = \pm 0.5\ years$; a peak of multiplicity m has an error $\sigma = \pm 0.5/m\ years$. This suggests that we have to evaluate a weighted average (proportional to $1/\sigma^2$) with weights m^2. A different argument is by stating that whenever a measure is repeated m times, the error of the mean of the measure is decreased by a factor $1/\sqrt{m}$. This suggests using a weighted average with weighs m. The weight m (instead of m^2) is perhaps better, as m^2 overweighs the higher multiplicities.

The reply to the 4th question *(d)* derives from consideration of some examples. Suppose to have a *point-like process* [i.e., a (0,1)-series], which is composed by 12 elements in this way (101000100000), identically repeated several times, and let us construct its $\mathfrak{arp}$. One obviously finds the *periodicity* 12, and all of its multiples as well. However, one also finds a minor, although well defined, series of peaks at $6, 18, 30, 42, \ldots, (2k+1)6, \ldots$ $(k = l, 2, \ldots)$. In fact, consider the given $(0,1)$-series, and notice that - by just changing one element 1 in it into a 0 - it becomes (100000100000), which has *periodicity* 6. Hence, this example can be reconsidered in terms of a superposition of two different point-like processes, i.e., (100000100000) plus (001000000000). The first point-like process has *periodicity* 6, and the second has *periodicity* 12. The first one has weight 2 with respect to the second one that has weight 1.

Concerning the 5th aforementioned question *(e)*, a subtraction of the background can be achieved by some moving average. For instance, one can plot, instead of $n(u,h)$

$$2\sqrt{n(u,h)} - 2\sqrt{\frac{1}{40}\sum_{k=1}^{20} n(u \pm k, h)} \tag{32}$$

where the sum is extended over both values of $n(u+k,1)$ and $n(u-k,h)$, and the choice of 20 elements is just indicative and arbitrary. This has[20] an error bar ± 1, and the 95% confidence interval is ± 1.96. This simple example applies a filter of the kind $\Pi(\pm 20)$, although the identical argument can be applied by means of every other filter, e.g. of the kind $\Lambda(\pm 20)$ (see Fig. 2).

The background trend of $\mathfrak{arp}$, however, can be simply inferred by a little algebra and a few trials. Let us call $f(t)$ the *point-like function* to be analyzed, $\mathfrak{Arp}(\mathrm{u}) = \mathrm{n}(\mathrm{u}, 1)$ its $\mathfrak{arp}$, and δ the Kronecker δ-symbol. Consider the following case histories.

I) One period p

$$f(t) = \sum_{m=0}^{M}\sum_{i=1}^{\infty} \delta_{i,r+mp} \tag{33}$$

$$\mathfrak{Arp}(\mathrm{u}) = \left[\sum_{\mathrm{i}=1}^{\infty}\sum_{\mathrm{m}=0}^{\mathrm{M}}\sum_{a=0}^{\mathrm{m}-1} \delta_{\mathrm{i},(\mathrm{m}-\mathrm{a})\mathrm{p}}\right] \delta_{pu} \tag{34}$$

In reality, the sum is never extended to infinity, being rather limited by the total time span of the time series. Graphically, the $\mathfrak{arp}$ displays peaks of decreasing intensity only at $u = kp$ $(k = 1, 2, \ldots)$. The general shape looks like a *triangular comb*, where every tooth of the comb is a peak.

II) Random $f(t)$

$$f(t) = const\ \mathfrak{E}(0, E) \tag{35}$$

where $\mathfrak{E}(a,b) \equiv 1$ for $a < t < b$, and $\mathfrak{E}(a,b) \equiv 0$ elsewhere, and E is the total time domain of definition of $f(t)$;

$$\mathfrak{Arp}(\mathrm{u}) = const \sum_{\mathrm{j}=1}^{\mathrm{M}} \mathfrak{E}(0, \mathrm{E} - \mathrm{j}) \tag{36}$$

Graphically, the $\mathfrak{arp}$ is a histogram that closely approximates a triangle, constructed by means of horizontal strips of linearly decreasing length. Call "*quasi-triangle*" this geometrical figure.

III) Two periods p_1 and p_2

$$f(t) = f_1(t) + f_2(t) = \tag{37}$$
$$= = \left\{\sum_{i=1}^{\infty}\left[\sum_{m_1=0}^{M_1} \delta_{i,r_1+m_1p_1}\right] + \left[\sum_{m_2=0}^{M_2} \delta_{i,r_2+m_2p_2}\right]\right\}$$

$$\mathfrak{Arp}(u) = A_1 + A_2 + A_{21} + A_{12} \tag{38}$$

where A_1 and A_2 are the $\mathfrak{arp}$s of f_1 and f_2 respectively, while

$$A_{12} = \sum_{i=1}^{\infty}\sum_{m_1=0}^{M_1}\sum_{n=0}^{m_1-1}\sum_{m_2=0}^{M_2} \delta_i, r_2 - r_1 + m_2p_2 - ap_1 \tag{39}$$

$$A_{21} = \sum_{i=1}^{\infty}\sum_{m_2=0}^{M_2}\sum_{n=0}^{m_2-1}\sum_{m_1=0}^{M_1} \delta_i, r_1 - r_2 + m_1p_1 - ap_2 \tag{40}$$

that are cumbersome expressions, the shape of which should be investigated, e.g., by computer. The aforementioned case history of the $(0,1)$ -series (101000100000) is one example of a superposition of two exact *periodicities*.

[20] This is derived from the same aforementioned argument before (30) and quoting Kendall and Stuart (1968), or by the argument leading to (2). As already mentioned, G. P. Gregori feels deeply indebted to the late Professor John Wilder Tukey (1915-2000) for this suggestion.

NCGT Journal
New Concepts in Global Tectonics
New Concepts in Global Tectonics Journal
Volume 14, Number 6, June 2026
ISSN number; ISSN 2202-0039

IV) Two random $f(t)$s

$$f(t) = const_1\ \mathfrak{E}(0,E) + const_2\ \mathfrak{E}(0,E) \equiv const\ \mathfrak{E}(0,E) \quad (41)$$

being

$$const \equiv const_1 + const_2 \quad (42)$$

Hence, the case IV coincides with the case II.

V) One period p plus a random $f(t)$

$$f(t) = f_1(t) + f_3(t) = \quad (43)$$

$$= \sum_{i=1}^{\infty}\sum_{m=0}^{M} \delta_{i,r+mp} + const\ \mathfrak{E}(0,E)$$

$$\mathfrak{Arp} = A_1 + A_3 + A_{13} + A_{31} \quad (44)$$

$$A_1 = \mathfrak{arp} \text{ of } f_1 \quad (45)$$

$$A_3 = \mathfrak{arp} \text{ of } f_3 \quad (46)$$

$$A_{13} = \sum_{i=1}^{\infty}\sum_{j=0}^{J}\sum_{m=0}^{M} \frac{1}{J}\delta_{i,r+mp-j} \quad (47)$$

$$A_{31} = \sum_{i=1}^{\infty}\sum_{m=0}^{M}\sum_{n=0}^{m-1} \frac{const}{M+1}\mathfrak{E}(0, M-r-a_p) \quad (48)$$

Graphically, A_1 is a *triangular comb*, and A_3 is a "*quasi-triangle*".

The shape of A_{13} is as follows: add together horizontal strips of increasing lengths, $r, r+p, r+2p, \ldots$. The result is again a "*quasi-triangle*", approximated by the line

$$A_{13} \sim -\frac{x}{p^J} + \left(\frac{M+1.5}{J}\right) - (p-r) \quad (49)$$

where x is the abscissa of the $\mathfrak{arp}$.

The shape of A_{31} is as follows. Add a rectangular *strip* (with left side at the origin) of horizontal length p and vertical width 1, say briefly a *strip* $(p \times 1)$, then a *strip* $(2p \times 2)$, then a *strip* $(3p \times 3)$, ... , then a *strip* $(kp \times k)$, $(k = 1, 2, \ldots)$. The resulting histogram looks like a parabola with negative curvature (apart the discontinuities in between integer values of the abscissa). Call it a "*quasi-parabola*", which (after some algebra) results

$$A_{31} = -\frac{(x-v)^2}{2\,p^2} + \quad (50)$$

$$+\frac{1}{2}\left[\frac{2M^3+3M^2+M}{2}\right]^{2/3}$$

$$v = E - r\ - M\,p \quad (51)$$

Summarizing, A_1 is a *comb*, A_3 and A_{13} are two *quasi-triangles*, and A_{31} is a *quasi-parabola*.

VI) When the system keeps memory of its past

Mere randomness requires that every datum, or every event, of the observational data series must keep no memory of any past occurrence. In the opposite extreme, whenever every occurrence keeps full memory of previous data, we must observe all events occurring simultaneously, and this is an ideal case history of perfect Lagrangian determinism.

Every physical intermediate condition - which is the normal occurrence in natural reality - has to be managed by means of the rationale of fractality, lognormality, and the Kapteyn class distributions (see Arley and Buch, 1950, or Paparo and Gregori, 2003, or Gregori et al., 2025w, or Gregori and Gregori, 2025).

For instance, let us refer to a data series of some given kind of events, such as, e.g., earthquakes of magnitude larger than some threshold etc. Mere randomness should require some kind of statistically constant time-lag in between any two subsequent events. That is, the distribution of these time lags must be normal with some given mean value and rms deviation.

Conversely, the deviation from ideal randomness is measured by considering that this distribution is lognormal, being more or less peaked towards small time lags. This physical circumstance can therefore be expressively checked by inspecting, by means of the *probit diagram*, whether this distribution is some more or less well defined lognormal distribution (see Arley and Buch, 1950, or also Paparo and Gregori, 2003).

As far as its corresponding $\mathfrak{arp}$ is concerned, the deviation from mere randomness implies a relative overcrowding of short - compared to longer duration - lags. That is, the *quasi triangle* of the random $\mathfrak{arp}$ will appear "inflated" at comparatively lower values. This inflation is the more pronounced the shorter is the time-lag that is comparatively more frequent in between any two subsequent events. However, the mathematical formal expression of every case history of this kind is cumbersome, and it results of no practical help.

In summary, in the case of an "inflated" *quasi triangle*, one gets the relevant physical information that events do occur clustered in time - more or less time-delayed compared with each other. For instance, earthquakes, or floods, or volcanic eruptions, or stress solitons, etc., owing to some physical reason occur while the system is experiencing an evolution of its internal structure and processes.[21] Therefore, some model must be investigated that should give a tentative physical explanation for this behavior.

VII) More intricate examples

It appears therefore formally cumbersome to treat more complicated case histories. Perhaps, a simple-minded approach is to guess in some way some tentative *periodicities*, or some physical model for the system, etc. Then, one can guess some tentative $f(t)$ over which the $\mathfrak{arp}$ is evaluated. Finally, $f(t)$ ought to be optimized by an iterative try-and-check procedure by least square fitting etc.

While guessing some tentative $f(t)$ one can include a few different random addenda, e.g. when referring to different epochs. For instance, random addenda could be introduced only for the epochs outside the lifespan of the chroniclers, etc. This is somewhat equivalent to estimating some function of probability of the datum availability. In any case, all this somewhat involved procedure can be interpreted as a reply to the aforementioned questions *(a)* through *(e)*. In addition, the use of (32) is comparably much

[21] For instance, in the case of earthquakes, the aftershock sequence (*Omori-Utsu law*) is the tail of a lognormal distribution (see Arley and Buch, 1950, or also Paparo and Gregori, 2003).

NCGT Journal
New Concepts in Global Tectonics
New Concepts in Global Tectonics Journal
Volume 14, Number 6, June 2026
ISSN number; ISSN 2202-0039

more direct, although, perhaps, in that way the trend of the background is not explained, rather it is just subtracted.

This entire discussion looks qualitative. This fact results, however, into a real advantage - while exploiting the *exploratory* analysis of a database, and while seeking hunches for a physical model for the interpretation of observations. The advantage of a mathematical tool is its logical flexibility and robustness. Every possibility can thus result important, which derives from this flexibility, as it eventually leads to the inference of some intuitive interpretation of the final evidence. On the other hand, no "thumb rule" can be given, as every physical case history has its specific requirements, which derive from physics, and from "intuition", not simply from mathematics and statistics.

6. Some case histories - The need for an intuitive approach to the *exploratory* analysis

Chinese climatological investigations

Wang Shao-Wu, and Zhao Zong-Ci (1981) report on an analysis on floods, droughts, etc. from China covering the time span $1470\ AD - 1979\ AD$ based on a remarkable collection provided by the *Central Meteorological Institute* et al. (1981). They search for space correlation among events in a systematic way - such as, e.g., the simultaneous occurrence of floods and droughts in different regions of China. They use the technique of *orthogonal empirical polynomials* (*EOF*), i.e., the methods related also to *principal component analysis* (*PCA*). As far as the temporal dependence is concerned, they evaluate power spectra of single station data series. They quantify the information into a five-grade scale, *1* through *5*, which denote, respectively, a climate either very wet, or wet, or normal, or dry, or very dry.

Banzon et al. (1992a) applied a different approach to the same database, in terms of a simple graphical representation (see Fig. 6 of Gregori et al., 2025f). A five-color code was chosen, and associated with the aforementioned *5*-grade climatic scale. The entire set of all data series was represented by the ensemble of *120* thin colored lines. One line refers to one of the 120 different regions of China (see Figs 7 and 8 of Gregori et al., 2025f). The number line corresponds to a site indicated in Fig. 6 of Gregori et al. (2025f) and listed in Tables 10 and 11 of Gregori et al. (2025f). Every point along a thin line corresponds to one year, and its color corresponds to the color code of that year in that region of China.

Upon simple visual inspection, it was clearly inferred that no real *periodicity* is evident into this multivalued time series of data. However, the most striking conclusion was that, in recent decades, the climate data appear abruptly much more variable, clearly envisaging a psychological effect. In fact - maybe owing to some comparatively smaller occupation of territory - during past years people were less sensible to climatic changes, i.e. they considered "normal" some events. Conversely, during some comparatively much more recent times, some events were considered "anomalous" and worthy of being recorded. The advent of a widespread meteorological network certainly resulted into a much more detailed and accurate recording of climatic data.

The historical documentation about climate variations in China has been the object of a careful analysis, including some controversies. See e.g. Zhang (1993), Lin et al. (1995), and Man (1998), and Gregori et al. (2025f, 2025g, 2025h, 2025i, 2025j). See also, however, Figs 46 and 47 of Gregori et al. (2025i), plus Figs 6, 7 and 8.[22]

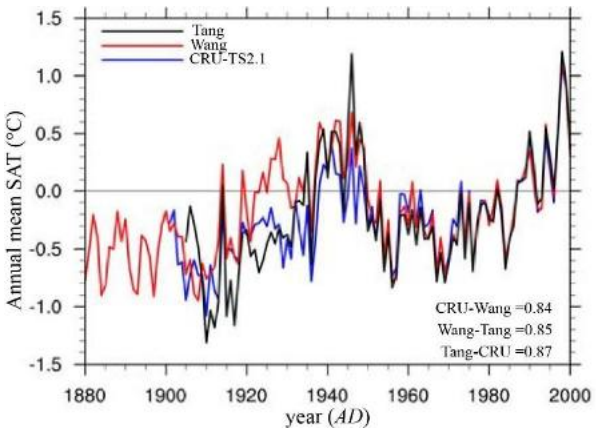

Fig. 6. "*Temperature series of China. Red: Wang et al. (1998, 1998a), blue: Tang and Ren (2005), black:* CRU, *average of 1971-2000 as referenced value*." Figure and captions after Ge et al. (2007). Reproduced with kind permission.

Piao et al. (2010) is a careful study on the recent climatic trend in China, and shows figures dealing with the interannual variation in the Yangtze River and Yellow River annual runoff, and with the change in glacier area at *22* monitoring stations in western China during the past $30 - 40\ years$.

However, the variability of climate in China depends on several drivers, and substantial changes occur during the years. For instance, a careful investigation was carried out by Ying et al. (2014). They summarize as follows their inference.

"*The interannual variability of seasonal precipitation in eastern China from fall to following spring is examined for the period of 1951-2004 based on observations at* 106 *stations.*

[22] For the *CRU* series see http://www.cru.uea.ac.uk/timm/grid.CRU-TS-2-1.html.

NCGT Journal
New Concepts in Global Tectonics
New Concepts in Global Tectonics Journal
Volume 14, Number 6, June 2026
ISSN number; ISSN 2202-0039

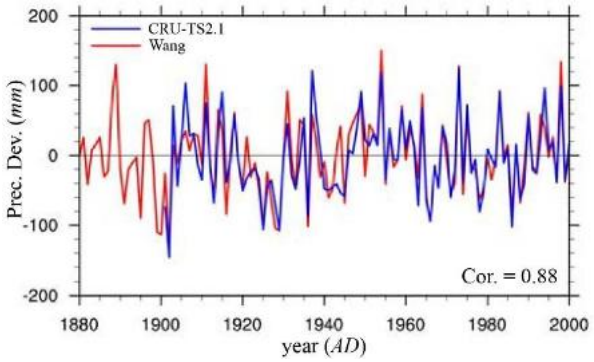

Fig. 7. "*Mean annual precipitation of China in the east of* $105°E$. *Red line: December-November of next year from Wang, blue line: January-December from* CRU *(Wen et al., 2006).*" Figure and captions after Ge et al. (2007). Reproduced with kind permission.

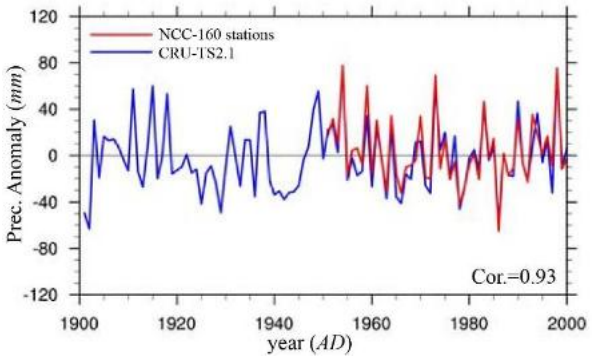

Fig. 8. "*Mean annual precipitation of China. Red line:* NCC *(*National Climate Center*)* 160 *stations, blue line:* CRU." Figure and captions after Ge et al. (2007). Reproduced with kind permission.

The temporal variability of seasonal mean values is decomposed into intraseasonal (fast) and slow (potentially predictable) components. EOF *analysis is then applied to both the fast and predictable components.*

We find that

(1) *the most predictable signal migrates in a north-south direction along with the annual cycle of the monsoon in east China, while spatial patterns of the leading fast modes does not change much;*

(2) *the predictable signal of precipitation in eastern China is associated with anomalous atmospheric circulation patterns having more zonally symmetric structures while the fast time-varying precipitation components are accompanied by wavy anomalous atmospheric circulation patterns;*

(3) *the most predictable signal has an apparent* 1*-season lagged correlation with the interannual variation of* SST *associated with* ENSO (El Niño Southern Oscillation)*;*

(4) *The fast rainfall component is largely attributed to the intraseasonal variabilities of the Siberian High over the Eurasian continent and the subtropical high associated with the Western-Pacific-Oscillation-like variabilities over the North Pacific; and*

(5) *The* ENSO *signal in the fall seasonal precipitation persisted throughout the entire* $54\ year$ *period while the signal in winter intensified significantly after the mid-1970s. This is attributed to the weaker/stronger intensification of* ENSO *anomalies in the tropical Pacific during the fall/winter."*

Volcanic series

A similar warning about the non-uniformity of the historical information applies, e.g., to every data series of the historical eruptions of a volcano, which unavoidably results into a relevant bias for every volcanic catalogue.

In the past, a volcano was considered just as a mountain that occasionally releases something looking much like fire. Whenever some volcanic activity was in progress, they considered it the "normal" state of the mountain, and they did not mind about recording this "normal" event.[23] Only after the Enlightenment – and mainly after Romanticism with the birth of the international network of environmental observatories - every observer became conscious of the need to provide some better record of natural phenomena. This change of feeling resulted into a cultural factor that affects, at present, the completeness and detail of every historical environmental information.

Since several years it has become customary to identify "anthropology" with the "history of culture". Hence, these cultural factors can be briefly called a consequence of "environmental anthropology". The impact of humankind on the environment - since the very early appearance of man on the Earth, including its effectiveness like a recorder of environmental proxy data - are just matters for "environmental anthropology". This fascinating item requires, however, a long study, independent of the concern of the present topical discussion.[24]

On other circumstances, the incompleteness of a data series can derive from non-anthropic factors. For instance, the magma emplacement rate from the Hawai'i hotspot during the last $\sim 40.000\ years$ was estimated upon considering the measured volumes of outpoured material within the Mauna Loa volcanic edifice (Lockwood, 1995).

[23] The ancient Greek mythology claimed that the God of Fire, *Hephæstus*, had his workshop inside a volcano, although they did not envisage one specific volcano. The Cnidian colony in the Lipari Island (in the Δ olian Islands) diligently reported to their mother land, i.e. to Greece, about an exceptionally violent eruption that involved the island of Vulcano. Hence, they began to believe that the workshop of *Hephaestus* was located inside the island of Vulcano. Since that time the name "*volcano*" was associated with every mountain that occasionally erupts either lava or other gases and/or materials. The ancient Romans changed the name of the God *Hephæstus* and called him "*Vulcanus*". The current name "volcano" derives therefore from the name of the island Vulcano. See Gregori (1997a).

[24] Some very preliminary studies are reported in Gregori (1997, 2001, 2002), Gregori and Gregori (1996, 1997, 1998, 1999, 2000, 2003, 1996a, 1999a), Gregori et al. (2000, 2000a), Colacino et al. (1988), and references therein. However, an almost endless number of other references ought to be quoted. For instance see Giosan et al. (2012) and references therein.

New Concepts in Global Tectonics Journal
Volume 14, Number 6, June 2026
ISSN number; ISSN 2202-0039

However, since older material is buried by more recent eruptions, some correction factor *vs.* time had to be guessed in order to get rid of this relevant bias.

Instead, no equivalent correction could be seemingly applied for guessing some Plinian eruption series of Vesuvius. Hence, no reliable - even only indicative - forecast can be made for any possible new Pompei eruption.[25]

In summary, whenever dealing with a historical data series, it is always worthwhile to take into account that the quality of the records systematically changed during time. Hence, a simple formal application of some algorithm may sometimes be inappropriate. This drawback can eventually result into devastating consequences, mainly when non-robust operators are applied, such as, e.g., when dealing with Fourier's algorithms, or power spectra, etc.

Differently stated, it is embarrassing - and eventually impolite with respect to some skillful applied mathematician, who in any case deserve great consideration - to stress that mathematics often approaches environmental data-sets by relying on "simplifying" assumptions. These assumptions are excellent according to the viewpoint of the mathematician, but are completely unrealistic when applied to natural data. This is quite a serious and frequent bias that is often encountered in several branches of Earth's and environmental sciences.[26]

Indeed, one can get rid of some "obvious" bias of the data series - mostly whenever this bias can be assessed in no other mathematically more involved formal way - by means of the apparently simple-minded *superposed epoch criterion*, including $\mathfrak{arp}$ or $\mathfrak{Cetra}$ etc., or even, whenever applicable, a simple graphical representation by some color code.

That is, physical "*intuition*" of phenomena - or *c.i.f.* as Enrico Fermi was joking - can find a great advantage from some simple graphical algorithm, because eye is the most powerful available analogue computer.

In addition, when dealing with climatology, it is worthwhile to emphasize the feasibility of investigation of space correlation by means of the standard approach in meteorology in terms of synoptic maps and processes etc.

*Earthquake series - "*Pole position*" analysis*

In disagreement with the entire aforementioned warning, earthquake series were generally always investigated in terms of temporal data series referred to *limited* space areas. Conversely, their spatial correlation was generally discussed only with reference to regional tectonics and some comparatively small areas. In contrast, every rationale of geodynamic phenomena - such as e.g. plate tectonics or other - was never tackled in terms of eventual statistical spatial and temporal correlations of earthquakes that occur in different parts of the world.

In fact, this possibility was always neglected (except, at most, in very few partial exceptions), because - according to the paradigm of plate tectonics - every seismic teleconnection was always considered *a priori* unlikely. This has always been almost a paradigm. However, no real logical reason can support this *a priori* assumption that, in every case, must be tested. In contrast, the serpentinization process (see Gregori and Hovland, 2025 and Hovland, 2026) clearly envisages the realistic occurrence of a teleconnection of seismicity even on the planetary scale.

An analysis of this kind can be easily carried out upon referring, e.g., to the set of earthquakes having magnitude above a given magnitude, and referring to a given total time span covered, e.g., by a given seismic catalogue of the world. Note that every catalogue has some unavoidable bias. On the other hand, a catalogue is the unique available observational database for an analysis that, on a simple intuitive ground, can be envisaged as follows.

We must take into account a key point. Every procedure should provide with evidence of features that are objectively intrinsic in natural reality, while every result ought to be avoided that derives from the simplifying assumptions that are implied by the algorithm. Taken for granted this warning, consider a conventional, more or less restricted, area of the globe. Call it "*pole position area*" (*ppa*). Re-define the origin of time at the time-instant of a seismic event that occurs inside the "*pole position area*": call it "*pole position event*" (*ppe*). Plot, on a world map, all seismic events of the seismic database, and represent every event with a symbol, drawn at the site of its epicenter, of size proportional to the time elapsed after the $t = 0$ *ppe*. For instance, draw a circle with radius proportional to such a time lag.

If, in some way, seismic activity propagates over the globe, it is thus possible to track its trajectory, and also to envisage its average speed of propagation. The physical model that envisages this possibility is the existence of the serpentosphere (see Gregori and Hovland, 2025; Hovland, 2026).

This analysis holds for every seismic event that occurs after the occurrence of every *ppe* event inside the *ppa*. However, a similar plot can also be drawn by referring to the seismic events that occurred before the $t = 0$ *ppe* of the pre-chosen *ppa*. In this case, the symbol, or circle, on the map has a size proportional to the advance time of an event of the catalogue before the $t = 0$ *ppe*. This second map shows the track, and to estimate the propagation speed, of the signal that finally leads to the occurrence of a seismic event inside the *ppa*.

[25] See, e.g., Santacroce (1987), Gregori (1993, 1996, 1996a), Santacroce et al. (1996). G. P. Gregori is indebted to Roberto Santacroce for this comment. The available historical information, dating back to the *3rd century BC*, permits to envisage some disquieting regularity, but only on much shorter time lags (see Gregori et al, 1992, 1994, and Gregori, 2002).

[26] For instance, it is a true sorrow to us to emphasize that this has been the case of the Elsasser-Bullard *MHD* geodynamo, which looked quite reasonable when it was formerly proposed, and required a very remarkable skill of professional mathematicians. In contrast, it later resulted incompatible with observational evidence, as Gregori (2002) extensively discussed.

ISSN number; ISSN 2202-0039

This *ppa* algorithm is simple and intuitive, and no false apparent evidence can derive from any kind of mathematical assumption. The unique bias can derive from the incompleteness of the seismic catalogue. This is a well-known concern for every seismologist. Hence, this warning deserves some additional comment.

One can apply the *ppa* algorithm to every different seismic catalogue, or to a catalogue that combines altogether all available catalogues - however, upon rejecting every repetition of the identical event. Every analysis is correct only when no false earthquake is included. On the other hand, the algorithm is robust, because even by including a small percent of false events no relevant implication affects the result.

As far as the threshold is concerned of the minimum earthquake magnitude, we must take into account a basic physical consideration (see Gregori et al., 2018). In fact, an earthquake is a planetary pathology that is eventually manifested at some given site whenever this site has the unlucky chance to be properly located in order to be an excellent monitoring device for the ongoing planetary sufferance.

The magnitude of the event depends on the local tectonic features, which are more or less suited to accumulate some more or less large amount of elastic energy. Hence, the magnitude of the event depends on occasional factors related to the *local* tectonic setting. That is, the magnitude is not a significant parameter aimed to characterize the "planetary pathology". Hence, the magnitude of an earthquake is not relevant for a geophysical analysis, rather the location of the epicenter is significant, and the occurrence time – while, obviously, the impact on humankind depends on the number of local inhabitants, on the construction technology of their houses and buildings, etc. However, this is not a geophysical concern.

Hence, the physical "completeness" can be hardly estimated of every given seismic catalogue. Thus, the robustness of the algorithm is crucial, because no really complete catalogue is available in a strict sense.

It is therefore concluded that the *ppa* algorithm gives evidence of some eventual features that are intrinsic in the observational database, with no additional bias of any kind, other than the intrinsic limitation derived from the way a catalogue was constructed.

The result of the *ppa* analysis can appear more or less credible. Therefore, the significance of every result must be evaluated, according to some general geophysical and geodynamic principles etc., according to "*intuition*", inside the framework of the global understanding of phenomena. However, in any case, no false evidence can result from the *ppa* algorithm *per se*.

Maybe, a previous study, which in some way resembles the approach by means of the *ppa* algorithm, is reported by O'Malley et al. (2018). In any case, the approach by these authors is consistent with the aforementioned "planetary pathology" concept that we must consider for explaining the local seismic events.

They state that one must consider a local cycle of tectonic stress buildup and release inside a fault zones. When a fault zone is near the end of its seismic cycle, a trigger is such that small forces enter into play in cascading failures, although – they stress – *"the extent of this effect on global seismicity is currently unknown."*

They investigate some available evidence about the ongoing triggering of earthquakes at a remote distance after large source events. They consider earthquakes with magnitudes M≥5.0. They analyze large events that occur during a time period of 3 $days$ after some large source event. Note that, compared to the *ppa* approach, this is a relevant limitation.

"*Earthquake occurrences display increases over baseline rates as a function of arc distance away from the epicenters. … The highest magnitude source events trigger more events, and the average global response indicates initial increased earthquake counts followed by quiescence and recovery. Higher magnitude earthquakes also appear to be triggered more often than lower magnitude events.*

The region with the greatest chance of induced earthquakes following all source events is on the opposite side of the Earth, within 30° *of the antipode.*"

O'Malley et al. (2018) stress that some speculations are often found in the literature concerning large-distance trigger of earthquakes. However, they are concerned with small magnitude (M≤4) events, and with a delay time > 8 hours. However, "t*he assumption remains that there is effectively no temporal and spatial dependence beyond the aftershock region…. The current understanding on the mechanics of how one earthquake could initiate another while being widely separated in distance and time has largely been conjectural and speculative …."*

Then, O'Malley et al. (2018) briefly summarize the case histories that, according to some authors, envisage a possible tele seismic connection. They claim that "*in any case, … the responding locations were likely close to the end of their seismic cycles... "* In fact, an earthquake occurs when a threshold is reached, being a sum of different concurrent drivers. They conclude that "*... regardless of mechanism, the results … represent the first discernible evidence that large earthquakes are associated with an increase in significant events around the globe and up to* 3 $days$ *later in time …"*

In this same respect, for the sake of completeness we must mention some additional previous analyses that in some way can be considered to be akin to the perspective of a global spacetime correlation of seismic activity. However, before evaluating their significance one must take into account the difference between an investigation in *mathematics* and an investigation in *geophysics*.

For instance, a conspicuous amount of literature deals with investigations on earthquakes, where every event is supposed to be the result of a coupling, both in space and time, of several oscillators. Some eventual time-phase shift is also introduced, or a dependence on spatial distance etc.

These astute investigations are carried out by skillful applied mathematicians, although they have to rely on a suitable set of assumptions etc. The first implicit assumption is that a seismic phenomenon can be considered like a process that can be likened to a sinusoidal oscillator. In contrast, an earthquake is a "*calorimetric*" phenomenon, i.e., a reservoir is progressively replenished, much like a

NCGT Journal
New Concepts in Global Tectonics
New Concepts in Global Tectonics Journal
Volume 14, Number 6, June 2026
ISSN number; ISSN 2202-0039

glass that is filled with water. Several sources contribute to increase the water level in the glass. One very last drop of water makes the water to overflow from the glass. An earthquake is just the same. Thus, the driver that originates the very last amount of energy that contributed to the reservoir is considered to be "the cause" of the earthquake. The case of volcanic eruption is analogous as mentioned in section 9.

In addition, the assumption is just *mathematical* that elementary oscillators located at different sites of the world are eventually mutually related in order to react one another according to some time-delayed trend in space etc. This is a reasonable and tentative "simple" scheme suited to carry out some tentative *mathematical* computation, although it is eventually devoid of realistic connection with natural reality. In fact, the scope of every computation of this kind only aims to show that some approximate relationship exists between a *mathematical* model and the natural sequence of seismic events.

For instance, suppose we represent a human body by means of several oscillators, coupled to one another. In this way, one can attempt to describe - or to predict – every kind of sickness, or death, or epidemics, etc. Obviously, in this mathematical model it is very hard to take into account the effect of the natural ageing of the human body, or its dependence on several different environmental factors, on food quality and amount, on climate, on kind of job, on parental physiological inheritance, etc. That is, this investigation would be an interesting study in *mathematics*, aimed to assess how far human physiology can be described by a "simple" algorithm. However, medical science must proceed independent of this approach. That is, we cannot confuse a *mathematical* with a *medical* investigation.

The reader, who is interested in the coupled oscillator approach applied to seismic events, can refer, e.g., to Bendick and Bilham (2017) who quote several previous references. No detail is here reported, and no discussion is here given, as the concern of those investigations is mainly mathematical. In any case, we must distinguish between an astute *mathematical* investigation - carried out on some geophysical data series by some skillful applied mathematician - and a *geophysical* investigation that relies on an ensemble of realistic observational information according to a multidisciplinary perspective by means of some *intuitive* - eventually robust - algorithm etc.

We must stress that this is not a criticism. Rather, we claim that these mathematical studies can be related to geophysical observations only *a posteriori*, whilst the focus of the present study is mostly devoted to direct geophysical investigation. On the other hand, we must consider the usefulness of every "mathematical" approach, although we must take into account a suitable warning.

For instance, Bendick and Bilham (2017) show Fig. 9, and the focus ought to be on the statement (in the figure captions) "*changes in the* l.o.d. *correlate with decadal fluctuations ...* "

It is more correct to state that changes in the *l.o.d.* and annual $M \geq 7$ earthquakes show that a common driver is responsible for simultaneous effects on both phenomena, but that, on other occasions, this cannot apply. That is, the term "correlate" is generally conceived with a more compulsory meaning. In fact, suppose to draw a scatter plot with changes in the $l.o.d.$ on abscissæ and annual $M \geq 7$ earthquakes on ordinates (every point corresponding to one and the same time instant). The plot will appear scattered and not approximately aligned along a straight line, as it is formally requested by "correlation analysis".

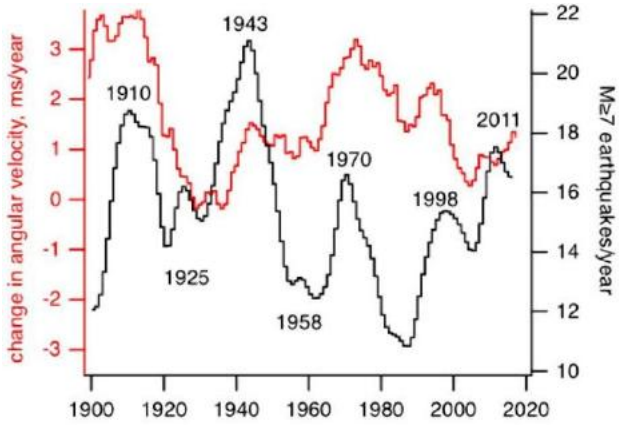

Fig. 9. "*Changes in the* l.o.d. *(Gross et al., 2004) correlate with decadal fluctuations in annual* $M \geq 7$ *earthquakes (Anderson, 1974; Shanker et al., 2001) (smoothed with* $10\ year$ *running mean). Peak seismic activity and rotational acceleration occur at* $15, 33, 60,$ *and* $88\ year$ *intervals.*" Figure and captions after Bendick and Bilham (2017). *AGU* copyright free policy.

Fig. 9 can be interpreted in different possible ways.

One can guess that e.m. stray currents (or Foucault currents) operate on the Earth much like the e.m. brake of a train. These stray currents cause a crisis of planetary crustal stress, and often this stress seems to be sufficient to trigger somewhere an earthquake (see Gregori et al., 2026a).[27] Note, however, that the phenomenon certainly is not periodical, as it responds to the whims of the solar wind flux.

Another possible interpretation deals with the location of the hypocenter with respect to some unknown bump of the *IC* (inner core), by which a strong earthquake can generate a "*sail effect*" on the *IC*. This is, in fact, the rationale for a possible investigation on the shape of the *IC*, and on its dynamics, as discussed in Gregori (2002). In fact, a well-known paradoxical fact is that some strong earthquakes cause a variation in the observed *l.o.d.* and pole motion, while other even stronger earthquakes have no similar effect. A strong earthquake generates a wave that cross through the whole planet. If the *IC* has some bump, the wave can push on it like wind on a *sail* (Fig. 10).

This seems to be the unique way suited to investigate the shape of the *IC*. In fact, some effects that are already

[27] In fact, the phenomenon seems relevant as, according to Straser (2025), and Straser et al. (2025, 2025a, 2025b, 2025c, 2025d, 2025e, 2026) and references therein, several strong earthquakes are related to large fluctuations in the solar wind, envisaging a consequent e.m. induction in the Earth.

NCGT Journal
New Concepts in Global Tectonics
New Concepts in Global Tectonics Journal
Volume 14, Number 6, June 2026
ISSN number; ISSN 2202-0039

measured, and reported in the literature, are interpreted like "*superrotation*" of the *IC*, although the interpretation is controversial, and not clear. See, e.g., the nice figures shown by Richards (2000), which started a series of several papers seeking the "*superrotation*" of the *IC*.

Controversial evidence later caused a decrease of attention on this phenomenon, while the interpretation outlined in Fig. 10 is certainly convincing with no counter-evidence. The effective exploitation of this approach is, however, computationally heavy, as one must deal simultaneously with two *SHE*s (*spherical harmonic expansions*), one *SHE* of the geomagnetic potential, and one *SHE* if the geodetic shape of the *IC*, which must be computed by observational evidence related to several strong earthquakes. See details in Gregori (2002).

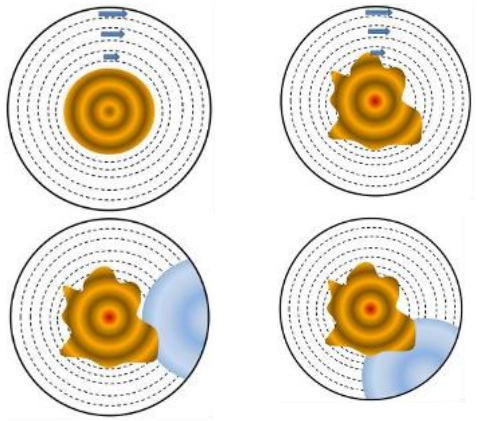

Fig. 10 - Out-of-scale cartoon showing the Earth observed from the North pole, and two case histories of a hypothetical earthquake with epicenter located somewhere in the equatorial belt. However, the concept is general and applies to every case history. The seismic wave propagates through the Earth body, and through the "*metallic*" fluid *OC* (outer core), until it reaches the hard "*magpol*" *IC*. While striking it, this phenomenon originates an anomalous "*sail effect"*, and a recoil that propagates until Earth's surface. The astronomical motion of the Earth is monitored by observatories located on the continental crust. Hence, a strong earthquake - through the *"sail effect"* caused by the seismic wave that hits the *IC* - originates a change in the astronomical motion of the Earth. *(a)* No *"sail effect"* occurs on a perfectly spherical *IC*, unlike for a non-spherical *IC* [*(b)*], and the *"sail effect"* depends on the location of the epicenter [*(c)* and *(d)*]. Unpublished figure.

Concerning the "*superrotation*" of the *IC*, we must remember the remarkable *Thesis* by Marco Marino (2004),[28] who carried out an impressive amount of data analysis, that was later interpreted in Gregori et al. (2025y). We report the abstract of Gregori et al. (2025y).

"*The standard way to compute the geomagnetic* SV *is by using maps of yearly means, i.e., by averaging over* $365\ days$*, and over* $366\ days$ *during leap years. The generally reported value is a* WD *by* $\sim 0.2^\circ\ year^{-1}$.

On the other hand, the observed WD *can be a beat between the* $1\ year$ *period of the orbital motion of the Earth, arbitrarily introduced by choosing either* 365 *or* $366\ days$*, and the actual rotation of the* IC *with respect to Earth's surface. Hence, the amount of the observed* WD *must vary, if the average is taken of magnetic records over some period* $[365.25 - \Delta t]$ *vs.* Δt*. This is the basic rationale of the present analysis. The INTERMAGNET database is used, available in 1999-2001 referred to complete records for* 73 *observatories.*

A stroboscopic effect is found that envisages an IC *that spins faster than Earth's surface, with an apparent period of* $\sim 369.75 \pm 0.5$ *rotations (number of rotations during one solar year of* $365.25\ days$*). Hence, the* IC *seems to spin faster than Earth's surface by* $\sim 370/365.25 \cong 1.01$*, or by* $\sim 1\%$.

Therefore, if this is correct, a reasonable final indicative value is, say, $\sim 370 \pm 0.3$ *rotations in* $1\ year$*, equivalent to a period (for one rotation) of* $\sim 0.9872 \pm 0.0008\ days \cong 23.69 \pm 0.02\ hours \cong 85,291 \pm 71\ sec$*. The reported observed* WD *of* $\sim 0.2^\circ\ year^{-1}$ *ought to be a beat due to the arbitrary reference to annual mean values over* $\sim 365.25\ days$*, while in reality the* IC *experiences a* WD *of* $\sim [4.5 \pm 0.5] \times 360^\circ / 365.25\ year^{-1} \cong [4^\circ.4 \pm 0.5]\ year^{-1}$.

This paradoxical evidence provided by the stroboscopic effect is $\sim 22\ times$ *larger than the expected* $\sim 0.2^\circ\ year^{-1}$ *(or, more exactly,* $\sim 0.24^\circ\ year^{-1}$ *concerning the specific data set used in the present computation). This has an unexpected physical implication.*

Upon a closer inspection on the data set used in this analysis, by means of a better algorithm than a simple visual inspection on geomagnetic maps, it is found a WD *of* $0.287^\circ\ year^{-1}$*, which is in fact close to the approximate* $\sim 0.24^\circ\ year^{-1}$ *. Hence, the discrepancy looks quite reasonable.*

A concern deals rather with the need to give a physical interpretation of the dramatically larger, and precise, estimate of $\sim [4.4^\circ \pm 0.5]\ year^{-1}$ *. A possible reasonable explanation is related to the geodetic figure of the* IC*. That is, the* IC *is likely to have spatially repeated bumps in longitude, in such a way that its real* WD *is* $0.287^\circ\ year^{-1}$*, while, by searching the stroboscopic effect, its speed is* $\sim 4.4^\circ/0.2^\circ = 22\ times$ *larger, due to some approximately regular "hills" and "valleys" on the* IC *surface.*" Hills and valley are qualitatively indicated in Fig. 10.

In addition, upon referring to the general problem of the search for *periodicities* or *cycles*, sometimes an algorithm, which is applied, gives some parameter that eventually displays some appearance of a possible periodical trend. It is often difficult to assess whether such a *periodicity* derives from the definition of the algorithm or from an intrinsic trend of observations.[29]

Another warning is about the common appeal to a comparison of an actual observational data series with a randomly generated series of events. This is certainly correct from the *mathematical* viewpoint - and this is the

[28] We feel indebted to Marco Marino for his job.

[29] In this respect, a reminder is deserved for the authoritative warning by Tukey (1977) about *(i)* the need to deal with plots that show very clear evidence, and *(ii)* about a prudential skepticism, concerning all what seems only tenuously evidenced.

NCGT Journal
New Concepts in Global Tectonics
New Concepts in Global Tectonics Journal
Volume 14, Number 6, June 2026
ISSN number; ISSN 2202-0039

proper way to test the effectiveness of an algorithm in terms of eventual bias etc. (if a *periodicity* is found also with a random series, the algorithm is not reliable). On the other hand, natural phenomena are never random (e.g., see Gregori et al., 2025w, and Gregori and Gregori, 2025). Everything happens due to a physical reason. Appealing to a random behavior, only for comparison purpose, is a way to confess our ignorance about several *d.o.f.*s (degrees of freedom) of the natural system. Therefore, a warning is about avoiding to give a physical meaning to a check (i.e., comparison with a speculated random sequence) that is aimed only to test the lack of bias of an algorithm.

In any case, a mathematical algorithm can enter into the geophysical discussion only when its effectiveness has been proven. In contrast, at every preceding stage it is only a matter for mathematical concern, by means of the specific arguments of highly specialized mathematics. In contrast, it is not yet useful for a geophysical investigation. We attain the best logical condition when an algorithm is conceived specifically to test a given physical mechanism, relying on "intuition", and this would be the ideal way to carry out *confirmatory* analysis.

In summary, on a geophysical ground the simple and intuitive *ppa* analysis ought to be carried out, e.g., in order to prove, or disprove, the serpentinization process envisaged by Martin Hovland and coworkers (see Gregori and Hovland, 2025; Hovland, 2026).

In contrast, concerning volcanism, the apparent time variation of the primary heat supply to volcanoes - derived from their respective time series of historical eruptions - appears synchronous all over the Earth (see Gregori et al., 1994), envisaging the existence of a unique "central fire".[30]

7. Generalizations

The entire aforementioned analysis can be generalized as follows.

Cross-dependence and $\mathfrak{bArp}$

Suppose that we deal with two data sets, dealing with two different *point-like processes*, let us call them process A and process B. The same algorithm $\mathfrak{Arp}$ can be applied to infer the dependence between A and B. The procedure is just the same, provided that the *pole position* is fixed on the basis of *one* data series, and $\mathfrak{arp}$ or $\sqrt{\mathfrak{arp}}$ is constructed by means of *strips* of *the other* data series.

A new situation arises when deciding whether the physical connection is such that A precedes B or viceversa. It is possible to carry out two different $\mathfrak{Arp}$ analyses (namely, one by assuming that A precedes B, and the other one by assuming that B precedes A). Even better, one can use a bilateral operator $\mathfrak{Arp}$, or $\mathfrak{bArp}$.

For clarity, suppose that the time origin (or let us equivalently call it "*pole position*") is fixed with respect to A, while *strips* of B are added to construct the $\mathfrak{arp}$. When a *pole position* has been fixed, the procedure of Fig. 1 implies that only the B events occurring *after* the time instant of the *pole position* are piled up within the $\mathfrak{arp}$. That is, every B *strip* in Fig. 1 needs to reject (by a matter of definition) all what occurs *before* the time instant of the pole position.

Conversely, the $\mathfrak{bArp}$ procedure is just the same, where, however, every B *strip* implies no data rejection (see Fig. 11). Thus, the $\mathfrak{arp}$ will result from the sum of non-cut *strips* of B events (and the time origin over every such a *strip* will be just changed according to the displacement of the *pole position* over it).

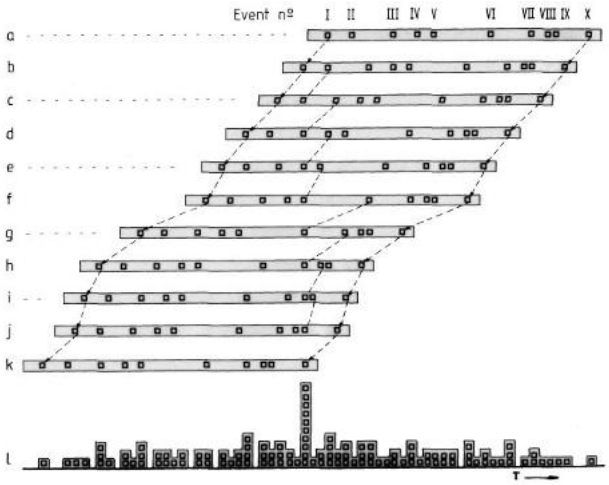

Fig. 11. Definition of bilateral $\mathfrak{Arp}$ or $\mathfrak{bArp}$. The same data sequence $\mathfrak{H}$ is considered as in Figs 1 and 3. Restart the stopwatch immediately after every event, exactly like in Fig. 1. However, don't reject the events for $t < 0$ within every *strip*. The resulting histogram ($\mathfrak{barp}$) is shown in l, and it is the sum of all *strips* $b, c, d, \ldots, k$. In the case of a random distribution of the *10* events within $\mathfrak{H}$, $\mathfrak{barp}$ approximately appears like an *isosceles triangle*. After Gregori et al. (1988) and Gregori (1990). With kind permission of the late Wilfried Schr^ der.

In this way, the result, i.e. the $\mathfrak{barp}$, instead of having approximately the shape of a *right-angled triangle* with right angle at the origin (like in Fig. 1), will look much like an approximately *isosceles triangle* resulting from the reflection (with respect to its vertical side through the origin) of the former *right-angled triangle* (like in Fig. 11).

Notice that should $\mathfrak{bArp}$ have been applied (instead of $\mathfrak{Arp}$) to the analysis of only one data series alone (as discussed in the previous sections), the result must appear symmetrical with respect to the vertical axis through the origin of T. Hence, the result would be a useless mirror duplication of the $\mathfrak{arp}$ or $\sqrt{\mathfrak{arp}}$, i.e. in this case $\mathfrak{bArp}$ is a useless complication with respect to $\mathfrak{Arp}$.

In the case of *two different* data series A and B, the advantage of $\mathfrak{bArp}$ with respect to $\mathfrak{Arp}$ is that one can inspect whether A precedes B or viceversa, by means of only one $\mathfrak{bArp}$ application.

Since $\mathfrak{bArp}$ is thus used for the analysis of cross-dependence[31] between two given processes A and B, it is

[30] This finding was one of the observational facts that triggered Gregori (2002). See also Gregori (2004, 2006e, 2009).

[31] The use of the term "*cross-correlation*" is here deliberately avoided because "*correlation*" means a specific technique referring to a linear correlation coefficient, etc., which is quite

NCGT Journal
New Concepts in Global Tectonics
New Concepts in Global Tectonics Journal
Volume 14, Number 6, June 2026
ISSN number; ISSN 2202-0039

sometimes convenient to call it $\mathfrak{x}\mathfrak{b}\mathfrak{Arp}$, where "$\mathfrak{x}$" stays for "*cross-dependence*".

Defining $\mathfrak{c}\mathfrak{Arp}$

The definition of *continuous* $\mathfrak{Arp}$ or $\mathfrak{c}\mathfrak{Arp}$ is as follows. Consider the case of two data series, one referring to a *point-like process*, say A, and the other to a continuous or smooth process, say $B(t)$.

A most obvious way is to choose the *pole position* on the basis of the *point-like process* A, and to construct the $\mathfrak{arp}$ by adding *strips* of $B(t)$. Similarly to the case mentioned before, also in this case it is convenient to use a bilateral $\mathfrak{Arp}$, i.e. $\mathfrak{c}\mathfrak{b}\mathfrak{Arp}$ or $\mathfrak{b}\mathfrak{c}\mathfrak{Arp}$.

Another possibility is by applying $\mathfrak{c}\mathfrak{Arp}$ directly to the continuous data series $B(t)$ alone: there is only need for specifying how to define the *pole position*. One criterion is to fix, e.g., some threshold such that every time one finds within $B(t)$ a maximum (or a minimum, or else) being above (or below) that given threshold. Then, a *pole position* is chosen at that instant of time. After that, the application of $\mathfrak{R}_{ES}$ and of $\mathfrak{Cetra}$ proceeds as above for the case of a *point-like process*.

Concerning the relation between $\mathfrak{c}\mathfrak{Arp}$ and the well-known and extensively used Fourier transform or power spectrum analysis of $B(t)$, note that a power spectrum is the Fourier transform of the auto-correlation function of $B(t)$ (e.g. BÂth, 1974, p. 83).

The process of constructing the output "histogram" of $\mathfrak{c}\mathfrak{Arp} \otimes \mathrm{B(t)}$, i.e. the $\mathfrak{carp}$, is somewhat similar to the process of the evaluation of the cross-correlation (as the cross-correlation analysis assumes to "superimpose", in some different way other than here above, a *strip* of $B(t)$ over the same $B(t)$, suitably time-shifted, etc.

However, independent of any detail of this formal mathematical analogy, $\mathfrak{c}\mathfrak{Arp}$ introduces the new substantial feature of the threshold: namely, a *pole position* needs to be fixed (or the stopwatch is reset to zero) every time the phenomenon goes beyond some given threshold. This choice can depend on physical arguments. Differently stated, at this instant of time, it is assumed that some physical, extreme process is triggered anew, while in all other circumstances the time variation of $B(t)$ is treated only as a "normal" smoothly varying phenomenon. In addition, unlike the Fourier algorithms, $\mathfrak{c}\mathfrak{Arp}$, applies even with incomplete data series, and this is an important advantage.

It is impossible to state *a priori* whether $\mathfrak{c}\mathfrak{Arp}$ is the best choice, or not. In some cases, it can be physically reasonable: whenever one deals, e.g., with a phenomenon that implies the yield of a structure (like an earthquake or a volcanic eruption, etc.) it is likely that, under suitable conditions, $\mathfrak{c}\mathfrak{Arp}$ can eventually work better than the standard power spectra. In several other cases, however, power spectra can sometime be better than $\mathfrak{c}\mathfrak{Arp}$.

Differently stated, physics - and not simply mathematics - should decide what is more appropriate. In general, both approaches should be tentatively used on the same database and their results compared with each other.

Concerning the error bar of $\mathfrak{carp}$, the key idea is to generate several random data series obtained by a suitable mixing of $B(t)$ with respect to t. This mixing should be carried out in such a way as to keep invariant some intrinsic features of the original data series $B(t)$. Several $\mathfrak{carp}$s can thus be obtained, and therefore their average and rms deviation evaluated. This deviation results reasonably constant (*vs.* the "trial" period T) when the average is evaluated over the $\sqrt{\mathfrak{carp}}$ much better than when the average is made over the $\mathfrak{carp}$ themselves. One specific example is discussed in Banzon et al. (1990).

$\mathfrak{Arp}$ *with no operator* $\mathfrak{D}$

Refer to[32] Table 4 and compare it with Table 1. Let us note that the whole $\mathfrak{Arp}$ analysis can be carried out also by avoiding to use the $\mathfrak{D}$ operator. Table 4 refers to the use of $\mathfrak{b}\mathfrak{Arp}$ (instead of $\mathfrak{Arp}$), where, however, bilateralism is optional. In addition, the output of $\mathfrak{Arp} \otimes \mathfrak{H}$ (or of $\mathfrak{b}\mathfrak{Arp} \otimes \mathfrak{H}$) is not a histogram like in the case of $\mathfrak{b}\mathfrak{Arp} \otimes \mathfrak{D} \otimes \mathfrak{H}$, but just a simple *string* of "almost Dirac δ-function points", which have an almost null probability of overlapping with one another. Then, one can apply $\sqrt{\Lambda \otimes \mathfrak{Arp} \otimes \mathfrak{H}} \pm 1/2$, and the entire subsequent procedure remains unchanged.

Table 4. Logical sequence of the 1D bilateral $\mathfrak{Arp}$ (or $\mathfrak{b}\mathfrak{Arp}$) analysis

$\mathfrak{H}$
$\mathfrak{b}\mathfrak{Arp} \otimes \mathfrak{H}$ $\pm\sqrt{\mathfrak{b}\mathfrak{Arp} \otimes \mathfrak{H}}$
$\sqrt{[\Lambda \otimes \mathfrak{b}\mathfrak{Arp} \otimes \mathfrak{H}]} \pm \frac{1}{2}$ not $\left\{\Lambda \otimes \left[\sqrt{\mathfrak{b}\mathfrak{Arp} \otimes \mathfrak{H}} \pm \frac{1}{2}\right]\right\}$
$\mathfrak{R}_{ES} \otimes \mathfrak{H}$
$\mathfrak{Cetra} \otimes \mathfrak{R}_{ES} \otimes \mathfrak{H}$

Strictly speaking, the result is not identical to what is obtained by applying the operator $\mathfrak{D}$ as in Table 1. However, the conclusions of the two methods ought to be expected to be similar to each other. The most relevant difference is that $\mathfrak{D}$ implies the application of a Π filter (of unit time span) over $\mathfrak{Arp} \otimes \mathfrak{H}$, i.e. $\Pi \otimes \mathfrak{Arp} \otimes \mathfrak{H} \approx \mathfrak{Arp} \otimes \mathfrak{D} \otimes \mathfrak{H}$. However, e.g. concerning the series of anomalous climatic events on the Tanaro/Bormida (Pavese and Gregori, 1984 and Gregori et al., 1988), the first procedure puts one "elementary square" of unit side in the $\mathfrak{D} \otimes \mathfrak{H}$ sequence whenever two or more anomalous climatic events are reported along one and the same year. On the contrary, the value of $\Pi \otimes \mathfrak{Arp} \otimes \mathfrak{H}$ puts as many "elementary squares" as the total number of reported anomalous events during that same year.

Another difference is that in Table 1 the operational sequence is adopted $\Lambda \otimes \left[\sqrt{\mathfrak{b}\mathfrak{Arp} \otimes \mathfrak{H}}\right]$ (and not $\sqrt{[\Lambda \otimes \mathfrak{b}\mathfrak{Arp} \otimes \mathfrak{H}]}$ in order to avoid to evaluate a weighted-running-average over different data having an uneven error bar. In contrast, in Table 4 the use of $\sqrt{[\Lambda \otimes \mathfrak{b}\mathfrak{Arp} \otimes \mathfrak{H}]} \pm 1/2$ appears unavoidable, because

different compared to the present approach. See Gregori et al. (2026e).

[32] After Gregori (1990). With kind permission of the late Wilfried Schrˆder.

NCGT Journal
New Concepts in Global Tectonics
New Concepts in Global Tectonics Journal
Volume 14, Number 6, June 2026
ISSN number; ISSN 2202-0039

$\mathfrak{Arp} \otimes \mathfrak{H}$ is a *string* of never overlapping "almost Dirac δ-function points", and it results (for every trial T) $\sqrt{\mathfrak{Arp} \otimes \mathfrak{H}} \approx \mathfrak{Arp} \otimes \mathfrak{H} \approx 0$ or 1. Hence, one must first "pile up", in some way by means of some Λ, the points of $\mathfrak{Arp} \otimes \mathfrak{H}$ before evaluating the square root. Then, one can state that the expected rms deviation is $\approx \pm 1/2$.

It should be noted that the $\pm 1/2$ standard deviation rule is a rigorous result in the 1D case, while here it is only the result of a logical extrapolation, by analogy to the previous rule. However, it should be suitably proven for the nD case (to our knowledge not yet done). In addition, this rigorous proof could – maybe - even depend on the definition of Λ.

In any case - from a practical viewpoint - these details deal with mathematical aspects that, on an intuitive basis, are not likely to affect significantly the physical conclusions, which rely on the *superposed epoch criterion*. Rather, these mathematical problems look like a minor refinement, according to the viewpoint of the geophysicist, who is concerned with other potential sources of errors.

All these generalizations of $\mathfrak{Arp}$, which are of no practical help in the 1D case, play an important role while discussing the nD case.

8. The nD case

The generalization to the nD case is discussed by drawing simple analogies to the 1D case.

Database preparation

For clarity purposes, refer to the case of an earthquake catalogue, and consider only events of magnitude above a given threshold. Every event is *point-like*, and characterized by a time instant of occurrence and by the (geographical) latitude λ and longitude φ of epicenter.

Other parameters are neglected, such as the hypocenter depth, earthquake magnitude, etc. It is also assumed that all aftershocks have already been rejected from the catalogue.

When dealing with every kind of physical application other than earthquakes, we assume that some similar pre-selections and checks have been carried out before applying the $\mathfrak{Arp}$ analysis.

Definition of the Pole Position

Avoid using the operator $\mathfrak{D}$, as otherwise one could feel embarrassed by the actual size to be choice of the "elementary nD cube" of "unit side". Use a $\mathfrak{barp}$.

As far as *time* is concerned, the *pole position* is easily defined: it is the time instant (*date and UT*) of some given earthquake. Concerning the space co-ordinates, let us state that a *pole position* is defined whenever a shock occurs inside some given pre-chosen region of the globe. This will be briefly called the "*pole position area*", or *ppa*.

Concerning the extension in space of the *ppa*, the smaller it is, the better the spatial resolution will be of the result. On the other hand, the smaller the *ppa* is, the smaller the number is of the available different events or "*pole position events*" (*ppe*) that occur inside the given *ppa*, the poorer the statistics is of the earthquakes that enter into the $n\mathfrak{Arp}$ procedure, and therefore the larger the earthquake catalogue must be, for getting statistically significant results. That is, we must find a compromise between a large or a small *ppa*, depending on the amount of the data contained in the catalogue.

Defining $n\mathfrak{barp}$

Refer to[33] Table 5. Select one given *ppe*, occurring within the chosen *ppa.* Then, re-label every earthquake of the whole catalogue by means of three new coordinates as follows. A new time t' (negative or positive) measured with respect to the time of occurrence of the chosen *ppe*. A new latitude λ' and longitude φ' defined in a new frame of reference having its North Pole at the center of the *ppa.*

Table 5. Logical sequence of the nD $\mathfrak{barp}$

$\mathfrak{H}$
Choice of the *pole position*
$n\mathfrak{barp} \otimes \mathfrak{H}$ $\pm\sqrt{n\mathfrak{barp} \otimes \mathfrak{H}}$
$\sqrt{[n\mathfrak{barp} \otimes \mathfrak{H}]} \pm \frac{1}{2}$ [or $\sqrt{[n\Lambda \otimes n\mathfrak{barp} \otimes \mathfrak{H}]} \pm \frac{1}{2}$]
$n\mathfrak{R}_{ES} \otimes \mathfrak{H}$

By this, with reference to every given choice of a *ppe*, all earthquakes in the catalogue are re-labelled by a new set of three co-ordinates t', λ', and φ'. Then, one can draw, for every fixed *ppe*, an "almost Dirac δ-function" point-distribution in a 4D "histogram", having three co-ordinates t', λ', and φ', and the fourth one for the number of events. That is, it is possible to associate to every *ppa* a "*3D strip*" to be piled up in order to construct a 4D histogram $n\mathfrak{barp}$.

Repeat this identical procedure for every different available *ppe* in the catalogue and pile up all the corresponding *3D strips* (as above) to construct a unique final 4D histogram: call it the $n\mathfrak{barp}$.

For instance, this $n\mathfrak{barp}$ can be conveniently imagined to be drawn - at a set of given intervals of time instants - over a spherical surface (λ', φ').

In this way, the $n\mathfrak{barp}$ is a very general mathematical entity. However, while carrying out the physical interpretation of the results, there will be need for consideration of different choices of $n\mathfrak{barp}$, i.e. every choice referring to a different pre-chosen *ppa* (see below).

Defining $n\Lambda$ *and* $n\mathfrak{R}_{ES}$

The filter $n\Lambda$ in nD can be practically obtained by simple generalization of the Λ filter in 1D. We must, however, consider a few differences.

Concerning the time co-ordinate t, the problem is identical to the lD case, as there is a *triangle effect*. Hence, one should use the same criterion as for 1D for getting rid of the *triangle effect* and of the unwanted trends (such as, e.g., the ~ 1600 *years periodicity* originated in the Tiber flood data by an anthropic non-geophysical factor; see Gregori et al., 1988, or see Fig. 5).

[33] After Gregori (1990). With kind permission of the late Wilfried Schr^ der.

NCGT Journal
New Concepts in Global Tectonics
New Concepts in Global Tectonics Journal
Volume 14, Number 6, June 2026
ISSN number; ISSN 2202-0039

Concerning the spatial co-ordinates λ' and φ' two new facts enter into play.

The first fact is that it is not possible to use just two simple running-weighted-averages, separately over λ' and φ', because averaging over φ' is meaningless close to the poles. Rather, one must carry out a weighted-running-average over the spherical surface (λ', φ'), e.g. by using a weight defined by means of a *circular cone* (as in Fig. 12 instead than of a *triangle* as in Fig. 2b), i.e. the weight is assumed to be a suitable linear function of the radial distance of the point being weighted, with respect to the point at which the weighted average is evaluated. In this way, all points (λ', φ') are treated in a homogeneous way independent of (λ', φ').

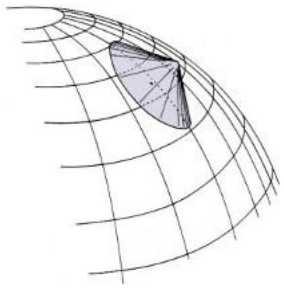

Fig. 12. Definition of a 2D filter over a spherical surface, similar to the 1D filter Λ for 1D (defined in Fig. 2b). This "*circular cone filter*" gives a weighted-running-average over a sphere, whereby every datum is assigned a (non-negative) weight that is linearly proportional to its distance from the center of the cone. This operation carries out a homogeneous filtering all over the spherical surface, independent of latitude and longitude. We can easily imagine other similar filters, e.g. by means of a weight defined by a 2D circular Gaussian function, etc. After Gregori (1990). With kind permission of the late Wilfried Schrˆ der.

The second fact is that there is no analogous *triangle effect* for λ' and φ'. As a matter-of-fact, the *triangle effect* in the case of the co-ordinate t occurs for the reason that, when taking a *strip* and fixing over it a time for the *pole position*, the total length of the data *strip* being available at any time - say, later than the *pole position event* - is accordingly changed, and the result of this shortening originates the *triangle effect*.

In contrast, when dealing with the pole position on the spherical surface (λ', φ'), one is just making a rotation of the latitude/longitude reference frame over this spherical surface, but there is no change in the total number of points. In fact, the *ppa* is a real region over the globe, hence the spatial extension of the (λ', φ') *strip* is always the same corresponding to the whole spherical surface. Thus, every *strip* is a complete repetition of the whole Earth's surface. Differently stated, a spherical surface - no matter how it is rotated – is always self-repetitive (in its total extension) as it contains no point at infinity.

Summarizing, since $n\mathfrak{bUrp}$ is a distribution of "almost Dirac δ-function" points, it is worthwhile to proceed by $\sqrt{[n\Lambda \otimes n\mathfrak{bUrp} \otimes \mathfrak{H}]}$, as its error-bar, owing to the same reasons as here above concerning the 1D case, it is reasonable to guess that it is $\approx \pm 1/2$.

After having defined $n\mathfrak{Ur}$, it is immediate to generalize $\mathfrak{R}_{ES}$ to the nD case, i.e. $n\mathfrak{R}_{ES}$. Therefore, one can supposed to have promptly got a 3D distribution (in λ', φ', and t') of a residual, from which all eventual unwanted trends, as well as the *triangle effect* for t', have been suitably subtracted.

Analysis of the residuals

As far as the present analysis is concerned, the generalization of $\mathfrak{Cetra}$ cannot be easily extended to the nD case. Consider that the generalization is almost immediate, concerning the time dependence, and the eventual *periodicity* of an event described by $(n-1)$ co-ordinates (i.e., the original n co-ordinates minus t). For instance, consider that the *cycle diagram* (such as in Fig. 3) is defined in terms of the probability of occurrence *vs.* an (n-1)D variety spanned by $(n-1)$ co-ordinates as above; the definition of the parameter p is always the same, independent of how large is $(n-1)$.

In contrast, the general problem of the analysis of the residuals cannot be simply treated in terms of a standardized and uniform way (as it was made in the 1D case by means of $\mathfrak{Cetra}$). Every specific case history can require a suitable practical approach that is likely to be defined separately in every different application.

In general, the problem is about how to make a graphical representation of the residuals gotten by $n\mathfrak{R}_{ES}$, e.g. on a computer monitor, in terms of, say, one different picture associated with every time instant. In practice, think about it in terms of a movie - every picture having the pre-chosen *ppa* located specifically somewhere, e.g. close to the center of the monitor. Suppose to use different colors for different values of the residual. If, say, a blue tone is associated to a high positive value of the residual, one should search for blue spots and how they are lit up sequentially in time - much like flashing-lights in a flipper game that monitors the trajectory of the ball.

This could actually occur in the analysis of an earthquake catalogue, where it can be expected that an earthquake results to be eventually indicative of a stress "*soliton*" that propagates somewhere through the Earth's crust. A similar picture can be given in terms of a pressure "*soliton*" that propagates - more properly one should call it a maximum surface elevation - over the surface of a pond where a stone has been thrown. Note that, in the case of a stone that falls in a pond, the effect displays a symmetrical ring, while in the Earth's crust the crustal anisotropy determines an asymmetrical propagation.

The concept of "*soliton*" in geophysical signals is explicitly considered by Mazur et al. (2008), who stress that "*solitons*" (and non-linear waves) frequently occur in the solar corona, in interplanetary space, in the Earth's magnetosphere, in topside ionosphere, in the atmosphere, and in the Earth's crust.

Specific theoretical and mathematical tools are available for describing ND-soliton structures and soliton turbulence gas. They rely on special nonlinear methods of signal analysis. Fourier algorithms "*fit well the detection of linear waves and determination of their properties, but they are not very effective for the examination of highly structured space plasma turbulence.*"

ISSN number; ISSN 2202-0039

The simplest algorithm starts by investigating the statistical relationships that exist - in the observed signal ensemble - between amplitudes, duration, velocity, etc. The next step is to compare these statistical properties with the expected theoretical relationships referring to a given soliton class. This is the observational test for identification.

Mazur et al. (2008) consider a few basic relationships referring to some types of solitons. They also discuss the validity and limitations of these relationships. In any case, they note that every simple statistical method of "*soliton*" identification needs for a substantial number of signals that, in principle, should occur with the same external conditions. Therefore, they discuss some more general algorithm etc. However, this is not pertinent for the present discussion.

Obviously, in the case of a climatic data catalogue, the expected trend of such a "*blue-flashing-light*" can be quite different. In addition, since a $\mathfrak{b}\mathfrak{Arp}$ was used, one can search for this flashing-light sequence, both *vs.* increasing and *vs.* decreasing time.

All this is intuitively clear. However, it is cumbersome - and, perhaps, sometimes even misleading - to attempt to imagine an automatic computerized procedure suited to recognize this interpretation of the residuals. It appears, rather, more convenient and practical to use first this visual and intuitive inspection by a computer movie. This helps the "*intuition*" process of the researcher. At a later time one can eventually envisage some mathematical *ad hoc* procedure suited for a quantitative formulation of the methodology, after having defined the procedure by direct visual analysis.

Concerning the physical interpretation of the results, this entire analysis is quite general. In fact, just one application of $\mathfrak{b}n\mathfrak{Arp}$ can give, in principle, a movie that gives the entire needed information. This movie could already result physically self-explanatory. On the other hand, one arbitrary choice remains in the procedure that appears unavoidable, i.e. the choice of a given *ppa*.

Therefore, there is a strict need to repeat the analysis several times for different *ppa* choices. The most appropriate choice of a *ppa* can be done following some reasonable criterion, e.g. either following a trial-and-error procedure, or according to some modeling for the physical interpretation (like, e.g., in the earthquake case, depending on tectonic features).

The whole aforementioned formal approach specifies all the required operative details that are required to implement the intuitive idea on the spacetime correlation of seismic activity, which happens in different parts of the globe, according to the anticipation made in section 6.

9. The physical interpretation

The basic idea for the $\mathfrak{Arp}$ operator - in its several forms and case histories – is the same as the *superposed epoch algorithm*.

If a *point-like process* is periodical in a strict sense with period T, its $\mathfrak{arp}$ must display a very regular sequence of peaks spaced by a time increment T. The $\mathfrak{arp}$ looks like a comb, with teeth of decreasing amplitude (see section 5).

Similarly, if the *point-like process* is randomly distributed vs. time, it can be easily realized that its $\mathfrak{arp}$ must appear like a perfect "*quasi-triangle*".

In general, as already formally stressed in detail in section 5, some intermediate case history is found, and the $\mathfrak{arp}$ looks like a superposition of some periodical component plus some percent of seemingly almost random background. A convenient way to proceed is to envisage the existence of a periodical component, and to evaluate the *cycle diagram* corresponding to the inferred leading *periodicity*. Subtract from the original data series the ideal perfect periodical phenomenon, resulting from the sum of several consecutive *cycle diagrams*. Then re-apply the same criterion to the residuals, in order to infer a second *periodicity*, etc. As far as possible, repeat the procedure iteratively. The analysis deals with the assessment of the *period families*, of their respective *forefather*, and of their mutual *relations*, as mentioned in section 3.

The case of a smooth phenomenon leads to the use of the operator $\mathfrak{Cetra}$, which ultimately responds to the same former key-idea, although in terms of continuous functions, rather than in terms of "yes" and "no" events.

All these items are the concern of the present entire previous treatment. From a simple and intuitive viewpoint, let us rather consider only the case history of a data series, which is not random, although it contains evidence for no clear *periodicity* – which can be distinguished from a clear background of random component.

That is, since the data series is not random, owing to a matter of definition, it is such that the occurrence of every event is in some way reminiscent of the past history of the system. The reason is that "randomness" is formally defined just as the case history in which every event - in a strict sense - is not reminiscent of the previous history of the system, neither it keeps memory of the future evolution of the system.

According to the rationale of the Kapteyn's class distribution (see Arley and Buch, 1950, or also Paparo and Gregori, 2003), this means that the statistical distribution must be *lognormal*, of the set of time intervals Δt elapsing between every two subsequent events. Upon a little thinking, it is concluded that, in the ultimate analysis, the $\mathfrak{arp}$ for this case history will display somewhere an upward "flattening", almost like a large "hill", compensated somewhere else by a corresponding gentle "valley" in order to keep a constant total integrated area of the $\mathfrak{arp}$ plot.

Finally - for the sake of completeness - let us recall that the plot of the aforementioned Δt vs. its order number of occurrence - i.e. not vs. time - is called "*Imbò's algorithm*", after Giuseppe Imbò (1899-1980).[34] This tool is very effective for the investigation of volcanic cycles. It is explicitly discussed and applied in Gregori (1993, 1996, 2002), and Gregori et al. (1992, 1994).[35]

[34] Director of the *Osservatorio Vesuviano* and Professor of Earth Physics at the *University Federico II* of Naples.

[35] Refer also to the original references Imbò (1928).

NCGT Journal
New Concepts in Global Tectonics
New Concepts in Global Tectonics Journal
Volume 14, Number 6, June 2026
ISSN number; ISSN 2202-0039

Let us recall that the physical meaning of this approach can be called a "*calorimetric criterion*", as it relies on the principle of the energy balance of the system. In terms of a correct analogy, the system operates like a pressure cooker. If the power supply that heats the cooker changes in time, the time interval - between every two subsequent whistlers of the security valve - will change accordingly, depending on the integral of the total heat that the cooker stored *vs.* time. That is, a whistler occurs every time that the system has reached a threshold of stored energy, corresponding to the weight of the security valve.

Every physical system can be tentatively treated according to this "*calorimetric*" criterion, by means of the *Imbò algorithm*. Whether the method results effective or not, its effectiveness depends on the physics of the system, and also on the data series that is analyzed.

For instance, this phenomenon occurs inside a geyser (e.g. Karlstrom et al., 2013). In the case of the time series of volcanic eruptions, it works very effectively, while it appears to be of little help for the treatment of the outliers in *AE* (acoustic emission) time series (see Gregori et al., 2026a).

For completeness sake, let us also point out that Imbò (1928) had formerly correctly applied this algorithm to the historical data series of all Etna's eruptions that had opened a new boca. However, at later times the researchers unduly abandoned this algorithm, maybe due to the limited available time series of historical eruptions when dealing with other volcanoes. However, there was also some misunderstanding, as it is stressed, e.g., by Bullard (1984, his Chapter 12). Volcanoes certainly display some apparent cyclic feature, but a reliable assessment ought to require a database that spans a much longer period of time, compared to the presently available historical eruption series.

The misunderstanding was originated by some studies by Thomas A. Jaggar,[36] while studying Kīlauea and Mauna Loa. He inferred that an $\sim 11\,year$ cycle exists, superimposed over a $\sim 132\,year$ cycle, composed of two parts, $\sim 66\,year$ each. Jaggar (1931, p. 3) wrote (reported by Bullard, 1984, p. 336): "*if the Earth magnetism and electricity are in some way associated with gravity, volcanism may be affected. If Earth's heat radioactivity affects volcanism, the Sun may in turn affect the Earth radiations. Finally, if volcanic emanations on the Earth are a last remnant of solar processes here, these processes by unknown means may be sympathetic with the Sun*." This is a sum of speculative guesses, based on the Buffon "*cooling cannon ball*" Earth's model.[37] However, Jaggar incorrectly envisaged that he had achieved observational evidence in support of his guess.

According to this same belief, Sassa (1936, p. 22), while reporting about the activity of the volcano Also, claimed that "*the volcanic mass and energy accumulated up to the latest period of the maximum number of sunspots were almost exhausted by a series of eruptions during that period* ... ."

However, Stearns and Macdonald (1946) carried out a careful study on Kīlauea, and found no support for Jaggar's guess. They found evidence for no $\sim 11\,year$ cycle, neither any way of relating its activity to sunspots. This finding determined the abandonment of the search for volcanic cycles.

We stress that a cycle does not imply a strictly periodic phenomenon, rather a sequence of comparatively more active and less active periods of time, with varying time lags between successive similar stages. In addition, we must consider the very complicated overlapping in solar-terrestrial effects, which occur either through the "*external way*" or through the "*internal way*" (see Gregori, 2002; Gregori et al., 2026a)

The database available in the 1920s was less rich than at present. Now, the effectiveness of the *Imbò algorithm* can be safely tested and true cyclic - though non-periodic - features can be reliably assessed (Gregori, 1993, 1996, 2002; and Gregori et al. 1992, 1994). Also the solar control on volcanism is thus shown,[38] although for time variations characterized by periods much longer compared to the $\sim 11\,year$ cycle, i.e. the phenomenon responds to the "*internal way*" and only to the spectral component, in the variation of the solar wind, with period $\gg 11\,years$.

10. Multivariate correlation analysis - The Gram analysis - Analysis of dependence

As a standard, a great amount of misunderstanding is often found in the literature, when dealing with multivariate problems, hence multivariate correlation analysis etc., and mostly when assuming a linear dependence. A full treatment of this item ought to require a much longer discussion.

For instance, sometimes authors attempt to envisage an algorithm that is suited for the application of their specific concern, e.g. by referring to some models etc. (see, e.g., Ke et al., 2009). See some mentions in Gregori et al. (2026e), with reference to the symmetric *Gram's matrix* $\| \varrho_{rs} \|$ (Courant and Hilbert, 1953), which sometimes is called "*matrix of moments*" or "*correlation matrix*" (see e.g. Cramèr, 1954 or Arley and Buch, 1950).

Let us suppose that we deal with M data series, every one composed of N elements, simultaneously measured at the same instants of time, i.e., in symbols let us call them $\{x_j(t_k)\}$ $(j = 1, 2, \ldots, M;\ k = 1, 2, \ldots, N)$. Let us call ϱ_{rs} the 2D correlation coefficient between $\{x_r(t_k)\}$ and $\{x_s(t_k)\}$ $(k = 1, 2, \ldots, N)$, i.e.

$$\varrho_{rs} = [x_r, x_s] \qquad (52)$$

where the [...] is the aforementioned *Gauss symbol*; see Gregori et al. (2026e).

[36] Thomas Augustus Jaggar, Jr. (1871-1953), American volcanologist, founder of the *Hawai'ian Volcano Observatory*, and its director during 1912-1940.

[37] This reminds about the experiments carried out by George-Louis Leclerc Comte de Buffon (1707-1788) by means of cooling cannon balls. It is surprising, and almost incredible, that this naïve concept is unconsciously shared today by almost all published papers.

[38] This finding was one key observational fact that determined Gregori (200).

New Concepts in Global Tectonics Journal
Volume 14, Number 6, June 2026
ISSN number; ISSN 2202-0039

It can be shown (Courant and Hilbert, 1953, p. 34-37) that a necessary and sufficient condition for the fact that the variates $\{x_j(t_k)\}$ ($j = 1, 2, \ldots, M;\ k = 1, 2, \ldots, N$) are linearly related one to another is that

$$det \parallel \varrho_{rs} \parallel = 0 \qquad (53)$$

That is, the rank of the *Gram determinant* represents the number of *d.o.f.*s of the physical system, according to the knowledge of the system expressed by the available series of measurements $\{x_j(t_k)\}$ ($j = 1, 2, \ldots, M;\ k = 1, 2, \ldots, N$).

Gregori et al. (2026e) consider the example when we do not know the gas law, while we have three data series referred to one gas sample. Gregori et al. (2026e) show how the algorithm can find the gas law.

A systematic application of this algorithm leads to what can be called "*analysis of dependence*". See Gregori et al. (2026e) for details.

11. Periods in natural phenomena

The previous sections deal with an attempt to highlight a few of the several procedures used by different authors for focusing on seemingly periodical phenomena in observational data series. It is excessively long to provide the reader with a feeling about the wide fan of different periods that are more often reported in the literature.

A warning is that, when reading about some investigation, every conscious-driven reader must rely on a suitable critical feeling, in order to evaluate the logical basis, the robustness, and the biases of every algorithm used in a given data analysis. All estimated approximate *periodicities* are intrinsically affected by error-bars that depend on the total time range of the database, on its completeness, and on its reliability.

Moreover, owing to the great variety of the quality of the time series to be analyzed, there is no general agreement about any standard method of analysis to be applied. Every author envisages his own approach - and in general different analyses give conclusions that are at least partially different from each other, even when they are applied to the identical data set (e.g., Fiorentino et al., 1988). This has in any case to be expected, as in general every given phenomenon is only approximately periodic, and every apparent *periodicity* is only a simplified way to look at the much greater complication of natural reality, compared to any ideal repetitiveness in time. Nevertheless, these apparent *periodicities* are effective in order to envisage what phenomena might be seemingly correlated, or not, with one another. Moreover, in general, either a periodic or a cyclic phenomenon is not simply sinusoidal, and - in the Fourier series representation - this deviation from any simple sinusoidal law is described by the appearance of higher order harmonics.

The discussion of the previous sections ought therefore to help while carrying out this critical evaluation. The following comments are an operative tool, hopefully useful for the reader, who wants to seek *periodicities*, and wants to know whether some other phenomena seemingly display some *periodicity*, which seems analogous to his findings. The result is almost frustrating, the primary cause being - in the ultimate analysis - the lack of truly linear relations between different observational parameters, and the concurrence of several simultaneous causes for driving every given phenomenon (see, e.g., Gregori et al., 2025w, and Gregori and Gregori, 2025, and references therein).

The best-known *cyclic*, not *periodic*, phenomenon is perhaps the sunspot cycle. The next best evident *cycle* is the *QBO* (quasi-biannual oscillation), i.e. an $\sim 27\ month$ cycle, formerly observed in the stratosphere along some wide equatorial belt (Lamb, 1972), and subsequently recognized in several atmospheric phenomena.

The solar rotation has $\sim 27\ days$, even though it varies regularly with solasr heliocentric latitude.

Other examples are often encountered. For instance, the average climate (dryness/wetness) of entire China clearly shows correlation among different sites, and a well-defined *cyclic* trend, although the phenomenon appears definitely *non-periodic* (see section 6, and Fig. 6 of Gregori et al., 2025f). Moreover, a *cyclic* phenomenon can also have some intrinsic scatter. For instance, during a basalt flood event, which generates a *LIP* (*Large Igneous Province*), the "magma flood" could last altogether $\sim a\ few\ Ma$, although with eventual gaps of quietness lasting $\sim several\ 10,000\ years$ (Rampino and Stothers, 1988, and references therein).

In general, Rezanov (1980) proposes a dependence of the *periodicity* (or *cycle* duration) *vs.* the intensity of the event, according to Fig. 13.

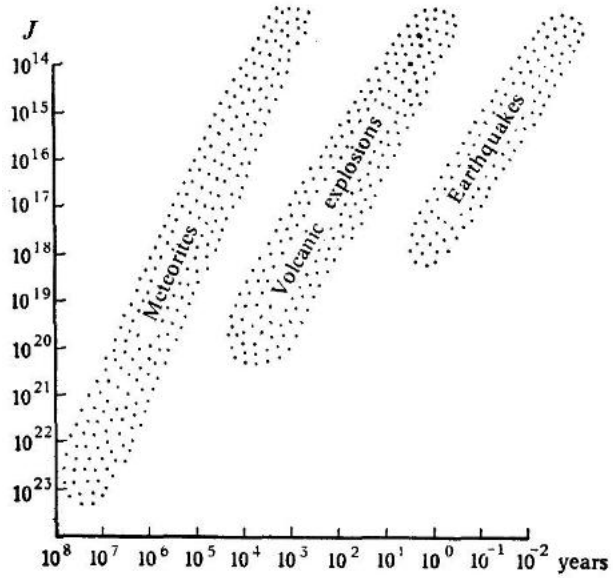

Fig. 13. Proposed approximate *periodicities* of different phenomena as a function of their respective energy. Redrawn after Rezanov (1980). Since 2008-2009 no either direct or indirect contact seems possible with *MIR Publishing* house, and no contact seems possible with the author.

Some tables are given in Lamb (1972, p. 242), where detailed references are given for every entry. Additional information is given, among others, by Hansen and Goldberg (1978), Wigley et al. (1981), Fischer (1986), Berger et al. (1989), Goodess et al. (1992), Fairbridge (1996), etc.

NCGT Journal
New Concepts in Global Tectonics

New Concepts in Global Tectonics Journal
Volume 14, Number 6, June 2026

ISSN number; ISSN 2202-0039

In general, different *cycles* or *periods* are believed to be associated with characteristic time scales of their own (Fig. 14).

Moreover, the steady persistence of the solar cycle during the last few centuries is the object of some controversy, particularly concerning the existence of the Maunder minimum during $AD\ 1645-1715$ (Schrˆder, 1988a, 1994; Treder and Schrˆder, 1992; Kopecky, 1996; Gregori et al., 2026c; Gregori and Leybourne, 2026c, and references therein). An important warning, however, is that the Sun is a very complicated and complex physical system that can hardly be fully represented by means of one *d.o.f.* alone. Sunspots are just one morphological feature, while geomagnetic activity, polar auroræ, tree rings, or more generally every other climatic proxy, etc. are other observational manifestations of the changes of the Sun. In general, it is possible that either one index (e.g. sunspots) denotes a "quiet" time, while another index (e.g. polar auroræ) shows activity. That is, it is oversimplifying to claim that the Sun is "*active*" or "*quiet*". The morphology of phenomena can be much more complicated compared to every "simple" or oversimplifying scheme. In fact, when the Sun is "*quiet*" all sunspots seem to coalesce into one or very few clusters. That is, the Sun is not "*quieter*", rather, the distribution of sunspots changes.

Upon considering in detail the several approximate estimates of the ages of *LIP*s, it appears that the *periodicity* of $\sim 27.4\ Ma$ is most relevant, which was observed both in the magma emplacement rate of Hawai'i's hotspot, and in the speed of the Pacific plate (Gregori, 2002; Gregori and Leybourne, 2021; Gregori et al., 2026a). This seems to be an almost permanent feature during the last $\sim 250\ Ma$, or even more. The reason for this *periodicity* - which however seems to have no equivalent period - seemingly relies in the deep Earth structure combined with the size of the Earth, and as a consequence of a non-linear response to the encounters of the Solar System with interstellar clouds. This gives an indirect justification for some observed correlation with astroblemes. However, this is an apparent correlation, deriving from the fact that a common cause influences both meteoroid recovery in the Oort reservoir, and the geodynamo with all its associated effects.

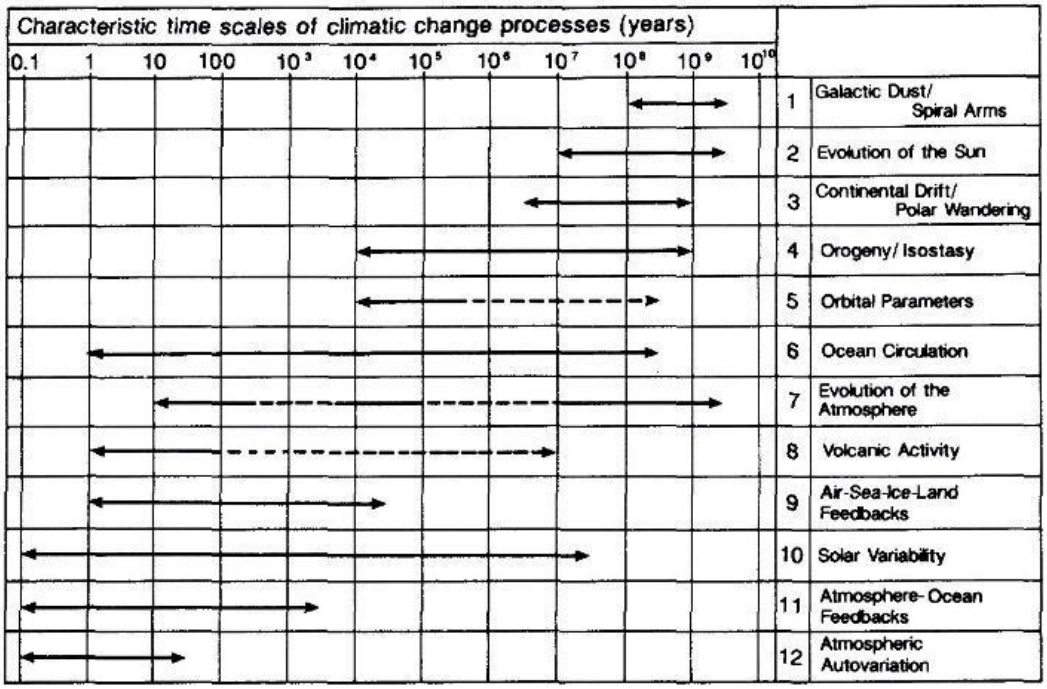

Fig. 14. "*Major mechanisms of climate change and their time scales of operation …* " Figure and caption after Goodess et al. (1992),[39] with data after Wigley et al. (1981). Reproduced with kind permission of Clare Goodess.

We remind about the symbol *PMC* (*planetary mass center*) that is defined by considering the motion of a hypothetical single planetary object with mass equal to all planetary objects except the Sun (altogether *352* objects including planets and asteroids). The *PMC* barycenter is considered, and how it moves relative to the Sun (see Scafetta et al., 2016 for details).

The review by Fairbridge[40] (1996) (that contains several references) is concerned with astrochronology during the last $\sim 15{,}000\ years$ in terms of a specific viewpoint or rationale, whereby the Sun and the planets are considered almost like a unique physical system that displays its own resonances.

In general, resonances are more or less pronounced, and affect several proxy-data series. Fairbridge and Sanders (1987) gives two tables, not here shown.

In particular, the Milanković periods ought to be considered like beats of other fundamental frequencies. That is, the dilemma is on whether *(i)* the Solar System behaves strictly periodically, almost like a high precision

[39] G. P. Gregori is indebted to the late Dr. Michele Conte for this important reference.

[40] Rhodes Whitmore Fairbridge (1914–2006), Australian geologist and expert on climate change.

NCGT Journal
New Concepts in Global Tectonics
New Concepts in Global Tectonics Journal
Volume 14, Number 6, June 2026
ISSN number; ISSN 2202-0039

clock, where every phenomenon is controlled by a strict Lagrangian determinism. The alternative possibility is *(ii)* that the system responds to some unpredictable inputs, although according to some intrinsic chaotic peculiarities. A third possibility *(iii)*, which is envisaged in the present study (Gregori, 2002; Gregori and Leybourne, 2021; Gregori et al., 2026a), is a non-linear process, resulting from an external forcing originated by the encounters with interstellar matter, plus an intrinsic cyclic modulation determined by some thresholds or reservoirs that must be attained or filled up, before triggering specific sequences of other phenomena.

Obviously, the discrimination between all these different possibilities - that, on the other hand, *per se* can even coexist altogether - should require the availability of complete, uniform, and adequately reliable data series. Since, at present, a high-quality database is likely to be beyond our reach - and it is likely to remain a utopia for a long time – we must consider these three possibilities altogether as equally possible explanations. In addition, they can eventually play different comparative roles *vs.* time while they drive different phenomena.

Referring explicitly to the two tables shown by Fairbridge (1996), he reminds about a trefoil recurrence pattern, shown by Charvàtovà (1995). Every leaf of the trefoil takes $19.8593\ years$, hence one full trefoil takes the "*Triad Cycle*" of $59.5779\ years$. Fairbridge (1996) proposes that this trefoil must be repeated three times ($9 \times 19.8593\ years = 178.7338\ years$) to return to the same approximate situation. This should correspond to a period first calculated dynamically by Josè (1965) and corresponding to the *Solar Orbital Precession* (*SOP*). "*During this 'Josè Cycle' the character of the Sunspot Cycle (mean period* $11.1212\ years$*) varies from minimum length (*$\sim 7-10\ year$*) maximum activity (highest 'Wolf number') to maximum length (*$\sim 12-16\ year$*) minimum activity (Fairbridge and Hameed, 1983).*"

Fairbridge and Sanders (1987) plotted *vs.* time the separation between Sun and barycenter of the Solar System during $770\ AD - 2030\ AD$. "*Charvàtovà and Stresik (1993) found that the highly symmetric trefoil sequences corresponded to high solar activity phases and the very irregular ('chaotic') orbital patterns to low activity*" (Fairbridge, 1996). Therefore, solar cycle, solar rotation, and sunspots, ought to respond more or less regularly or chaotically to planetary triggers. *"Sometimes confused with the* $178.73\ year$ SOP *or* 'Josè Cycle' *is a* $177.9392\ year$ *period known as the* 'King-Hele Cycle' *(*K-HC*), which is based on the aphelion/perihelion cycle of Jupiter (*9.8855×18*) and its resonance with the* SSC *(i.e. sunspot cycle,* 11.12×16*). The latter, plotted as positive and negative in its magnetic orientation, generates a* $22\ year$ *period, the* 'Hale Cycle' ... " Also this quotation is from Fairbridge (1996) who also specifies that the *Triad Cycle* $19.85930.88\ years$ "*displays a systematic drift, to repeat at intervals of* $417\ year$ *(*7 Triads*) and* $476\ year$ *(*8 Triads*), to create a* $893.6685\ year$ *cycle*." This is approximately equal to: *48* times the lunar nodal period, *80* times the sunspot cycle, *25* times the Brückner period, *5* times the *SOP*, and *3* times the Saturn-Jupiter-Earth-Venus-lunar resonance of $297.8\ years$. He concludes: "*this is hardly the simplest form of Kepler's 'divine' clockwork ...* "

According to several authors, the cause of several long-period phenomena can be reckoned to the tidal effects by planets on the Sun body, and the associated typical periods are listed in two tables Fairbridge and Sanders (1987).

Some indicative explanation, with no presumption for completeness, is as follows.

Fairbridge and Sanders (1987) consider the orbital periods and angular motion of Jupiter, Saturn, Uranus and Neptune, and the "lap" of couples of planets, i.e. the "beat frequency" (or time requested to recover to an identical relative location), associated also to the phase of the barycenter of the system, which drifts with an angular amount per lap.

Then, they note that *135 Sat/Jup laps* (*SJL*) = *59 Ura/Sat laps* (*USL*) = $2680.65\ years$, which is the resonance drift cycle. In addition, $2680.65\ years = 15 \times 178.71\ years$, and $178.73(\pm 0.27)\ years$ is the Sun's *orbital symmetry progression* cycle (*OSP*) that relates planetary motions to the sunspot cycle (*SSC*). Moreover, $178.71\ years = 3 \times 59.57\ years$, and $59.57\ years$ is the "*OSP Triad Cycle*".

The *SSC* ($11.2 \pm 6\ years$) is such that *OSP/SSC* = 16.07, and *APR/SSC* = 8400, where *APR* is the *all-planet-restart* (93,408 $years$ according to Stacey, 1967).

Other noteworthy relations are:

$$SJL \times 9 = 178.73\ years$$
$$SJL \times 16 = USL$$
$$SJL \times\times 7 = 317.74\ years\ (USJL)$$
$$OSP\ Triad\ Cycle = 59.57\ years$$
$$OSP \times 32 = 288 \times SJL = 126 \times USL = 5719.4\ years$$
$$16 \times OSP = 63 \times USL = 2859.7\ years\ (USJR)$$
$$USJL \times 3 = 953.22\ years$$
$$USJL \times 9 = 2859.7\ years\ (USJR)$$
$$NUL/OSP \cong 4111\ years = 24\ OSP$$
$$NUL \times 13 = 2224\ years$$
$$APR = 21 \times OPR = 545 \times NUL = 2058 \times USL$$
$$= 1568 \times OSP\ Triads$$
$$= 522.67 \times OSP = 4704 \times SJL\ years$$
$$3 \times SJL = 1\ Triad = 59.571\ years$$

Some authors, however, seem to be somewhat concerned about a real leading role played by tidal effects. This item is highly controversial. In this respect, according to the present study, a two-fold warning should be considered. On the one hand, we must take into account the role of the time-varying generation of endogenous heat by the *TD* (tide-driven) geodynamo, i.e. the Earth's *electrocardiogram* (Gregori, 2002; Gregori and Leybourne, 2021; Gregori et al., 2026a). On the other, this mechanism, which is fundamentally powered by a tidal source, is not linear and it is controlled by several others drivers, which determines the rate of power production.

Recall the tentative synthesis of the natural cycles that has been proposed by Mortari (2010), who envisages that several cycles are successive multiples, finally envisaging a cycle of $\sim 180\ Ma$, which could be associated to the estimated $\sim 100-200\ Ma$ cycle of continental generation and subsequent total disappearance by weathering and erosion.

ISSN number; ISSN 2202-0039

The great complication ought to be pointed out of the whole set of possible *periodicities* that could be associated with this peculiar kind of primary trigger. The non-linearity of the "climate" system must be emphasized, combined with the much indirect evidence inferred from every given observed phenomenon when it is considered alone.

In addition, the observational database is affected either by *(i)* the simultaneous variously amplified resonance and/or by *(ii)* the time-delayed effects that result from the overlapping of different concurrent causes, drivers, and control factors, which at different times play a different percent role in affecting the given phenomenon, etc. Therefore, one can envisage no simple thumb rule concerning natural *periodicities*. For a more general discussion of the universe from a wider perspective refer to Gregori et al. (2025w), and to the more plain account given in Gregori and Gregori (2025).

Appendix - Walsh and related functions

It is sometimes convenient to define a set of orthonormal base-functions that are step-functions, rather than continuous functions. They are extensively used for designing electronic devices and have been used also in seismology (instead of Fourier analysis) in order to save computer memory and computing time, and to use microprocessors (see references given in Beauchamp, 1984 or, for an application to the Earth gravitational potential, Meng and Cai, 1992).

A wide choice of different functions of this class can be found in the literature. Refer to Beauchamp (1984), while a more extensive mathematical treatment is Golubov et al. (1987). These functions are defined in a finite domain that - unless otherwise stated - will be supposed $0 \leq t \leq 1$ (the independent variable will be here called t, since time is the most usual case when dealing with these functions).

Let us recall the *Rademacher (1922) functions*, and the *Walsh (1923) functions* (which are, maybe, the best known of this class). In general, they look like complete sets of "*rectangular wave*" functions, taking two amplitudes $+1$ or -1. The *Haar (1910) functions* are a complete set of "*rectangular wave*" forms, and have several advantages, including a faster convergence of the series expansions when dealing with specific applications.

Several other choices were proposed to deal specifically with some given problems, for seeking faster convergence series. For instance, *slant functions* (Enomoto and Shibata, 1971; Pratt et al., 1972; Shibata, 1972; and Fino and Algazi, 1974) were specifically envisaged for image transmission purposes. They permit to compact the image energy into only a few functions, thus improving transmission efficiency.

Another set of orthogonal functions is the *Karhunen-Loève series* (Ahmed and Rao, 1975) that have specific advantages for some applications, but (compared with the previous sets) have a few other computational drawbacks. *Hybrid series* (i.e., making mixed use of *Walsh* and *Haar functions*) were proposed by Rao et al. (1975) and by Huang (1980).

Some extensive formal investigations were developed on all these step functions. Harmuth (1972) proposed the term "*sequency*" as *"one-half of the average number of zero crossings per unit time interval*". When a set of functions is ordered according to their respective sequency, this is called a *sequency ordering*.

Different ways of ordering the *Walsh functions* are used, depending on whether they are needed for theoretical use or for a specific application. The three best known ordering criteria are as follows.

- The *sequency order*, or "*ordered form*", or "*Walsh order*", or "*Walsh-Kaczmarz order*", that was originally used by Walsh.
- The *dyadic order*, or *Paley order*, originally proposed by Paley (1932), is based on the generation of *Walsh function* by successive *Rademacher's functions*.
- The *natural order*, or *Hadamard order* (or *Kronecker order*), that follows from the generation of the *Walsh functions* by means of the *Hadamard matrix*. The *Walsh functions*, when ordered in this way, were formerly proposed by Henderson (1970).

A few additional ways of *ordering* are mentioned by Beauchamp (1984) who gives also the respective references. The way of *ordering* can result important for specific theoretical derivations.

The phasing of an ordering is concerned with the criterion dealing with the choice of the phase of every ordered *Walsh function*. For instance, the *sequency* order (which resembles the standard phasing of sine and cosine functions) is called *Harmuth phasing*, unlike the *dyadic* or the *natural order*, which implies that all functions start at the level $+1$. Hence, they are said to use a *positive phasing*.

The *Walsh functions* can be generated in different ways. Formal recurrence relations can be derived in different ways (see Beauchamp, 1984 for details).

Formal relations between these *ordered* functions are reported in the literature (see Beauchamp, 1984; e.g. Pichler, 1968 and Tam and Goulet, 1972).

Analogous results hold for the *Harr functions*.

An interesting analogy with the sine and cosine functions is concerned with the Nyqvist limit implied by the sampling theorem. Namely, for sine and cosine functions a sampling rate is needed of at least 2ν (where ν is the maximum frequency that one wants to consider). In the case of the *Walsh* and *related functions*, the situation is worse than in the sine and cosine case (Kac, 1970). In fact, if one wants to consider a maximum frequency ν, first find out the smallest power of 2, say 2^k, such that $2k > \nu$. Then, the sampling rate needed must be at least $2k + 1$.

The relative advantages and disadvantages of a standard Fourier approach, or of using the *Walsh* and *related functions*, were discussed by Beauchamp (1973) and by Risch and Brubaker (1973).

Beauchamp (1984) contains also a discussion of the generalization of the *FFT* to the case of *Walsh* and *related functions*, as well as of the analysis analogous to Fourier analysis, of correlation and convolution, of spectral analysis (or, more exactly, of *sequency* analysis), of digital filtering, of aliasing, etc. The problem sometimes is much more than

ISSN number; ISSN 2202-0039

a simple generalization by analogy, implying some substantial new theoretical aspects.

It is impossible to give in a few pages an idea of all the theoretical developments and different applications. The few mentions here given aim to be just a simple indication of the existence of such an entire theory. The formal development of the theory given by Golubov et al. (1987) is even more extensive than the account given in Beauchamp (1984).

Acknowledgements

G. P. Gregori feels particularly indebted to the late Prof. John W. Tukey for his crucial suggestions. G. P. Gregori feels honored for his input.

We thank all friends and colleagues who, in different ways, and at different times during several decades, contributed to the exploitation of the ideas that are here expressed.

Author's Contributions

G. P. Gregori has the main responsibility, and initiative based on several decades of reflection. B. A. Leybourne contributed to the final drafting of the paper. This entire study derived from a long-lasting cooperation with several scientists and resulted from the emergence of true long-lasting discussions.

Funding Information

All investigations here mentioned were carried on our own support. G. P. Gregori was supported by his professional employment. B. A. Leybourne is a semi-retired self-funded independent researcher.

Data Availability Statement

No specific data are considered.

Ethics

This article is original and contains unpublished material. Authors declare that there are not ethical issues and no conflict of interest that may arise after the publication of this manuscript.

References

Ahmed, N., and K. R. Rao, 1975. *Orthogonal transforms for digital signal processing*. Springer-Verlag, Berlin.

Alessandrini, B., G. F. Papi, G. de Franceschi, and G. P. Gregori, 1987. The secular variation of the geomagnetic field and the shape of the Earth. *Physics of the Earth and Planetary Interiors*, 48: 84-114; DOI:10 .1016/0031-9201(87)90114-2

Anderson, D. L., 1974. Earthquakes and the rotation of the Earth, *Science*, **186**, 49–50; DOI:10.1126/science.186.4158.49.

Arley, N., and K. R. Buch, 1950. *Introduction to the theory of probability and statistics*. Science Editions, John Wiley and Sons, Inc., New York; pp: 1-240.

Banzon, V. P., G. de Franceschi, and G. P. Gregori, 1992. The mathematical handling and analysis of non-homogeneous and incomplete multi-variate historical data series. In B. Frenzel, (ed.), *Paläoklimaforschung-Palaeoclimate Research*, (Spec. issue: *ESF* Project-European Palaeoclimate and Man 2, Proceedings of the *ESF* Meeting on *Climate in Europe in the last 10000 years*, Mainz, Germany, March 1990). Akademie der Wissenschaften und der Literatur, Mainz, European Science Foundation, Strasbourg, and Gustav Fischer Verlag, Stuttgart, Jena, and New York; pp.: 137-150.

Banzon, V. P., M. Colacino, G. de Franceschi, L. Diodato, G. P. Gregori, M. P. Pavese, and R. Santoleri, 1990. Tiber floods, anomalous climatic events in the upper Po valley, and volcanic activity. In W. Schrˆder, (ed.), *Advances in geosciences*. Interdivisional Commission on History of IAGA, Bremen-Roennebeck; pp: 73-79.

Banzon, V.P., G. P. Gregori, R. Leonardi, G. de Franceschi, and Wei-Chyung Wang, 1992a. An analysis of the *510* year data series of the dryness/wetness index for *120* regions of China. In W. Schrˆder, and J.-P. Legrand, (eds), *Solar terrestrial variability and global change,* Interdivisional Commission on History of IAGA, Bremen-Roennebeck, pp.: 223-238.

BÂth, M., 1974. *Spectral analysis in geophysics*. Elsevier Scientific Publ. Co., Amsterdam etc.; pp.:1-563.

Beauchamp , K. G., 1984. *Applications of Walsh and related functions, with an introduction to sequency theory*, Academic Press, London, etc.; pp.:1- 308.

Beauchamp, K. G., 1973. Waveform synthesis using Fourier and Walsh series, *Proc. Theory Applic. Walsh Functions*, Hatfield Polytechnic, England.

Bendick, R., and R. Bilham, 2017. Do weak global stresses synchronize earthquakes? *Geophys. Res. Lett.*, 44: 8320–8327; DOI:10. 002/2017GL074934

Berger, A., S. Schneider, and J. Cl. Duplessy, (eds), 1989. *Climate and geosciences. A challenge for science and society in the 21st century*, Kluwer Acad. Press, Dordrecht etc.; pp.:1-724.

Brillinger, D. R., 1975. Statistical inference for stationary point processes. In M. L., Puri, (ed.), *Stochastic processes and related topics*, Academic Press, New York; pp.: 55-99.

Brillinger, D. R., 1975a. *Time series: data analysis and theory*. Holt, Reinhart and Winston, New York.

Brillinger, D. R., 1976a. Estimation of the second-order intensities of a bivariate stationary point process, *J. R. Statist. Soc., Ser. B, (Methodol.)*, 38, (1): 60-66.

Brillinger, D. R., 1976b. Measuring the association of point processes: a case history, *Am. Math. Month*., 83, (1): 16-22.

Brillinger, D. R., 1979. Analyzing point processes subjected to random deletions, *Can. J. Statist*., 7, (1): 21-27.

Brillinger, D. R., H. L. Bryant, and J. P. Segundo, 1976. Identification of synaptic interactions, *Biol. Cybernetics*, 22, 213-228.

ISSN number; ISSN 2202-0039

Bryant, H. L. A. R. Marcos, and J. P. Segundo, 1973. Correlations of neuronal spike discharges produced by monosynaptic connections and common inputs, *J. Neurophysiol.*, 36: 205-225.

Bullard, F. M., 1984. *Volcanoes of the Earth*. II Revised Edition, University of Texas Press, Austin; pp.:1-.629.

Cai, Wenju, T. Cowan, and M. Raupach, 2009. Positive Indian Ocean Dipole events precondition southeast Australia bushfires, *Geophys. Res. Lett.*, 36: L19710 [6 pp.]; DOI:10.1029/2009GL039902.

Castillo, E., 1988. *Extreme values theory in engineering,* Academic Press, London etc.; pp.:1-404.

Central Meteorological Institute. Peking University, Nanking University, etc., 1981. *Yearly Charts of Dryness/Wetness in China for the last 500-year period*, Atlas Press; pp.:1-332.

Chapman, S., and R. S. Lindzen, 1970. *Atmospheric tides. Thermal and gravitational*. D. Reidel Publishing Co., Dordrecht; pp.:1-200.

Charvátová, I., 1995. Solar-terrestrial and climatic variability during the last several millennia in relation to solar inertial motion, *J. Coastal Res*., 17: 343–354.

Charvàtovà, I., and J. Střeštík, 1993. Long-term climatic changes in connection with solar motion. In E. Ruzickovà, and A. Zeman, (eds). *PAGES-Stream I.* Prague: Acad. Sci. Czech., Rep., Geol. Inst.; pp.: 47-54.

Christensen-Dalsgaard, J., and S. Frandsen, 1988. Advances in helio- and asteroseismology, *Proc. of the 123th IAU symp.,* Aarhus, Denmark, July 7-11, 1986. D. Reidel Pubì. Co.; pp.:1-604.

Colacino, M., G. P. Gregori, M. R. Valensise, F. Chiarini, and M. Mastrogregori, 1988. Climate as a historiographical problem. In W. Schrˆder, (ed.). *Past, present and future trends in geophysical research*. 342 pp., Interdivisional Commission on History of IAGA, Bremen-Roennebeck; pp.: 212-249.

Courant, R., and D. Hilbert, 1953. *Methods of mathematical physics. Vol*. I, 561 pp., *Vol.* II, *Partial differential equations*. 830 pp., Interscience Publishers, New York and London. First published in German, *Methoden der mathematischen Physik*, Berlin, 1924.

Cox, Sir D. R., and H. D. Miller, 1965. *The theory of stochastic processes*, Methuen and Co., Ltd., London-New York; pp.:1-398.

Cramér, H., 1954. *Mathematical methods of statistics*. Princeton University Press, Princeton, N. J.; pp.:1-575.

Eddy, J. A., 1978. *The new solar physics,* AAAS Selected Symposium 17, Westview Press, Boulder, Co.; pp.:1-214.

Enomoto, H., and K. Shibata, 1971. Orthognal transform coding system for television signals, *Proc. Applic. Walsh Functions*, Washington, D.C., AD727000: 11-17.

Eriksson, C., A. Omstedt, J. E. Overland, D. B. Percival, H. O. Mofjeld, 2007. Characterizing the European sub-arctic winter climate since 1500 using ice, temperature, and atmospheric circulation time series, *J. Climate*, 20, (21): 5316–5334. DOI:10.1175/2007JCLI1461.1

Fairbridge, R. W., 1996. Spectra of solar-terrestrial proxies (auroras, tree rings, varves, ice cores), and a proposed astrochronology of the last 15,000 years. In W.Schrˆder and M. Colacino, (eds). Global change and history of geophysics. *Mitteilungen des Arbeitskreises Geschichte der Geophysik der DGG*, 15, Jahrgang (1996), (1-4): 89-1121-291. Science Edition / IDCH-IAGA / AKGGKP (Arbeitskreis Geschichte der Geophysik und Kosmischen Physik der DDG), Bremen-Roennebeck and Potsdam.

Fairbridge, R. W., and J. E. Sanders, 1987. The Sun's orbit, AD 250-2050: basis for new perspectives on planetary dynamics and Earth-Moon linkage. In M. R.,Rampino, J. E. Sanders, W. S. Newman, and L. K. Kˆnigsson, (eds). *Climate-history, periodicity, and predictability*, 588 pp., Van Nostrand Reinhold, New York; pp.: 446-471: bibliography: 475-541.

Fairbridge, R. W., and S. Hameed, 1983. Phase coherence of solar cycle minima over two 178-year periods. *Astron. J*., 88, (6): 867-869.

Ferrari, A., 2002. Enrico Fermi astrofisico. *Giorn. Astr*., 29, (2): 2-7.

Fino, B. J., and V. R. Algazi, 1974. Slant Haar transform, *Proc. IEEE (Lett.)*, 62: 653-654.

Fiorentino, E-, G. P. Gregori, G. de Franceschi, B. Alessandrini, M. Colacino, A. Guerrini, A. Meloni, R. Purini, R. Santoleri, M. Silvestri and C. Valenti, 1988. Multi-variate analysis of historical data series. In W. Schrˆder, (ed.), *Past, present and future trends in geophysical research*, Interdivisional Commission on History of IAGA, Bremen-Roennebeck; pp.: 251-318.

Fischer, A. G., 1986. Climate rhythms recorded in strata. *Ann. Rev. Earth Planet. Sci*., 14: 351-376.

Ford, E. A. K., R. E. Hibbins, and M. J. Jarvis, 2009. QBO effects on Antarctic mesospheric winds and polar vortex dynamics, *Geophys. Res. Lett.*, 36 : L20801 [6 pp.]; DOI:10.1029/2009GL039848

Fougère, P. F., (ed.), 1990. *Maximum entropy and Bayesian methods*, Kluwer Acad. Publ., Dorcrecht etc.; pp.:1-480.

Frick, P., A. Grossman, and P. Tchamitchian, 1998, Wavelet analysis of signals with gaps. *J. Math. Phys.* ,39: 4091.

Frick, P., S. L. Baliunas, D. Galyagin, D. Sokoloff, and W.Soon, 1997, Wavelet analysis of stellar chromospheric activity variations. *Astrophys. J.:* 483, (1): 426-483; DOI 10.1086/304206

Galambos, J., 1978. *The asymptotic theory of extreme order statistics*, John Wiley & Sons Inc.; pp.:12-368.

Ge, Quansheng, Wang Shaowu, Wen Xinyu, and Hao Zhixin, 2007. Climate change during the Holocene in China, *China Nat. Rep. Met. Atmos. Sci. (2003-2006)*, Report No.11 [to *IUGG* General Assembly, Perugia], 26 pp.

Ghil, M., M. R. Allen, M. D. Dettinger, K. Ide, D. Kondrashov, M. E. Mann, A. W. Robertson, A. Saunders, Y. Tian, F. Varadi, and P. Yiou, 2002. Advanced spectral methods for climatic time series, *Rev. Geophys.*, 40, (1): 1003; DOI:10.1029/2000RG000092

Giosan, L., D. Q. Fuller, K. Nicoll, R. K. Flad, and P. C. Clift, (eds), 2012. Climates, landscapes, and civilizations, *Geophys. Monograph Ser*., 198, AGU, Washington, D. C.; pp.:1-226

Godin, G., 1972. *The analysis of tides*. University of Toronto Press; pp.:1-264.

Golubov, B., A. Efimov, and V. Skvortsov, 1991. *Walsh series and transforms*, Kluwer Academic Publishers, Dordrecht, etc; pp-:1-368. Translation of "*Riad'i i preobrzobaniia Woltsha-Teoria i primeneniia*", Nauka, Moscow, 1987.

Goodess, C. M., J. P. Palutikof, and T. D. Davies, 1992. *The nature and causes of climate change. Assessing the long-term future*. Behaven Press, London, and Lewis Publishers, Boca Raton, Ann Arbor; ISBN 1852932295; pp.:1-248.

Gregori, G. P., 1990. A Few Mathematical Procedures for the Analysis of Incomplete Historical Data Series. In W. Schrˆder (ed.), *Advances in geosciences*, Interdivisional Commission on History of IAGA, Bremen-Roennebeck, pp: 80-127

Gregori, G. P., 1993. Geo-electromagnetism and geodynamics: "corona discharge" from volcanic and geothermal areas. *Physics of the Earth and Planetary Interiors*, 77: 39-63; DOI:10 .1016/S0031-9201(02)00211-X

Gregori, G. P., 1996. The next eruption of Somma-Vesuvius. In V. Piccione, and C. Antonelli (eds), *Proceedings of the 4th Workshop of Progetto Strategico Clima, Ambiente e Territorio nel Mezzogiorno*, Lecce, November 11-14, 1991, 2 vol., CNR, Roma; pp.: 399-468

Gregori, G. P., 1996a. Satellite, volcanoes, and global change. *Earth Space Review*, 5, (1), 17-26.

Gregori, G. P., 1997. Historical data and global change. Case studies. In W. Schrˆder (ed.), Physics and Geophysics with Special Historical Case Studies (A Festschrift in Honour of Karl-Heinrich Wiederkehr). *Mitteilungen des Arbeitskreises Geschichte der Geophysik der DDG*, 16, Jahrgang (1997): (2/5): and Newsletter of IDCH-IAGA, (25), Science Edition / IDCH-IAGA / AKGGKP (Arbeitskreis Geschichte der Geophysik und Kosmischen Physik der DDG): Science Edition, Bremen Roennebeck and Potsdam, pp: 183-210

Gregori, G. P., 2001. Self-consciousness in Earth's sciences - Some personal reflections. In W. Schrˆder (ed.), Wege zur Wissenschaft, Gelehrte erz‰hlen aus ihrem Leben – Pathways to science, Scientists tell of their life and work, *Beiträge zur Geschichte der Geophysik und Kosmischen Physik des Arbeitskreises Geschichte der Geophysik und Kosmischen Physik*, (4), W. Schrˆder, AKGGKP, Bremen-Roennebeck, pp: 123-133

Gregori, G. P., 2002. Galaxy – Sun – Earth relations. The Origin of the Magnetic Field and of the Endogenous Energy of the Earth, with Implications for Volcanism, Geodynamics and Climate Control, and Related Items of Concern for Stars, Planets, Satellites, and Other Planetary Objects. A Discussion in a Prologue and Two Parts. *Beiträge zur Geschichte der Geophysik und Kosmischen Physik*, Band 3, Heft 3: pp. 1-471 [Available at http://ncgtjournal.com/additional-resources.html]

Gregori, G. P., 2004. The geodynamo and Galaxy–Sun–Earth relations. Implications for geodynamics, climate, and for the origin of the magnetic field of planets, satellites, and larger celestial bodies. In *Schröder (2004)*, 161-165.

Gregori, G. P., 2006e. The Earth's interior-Myth and science. In Case studies in physics and geophysics. W. Schrˆder, (ed.), *Beiträge zur Geschichte der Geophysik und Kosmischen Physik*, special issue (2006/2), (*Journal for the history of Geophysics and Cosmical Physics*), Science Editions, AKGG, Bremen-Roennebeck; pp: 108-126

Gregori, G. P., 2009. The Earth's interior – Myth and science, *New Concepts in Global Tectonics, Newsletters*, (53): 57-75. [Revised edition of Gregori (2006e).]

Gregori, G. P., A. Incoronato, and M. Marino, 2025y. Search for a stroboscopic effect in the geomagnetic secular variation (*SV*)- Superrotation and geodesy of the inner core (*IC*). *New Concepts in Global Tectonics, Journal*, 13, (5): 682-710.

Gregori, G. P., and B. A. Leybourne, 2021. An unprecedented challenge for humankind survival. Energy exploitation from the atmospheric electrical circuit, *American Journal of Engineering and Applied Science*, 14 (2): 258-291; DOI:10.3844/ajeassp.2021.258.291

Gregori, G. P., and B. A. Leybourne, 2025i. Wildfires from the Banda Sea through Beijing and through Karakoram. *New Concepts in Global Tectonics, Journal,* 13, (6): 854-887

Gregori, G. P., and B. A. Leybourne, 2025j. The energy supply to hurricanes. *New Concepts in Global Tectonics, Journal,* 13, (5): 731-786

Gregori, G. P., and B. A. Leybourne, 2026c. The solar cycle and MiniMax - Effects on other planets. *New Concepts in Global Tectonics, Journal,* 14, (4): 362-387

Gregori, G. P., and B. G. Gregori, 2025. *The universe out of the box - New foundations of physics - Rhythms, Golden Ratio, origin of life, antifragility*, Europe Books, pp: 1-306

Gregori, G. P., and L. G. Gregori, 1996. Viewpoints in archæoastronomy. An invitation to the prehistory of Earth's science. In Schrˆder, W., and M. Colacino, (eds). Global change and history of geophysics. *Mitteilungen des Arbeitskreises Geschichte der Geophysik der DGG*, 15, Jahrgang (1996), (1-4), Science Edition / IDCH-IAGA / AKGGKP (Arbeitskreis Geschichte der Geophysik und Kosmischen Physik der DDG), Bremen-Roennebeck and Potsdam, p.: 228-288

Gregori, G. P., and L. G. Gregori, 1997. Archæoastronomy II-An invitation to the prehistory of environmental science. In Schrˆder, W., (ed.), Geomagnetism and aeronomy (with special historical case studies), *IAGA Newsletter 29/1997*, Science Edition / *IDCH* of *IAGA* / *AKGGKP* (Arbeitskreis Geschichte der Geophysik und Kosmischen Physik der *DDG*), Bremen-Roennebeck and Potsdam, p.: 6-64

Gregori, G. P., and L. G. Gregori, 1998. Solar-terrestrial relations. A reminder. *Acta Geodaetica et Geophysica Hungarica*, 33 (2/4): 391-459; DOI:10.1007/BF03325551

Gregori, G. P., and L. G. Gregori, 1999. Prehistory of geophysics, anthropology, and archaeoastronomy. In W. Schrˆder, (ed.), Physics and Geophysics (A Compilation with Special Historical Case Studies), History Commission of the German Geophysical Society, *Mitteilungen des Arbeitskreises Geschichte der Geophysik der DGG*, 18, Jahrgang (1999), Heft 1-3, Science Edition/DGG, Bremen; pp.: 246-267

Gregori, G. P., and L. G. Gregori, 2000. Archæoastronomy (an updating), and anthropological aspects of architecture. With an Appendix on "Architectural symmetries in ancient circular or semicircular buildings" (by L. G. Gregori). In Schrˆder, W., (ed.). Geomagnetism (research, past and present), *Newletter of the IDCH of IAGA*, (40), Science Edition, Bremen-Roennebeck, p.: 188-224

Gregori, G. P., and L. G. Gregori, 2003. Archæoastronomy and the study of global environmental change. *Riv. Ital. Archeoastron.,* 1, 3-20.

Gregori, G. P., and M. T. Hovland, 2025. Go for the anomaly – a golden strategy for discovery? Seepology & the origin and crucial role of the biosphere - Earth and planetary objects - Supercritical water and serpentinization. *New Concepts in Global Tectonics, Journal,* 13, (9): 1337-1491

Gregori, G. P., B. A. Leybourne, and J. R. Wright, 2026c. The solar cycle and MiniMax. *New Concepts in Global Tectonics, Journal,* 14, (4): 323-361

Gregori, G. P., B. A. Leybourne, Dong Wenjie, and Gao Xiaoqing, 2025f. The Tang Maocang school. The uplift of Himalaya – shallow geotherms – palæoclimate – endogenous heat. *New Concepts in Global Tectonics, Journal,* 13, (8). 1026-1039

Gregori, G. P., B. A. Leybourne, Dong Wenjie, and Gao Xiaoqing, 2025g. The timing of the uplift of Himalaya and the Third Pole. *New Concepts in Global Tectonics, Journal,* 13, (8): 1040-1079

Gregori, G. P., B. A. Leybourne, Dong Wenjie, and Gao Xiaoqing, 2025h. Shallow geotherms. *New Concepts in Global Tectonics, Journal,* 13, (8): 1080-1169

Gregori, G. P., B. A. Leybourne, G. Paparo†, and M. Poscolieri, 2026a. The global Sun-Earth circuit. *New Concepts in Global Tectonics, Journal,* 14, (4): 234-272

Gregori, G. P., G. M. Gregori, G. Iannone, and B. A. Leybourne, 2026e. The rejection of outliers, *New Concepts in Global Tectonics, Journal*, 14, (6): present issue.

Gregori, G. P., M. Colacino, M. R. Valensise, and L. G. Gregori, 2000. Why a history of geophysics? In W. Schrˆder (ed.), *Geschichte und Philosophie der Geophysisk (History and Philosophy of Geophysics)*, Beitr%ge zur Geschichte der Geophysik und Kosmischen Physik der DDG, 2, and Newsletter of IDCH-IAGA (42), W. Schrˆder, and AKGGKP (Arbeitskreis Geschichte der Geophysik und Kosmischen Physik der DDG), Bremen-Roennebeck and Potsdam; pp.: 112-122

Gregori, G. P., M. T. Hovland, B. A. Leybourne, S. Pellis, V. Straser, B. G. Gregori, G. M. Gregori, and A. R. Simonelli, 2025w. Air-earth currents and a universal "law": filamentary and spiral structures - Repetitiveness, fractality, golden ratio, fine-structure constant, antifragility and "statistics" - The origin of life, *New Concepts in Global Tectonics, Journal*, 3, (1): 106-225

Gregori, G. P., Michele Colacino, Wilfried Schrˆder, and Lucia G. Gregori, 2000a. Mankind *vs.* environment-echoes from the past, and present challenges. In W. Schröder, (ed.). Long and short term variability in Sun's history and global change. *Newsletter of IDCH-IAGA*, (39): 302-318. Science Edition, Bremen-Roennebeck, Germany.

Gregori, G. P., R. Santoleri, M. P. Pavese, M. Colacino, E. Fiorentino and G. de Franceschi, 1988. The analysis of point-like data series. In W. Schrˆder (ed.), *Past, Present and Future Trends in Geophysical Research,* Interdivisional Commission on History of IAGA, Bremen-Roennebeck, pp.: 146-211

Gregori, G. P., V. Banzon, and R. Leonardi, 1994. The cycles of volcanoes, and the global synchronism of the time variation of their heat source. In W. Schrˆder, and M. Colacino (eds), Geophysics: past achievements and future challenges. *Newsletter of IDCH-IAGA*, (20), Science Edition / IDCH of IAGA, Bremen-Roennebeck, pp 152-191.

Gregori, G. P., V. P. Banzon, R. Leonardi, and G. de Franceschi, 1992. Geomagnetic activity versus volcanic cycles and their forecasting. Application to Etna and Vesuvius. In W. Schrˆder, and J.-P. Legrand, (eds), Solar Terrestrial Variability and Global Change,: IDCH of IAGA, Bremen-Roennebeck, pp: 188-222

Gregori, L. G., 1997a. The myth of Hephaestus and the activity of the island of Vulcano. In W. Schrˆder, (ed.). Geomagnetism and aeronomy (with special historical case studies), *IAGA Newsletter* 29/1997, Science Edition / IDCH of IAGA / AKGGKP (Arbeitskreis Geschichte der Geophysik und Kosmischen Physik der DDG), Bremen-Roennebeck and Potsdam; pp. 295-314.

Gregori, L. G., and G. P. Gregori, 1999a. The consciousness of time and the conquest of space. The dawn of civilisation, anthropology, and archaeoastronomy. *Annals of the New York Academy of Sciences*, 879: 158-163

Gregori, L. G., and G. P. Gregori. 1996a. The knowledge of territory in ancient civilisations. Temples and sacred sites as prehistoric geodetic networks? *Archeologia e Calcolatori*, 7: 193-212.

Griffith, J. S., and Dr. G. Horn, 1963. Functional coupling between cells in the visual cortex of the unrestrained cat. *Nature,* 199: 876-876 and 893-895.

Gumbel, E. J., 1958. *Statistics of extremes*, Columbia University Press, New York and London; pp.: 1-375.

Gusev, A. A. 2008. On the reality of the 56-year cycle and the increased probability of large earthquakes for Petropavlovsk-Kamchatskii during the period 2008–2011 according to lunar cyclicity, *J. Volc. Seism*., 2, (6): 424-434. Original Russian text in *Vulkanologiya i Seismologiya*, 2008, (6): 55–65.

Haar, A., 1910. Zür Theorie der orthogonalen Funktionenesysteme, *Math. Annal*., 69: 331-371.

ISSN number; ISSN 2202-0039

Hansen, J. R., and R. A. Goldberg, 1978. *Sun, weather and climate*. NASA SP-426, Washington, D.C.; pp.:1-360.

Harmuth, H. F., 1972. *Transmission of information by orthogonal functions*, 2nd ed., Springer-Verlag, Berlin.

Henderson, K. W., 1970. Comment on "Computation of the fast Walsh-Fourier transform", *IEEE Trans. Comput*., C-19: 850-851.

Hovland, M. T., 2026. The 18 best discoveries I have done (together with others), *New Concepts in Global Tectonics, Journal*, 14, (5): 395-406.

Huang, D. M., 1980. Walsh-Hadamard-Haar hybrid transforms, *IEEE Proc. Int. Conf. Pattern Recognition, 5th*: 180-182.

Imbò, G., 1928. Variazioni cicliche nella successione dei periodi di riposo etnei. *Bull. Volcanologique*, (15/18): 80-88.

Jaggar, T. A., 1931. Volcanic cycles and sunspots. *Volcano Lett*., (326).

Jenkinson, A. F. (1969), Estimation of maximum floods, World Meteorological Organization, *Technical Note* No 98, ch. 5: 183-257.

Jevrejeva, S., A. Grinsted, J. C. Moore, and S. Holgate, 2006. Nonlinear trends and multiyear cycles in sea level records, *J. Geophys. Res.: Oceans (1978–2012)*, 111, (C9) : C09012 [11pp.]; DOI:10.1029/2005JC003229

José, P. D., 1965. Sun's motion and sunspots. *Astron. J*., 70, (3): 193-200.

Kac, S. C., 1970. Sampling theorem in Walsh-Fourier analysis, *Electron. Lett*., 6, (14): 447-448.

Karlstrom, L., S. Hurwitz, R. Sohn, J. Vandemeulebrouck, F. Murphy, M. L. Rudolph, M. J. S. Johnston, M. Manga, and R. B. McCleskey, 2013. Eruptions at Lone Star Geyser, Yellowstone National Park, USA: 1. Energetics and eruption dynamics, *J. Geophys. Res. Solid Earth,* 118: 4048–4062; DOI:10.1002/jgrb.50251

Kay, S. M., and S. L. Marple, 1981. Spectrum analysis-a modern perspective. *Proc. IEEE*, 69, (11): 5-51.

Ke, Zongjian, Wenjie Dong, Peiqun Zhang, Jin Wang, and Tianbao Zhao, 2009. An analysis of the difference between the multiple linear regression approach and the multimodel ensemble mean, *Adv. Atmosph. Sci.*, 26, (6): 1157; DOI:10.1007/s00376-009-8024-8

Kendall, M. G., and A. Stuart, 1969, 1973, 1968. *The advanced theory of statistics: vol. 1-Distribution theory,* (third edition), 439 pp., 1969, *vol. 2-Inference and relationship,* (third edition), 723 pp., 1973, *vol. 3 - Design and analysis, and time series* (second edition), *557* pp., 1968, Charles Griffin and Co., Ltd., London.

Kopecky, M., 1996. The maximum Wolf's sunspot numbers of 11-year cycles during the 16th, 17th and 18th century. In W. Schrˆder, and M. Colacino (eds), Global change and history of geophysics. *Mitteilungen des Arbeitskreises Geschichte der Geophysik der DGG,* 15, Jahrgang (1996), (1-4): pp 113-116. Science Edition / IDCH-IAGA / AKGGKP (Arbeitskreis Geschichte der Geophysik und Kosmischen Physik der DDG), Bremen-Roennebeck and Potsdam.

Kuhn, T. S., 1962 or 1970. *The structure of scientific revolutions*, Univ. of Chicago Press, Chicago; pp.:1-210.

Kulhanek, O., 1976. *Introduction to digital filtering on geophysics*. Elsevier Publ. Co., Amsterdam, etc.; pp.:1-168

Lamb, H. H., 1972. *Climate: present, past and future. Volume 1, Fundamentals and climate now*. Methuen and Co. Ltd, London; pp.:1-613.

Lawrence, R. J., 1988. The lognormal as event-time distribution. In E. L. Crow, and K. Shimizu (eds). *Lognormal distributions. Theory and applications*. 387 pp., Marcel Dekker. Inc., New York and Basel; pp.: 211-228.

Lee, W. H. K., and D. R. Brillinger, 1979. On Chinese earthquake history-An attempt to model an incomplete data set by point process analysis, *Pure Appl. Geophys*., 117: 1229-1257.

Liang, X. San, 2014. Unraveling the cause-effect relation between time series, *Phys. Rev*., E 90: 052150; DOI:10.1103/PhysRevE.90.052150

Liao, M., and T. Shimokawa, (1999. A new goodness-of-fit test for type-I extreme-value and 2-parameter weibull distributions with estimated parameters. *Journal of Statistical Computation and Simulation*, 64, (1): 23–48. https://doi.org/10.1080/00949659908811965

Lin, Xuechun; Yu Shuqiu, and Tang Guoli, 1995. Series of average air temperature over China for the last 100-year period, *Scientia Atmospherica Sinica*, (05); DOI:cnki:ISSN:10069895.0.1995-05-001

Lisitzin, A. P., 1974. *Osadkoobrazovanie v Okeanach*, Izdatelstvo Nauka, Moscow; pp.:1-438.

Lockwood, J. P., 1995. Mauna Loa eruptive history. The preliminary radiocarbon record. In J. M., Rhodes, and J. P. Lockwood, (eds), Mauna Loa revealed: structure, composition, history, and hazards, *Geophysical Monograph*, 92: 1-360.

Man, Z., 1998. Climate in Tang dynasty of China: discussion for its evidence, *Quaternary Sci*., (01); DOI:cnki:ISSN:1001-7410.0.1998-01-003

Marino, M., 2004. Analisi in armoniche sferiche del campo geomagnetico e ipotesi della rotazione differenziale del nucleo interno terrestre. *Thesis*, *Università degli Studi di Napoli "Federico II"*.

Mazur, N. G., V. A. Pilipenko, and K.-H. Glassmeier, 2008. Methods to detect solitons in geophysical signals: the case of the derivative nonlinear Schrˆdinger equation. In R. V.Donner, and S. M. Barbosa, (eds). Nonlinear time series analysis in the geosciences - Applications in climatology, geodynamics and solar-terrestrial physics, *Lecture Notes in Earth Sciences*, 112, Springer-Verlag, Berlin and Heidelberg; pp.: 311-326; DOI:10.1007/978-3-540-78938-3_14.

Melchior, Baron P., 1978. *The tides of the planet Earth*. Pergamon Press, Oxford, etc.; pp.:1-609.

Meng, Jiachun, and Cai Ximei, 1992. Walsh-Fourier series expansion of the Earth's gravitational potential. In O. L.Colombo, (ed.). *From Mars to Greenland: charing gravity with space and airborne instruments. Fields, tides, methods, results*. Springer-Verlag, New York etc.; pp.: 339-347.

ISSN number; ISSN 2202-0039

Moore, J. C., A. Grinsted, and S. Jevrejeva, 2005. The new tools for analyzing the time series relationships and trends, *EOS, Trans. Am. Geophys. Un*., 86, (24): 226.

Mortari, R., 2010. *I ritmi segreti dell'universo*, pp.:1-336, (III ed.) Aracne editrice s.r.l., Roma. The I ed. appeared in 1988, the II ed. in 1999.

O'Malley, R. T., D. Mondal, C. Goldfinger, and M. J. Behrenfeld, 2018. Evidence of systematic triggering at teleseismic distances following large earthquakes, *Sci. Rep.*, 8, (1): article no. 11611; DOI:10.1038/s41598-018-30019-2

Paley, R. E., 1932. A remarkable set of orthogonal functions, *Proc. Lond. Math. Soc.,* 34: 241-279.

Paparo, G., and G. P. Gregori, 2003. Multifrequency acoustic emissions (AE) for monitoring the time evolution of microprocesses within solids. *Reviews of Quantitative Nondestructive Evaluation*, 22, (*AIP Conference Proceedings ed. by D. O. Thompson and D. E. Chimenti)*, pp.: 1423-1430.

Pavese, M. P., and G. P. Gregori, 1984. An analysis of six centuries (XII through XVII A.D.) of climatic records from the upper Po valley. In W. Schrˆder, (ed.). Historical events and people in geosciences, *Selected papers from the symposia of the Interdivisional Commission on History of IAGA during the IUGG General Assembly*, held in Hamburg, 1983, Verlag Peter Lang, Jupiterstrasse 15, CH-3015 Bern; pp.: 185-220.

Pavese, M. P., V. P. Banzon, M. Colacino, G. P. Gregori, and M. Pasqua, 1992. Three historical data series on floods and anomalous climatic events in Italy. In R.S. Bradley and P.D. Jones (eds), *Climate since A. D. 1500*, Routledge, London and New York; pp: 155-170.

Percival, D. B., and A. T. Walden, 2000. *Wavelet methods for time series analysis*. Cambridge University Press; pp.:1-594.

Percival, D. B., James E. Overland, and H. O. Mofjeld, 2004: Modeling North Pacific climate time series. In D. R. Brillinger, E. A. Robinson, and F. P. Schoenberg, (eds). *Time series analysis and applications to geophysical systems*, Springer-Verlag; pp.: 151−167.

Piao, Shilong, P. Ciais, Yao Huang, Zehao Shen, Peng Shushi, Junsheng Li, Liping Zhou, Hongyan Liu, Yuecun Ma, Yihui Ding, P. Friedlingstein, Chunzhen Liu, Kun Tan, Yongqiang Yu, Tianyi Zhang, and Jingyun Fang, 2010. The impacts of climate change on water resources and agriculture in China, *Nature*, 467: 43–51; DOI:10.1038/nature09364

Pichler, F., 1968. Synthese linearer periodische zeitvariabler Filter mit vorgeschreibenen sequenzverhalten, *AEU* 22: 150-161.

Pratt, W. K., L. R. Welch, and W. H. Chen, 1972. Slant transforms for image coding, *Proc. Appl. Walsh Functions, Washingotn D.C*., AD744650: 229-234.

Prescott, P., and A. T. Walden, 1980. Maximum likelihood estimation of the parameters of the generalized extreme-value distribution, *Biometrika*, 67: 723-724. https://api.semanticscholar.org/CorpusID:122871145

Quinn, J. M., 2010. *Global warming. Geophysical counterpoints to the enhanced greenhouse theory.* Dorrance Publishing Co., Inc., Pittsburgh, USA; pp.:1-118.

Rademacher, H., 1922. Einige S%tze von allgemeinen Orthogonalfunktionen, *Math. Annal*., 87: 122-138.

Rampino, M. R., and R. B. Stothers, 1988. Flood basalt volcanism during the past 250 million years. *Science*, 241: 663-668.

Rao, R. K., M. A. Naramsimhan, and K. Revulieri, 1975. Image data processing by Hamdamard-Haar transform, *IEEE Transf. Comput*., C24: 888-894.

Rezanov, I. A., 1980. *Catastrophes in the Earth's history*, Mir Publ., Moscow. Revised English edition published in 1984; pp.: 1-167.

Risch, P. R., and T. A. Brubaker, 1973. Evolutionof data reconstruction using Walsh functions, *Electron. Lett*., 9: 489-490.

Salcedo, G. E., R. F. Porto, and P. A. Morettin, 2012. Comparing non-stationary and irregularly spaced time series. *Computational Statistics and Data Analysis*, 56: 3921.

Santacroce, R. (ed.), 1987. Somma-Vesuvius. *Quad. Ric. Sci.*, (114), (*Progetto Finalizzato 'Geodinamica', Monografie finali* vol. 8), CNR, Roma; pp.: 1-251.

Santacroce, R., M. Rosi, A. Sbrana, R. Cioni, and L. Civetta, (eds), 1996. Vesuvius. A decade volcano. *Workshop handbook. IAVCEI and GNV* (*Gruppo Nazionale per la Vulcanologia of the Italian CNR*).

Sassa, K., 1936. Micro-seismometric study on eruptions of the volcano Aso. *Mem. Coll. Sci. Kyoto Imp. Univ.*,19, (1): 11-56 (+4+3).

Scafetta, N., and R. C. Willson, 2013. Multiscale comparative spectral analysis of satellite total solar irradiance measurements from 2003 to 2013 reveals a planetary modulation of solar activity and its nonlinear dependence on the 11 yr solar cycle, *Pattern Recognition Phys.,* 1: 123-133; DOI:10.5194/prp-1-123-2013

Scafetta, N., F. Milani, A. Bianchini, and S. Ortolani, 2016. On the astronomical origin of the Hallstatt oscillation found in radiocarbon and climate records throughout the Holocene, *Earth Sci. Rev.,* 162: 24-43; DOI:10.1016/j.earscirev.2016.09.004

Schove, D. J., (ed.), 1983. *Sunspot cycles*. Hutchinson Ross Publishing Co., Stroudsbourg, Pennsylvania; pp.:1-410.

Schrˆder, W., 1988a. Aurorae during the Maunder minimum, *Meteorol. Atmos. Phys.,* 38: 246-251.

Schrˆder, W., 1994. Behaviour of auroras during the Spˆrer minimum (1450-1550), *Annales geophys*., 12, (8): 808-809; DOI:10.1007/s00585-994-0808-7.

Shanker, D., N. Kapur, and V. Singh, 2001. On the spatio temporal distribution of global seismicity and rotation of the Earth - A review, *Acta Geod. Geoph. Hung*., 36: 175–187.

Shibata, K., 1972. Waveform analysis of image signals by orthogonal transformation, *Proc. Appl. Walsh Functions, Washington, D.C*., AD744650: 210-215.

Simkin, T., and L. Siebert, 1994. *Volcanoes of the world*, II ed., Geoscience Press, Inc., Tucson, Arizona; pp.:1-349.

Soon, W., V.M. Velasco Herrera, R.G. Cionco, S. Qiu, S. Baliunas, and R. Egeland, 2019. Covariations of

ISSN number; ISSN 2202-0039

chromospheric and photometric variability of the young Sun analogue HD 30495: evidence for and interpretation of mid-term periodicities. *Monthly Notices of the Royal Astronomical Society*, 483: 2748.

Stearns, H. T., and G. A. Macdonald, 1946. Geology and ground water resources in the Island of Hawaii. Division of Hydrography, Territory of Hawaii, *Bulletin of Honolulu*.

Straser, V., 2025. Ionizations in the atmosphere, vapor clouds and earthquakes, *New Concepts in Global Tectonics, Journal*, 13, (10): 1505-1510.

Straser, V., G. Cataldi, and D. Cataldi, 2025. Solar and Earth's geomagnetic activity related to the M6.3 earthquake recorded in Mauritius, Réunion region on September 26, 2024, *New Concepts in Global Tectonics, Journal*, 13, (1): 23-35.

Straser, V., G. Cataldi, and D. Cataldi, 2025a. Solar and Earth's geomagnetic activity related to the M6.2 Earthquake recorded in Costa Rica on October 12, 2024, *New Concepts in Global Tectonics, Journal*, 13, (1): 36-44.

Straser, V., G. Cataldi, and D. Cataldi, 2025b. Solar and Earth's geomagnetic activity related to the M6.2 earthquake recorded in Chile on November 8, 2024, *New Concepts in Global Tectonics, Journal*, 13, (4): 546-555.

Straser, V., G. Cataldi, and D. Cataldi, 2025c. Solar and Earth's geomagnetic activity related to the M6+ earthquake recorded between 12 and 18 November 2024, *New Concepts in Global Tectonics, Journal*, 13, (4): 556-563.

Straser, V., G. Cataldi, and D. Cataldi, 2025d. Solar and Earth's geomagnetic activity related to the M6 earthquake recorded on October 30, *New Concepts in Global Tectonics, Journal*, 13, (7): 983-992.

Straser, V., G. Cataldi, and D. Cataldi, 2025e. Local electromagnetic precursors: mechanisms and pre-seismic monitoring through low frequency bands, *New Concepts in Global Tectonics, Journal*, 13, (10): 1537-1553.

Straser, V., G. Cataldi, and D. Cataldi, 2026. Space weather related to potentially destructive seismic activity, *New Concepts in Global Tectonics, Journal,* 14, (2), 220-224.

Tam, L. D. C., and R. Y. Goulet, 1972. On arithmetic shift for Walsh functions, *IEEE Trans. Comp.,* C21: 1451-1452.

Telesca, L., 2007. Cycles, scaling and crossover phenomenon in length of the day (LOD) time series, *Physica A*, 379: 459-464; DOI:10.1016/j.physa.2007.02.064

Torrence, C., and G. Compo, 1998. A practical guide to wavelet analysis. *Bulletin of the American Meteorological Society*, 79: 61.

Treder, H.-J., and W. Schrˆder, 1992. Cosmical influence on the geological time. *Acta Geod. Geophys. Mont. Hung.*, 27, (2-4): 241-249.

Tsirulnik, L. B., T. V. Kuznetsova, and V. N. Oraevsky, 1997. Spectral method of global minimum (MGM) and its application to problems of heliospheric and planetary physics, *Planet. Space Sci*., 45, (2): 241-250.

Tukey, J. W., 1977. *Exploratory data analysis*. Addison-Wesley Publ. Co., Reading. Massachusetts, etc.; pp.:1-688.

Velasco Herrera, V.M., W. Soon, D.V. Hoyt, and J. Murakˆzy, 2022. Group sunspot numbers: a new reconstruction of sunspot activity variations from historical sunspot records using algorithms from machine learning, *Solar Physics*, 297: 8, DOI:10.1007/s11207-021-01926-x

Walsh, J. L., 1923. A closed set of orthogonal functions, *Ann. J. Math*., 55: 5-24.

Wang, Shao-Wu, and Zhao Zong-Ci, 1981. Droughts and floods in China, 1470-1979. In T. M. L. Wigley, M. J. Ingram, and G. Farmer (eds), *Climate and history-Studies in past climates and their impact on Man*, 530 pp., Cambridge University Press, Cambridge; pp.: 271-288.

West, B. J., 1982. Stochastic predictions of cataclysmic events. *AIP Conference Proceedings,* 82, (1): 263-274. American Institute of Physics.

Whyte, M. A., 1977. Turning point in Phanerozoic history, *Nature*, 267: 679-682; DOI:10.1038/267679a0

Wigley, T. M. L., M. J. Ingram, and G. Farmer (eds), 1981. *Climate and history-Studies in past climates and their impact on Man*, Cambridge University Press, Cambridge; pp.: 1-530.

Ying, Kairan, Tianbao Zhao, Xiao-Wei Quan, Xiaogu Zheng, and C. S. Frederiksen, 2014. Interannual variability of autumn to spring seasonal precipitation in eastern China, *Clim. Dyn.,* [19 p.]; DOI:10.1007/s00382-014-2411-2

Zhang, D., 1993. A study on the Medieval warm period in China, *Quaternary Sci.,* (01); DOI:cnki:ISSN:1001-7410.0.1993-01-001

Zolitschka, Bernd, 1986. *Warvenchronologie des Meerfelder Maares (Westeifel),* 119 pp. Diplomarbeit. University of Trier.

Acronyms

AE – acoustic emission
AI - Artificial Intelligence
APR - all-planet-restart
Arp - Automatic Research for Periodicities (operator)
bArp – bilateral Arp (operator)
cArp – continuous Arp (operator)
Cetra - Computing Errors, Trends, and Associated parameters (operator)
Cydia - cycle diagram (operator)
d.o.f. – degree of freedom
DFA - detrended fluctuation analysis
ENSO – El Niño Southern Oscillation
EOF - empirical orthogonal polynomials
FFT - Fast Fourier Transform
IC – inner core
IOD - Indian Ocean Dipole
K-HC - King-Hele Cycle
l.o.d. – length of the day
LIP - large igneous province
magpol – magnetic polarization (state of matter)

New Concepts in Global Tectonics Journal
Volume 14, Number 6, June 2026
ISSN number; ISSN 2202-0039

MEM - maximum entropy methods
MGM - method of global minimum
$nb\mathcal{A}rp$ – nD bilateral Arp (operator)
$n\mathcal{R}_{es}$ – nD operator on residuals
NUL - $NUL \times 13 = 2224\ years$
OC – outer core
OSP - orbital symmetry progression (cycle)
PCA - principal component analysis
PMC - planetary mass center
ppa - pole position algorithm
ppa - pole position analysis
ppa - pole position area"
ppe - pole position event
QBO - Quasi Biannual Oscillation
$\mathcal{R}_{es}$ – operator on residuals
SHE - spherical harmonic expansion
SJL - Sat/Jup laps
SOP - Solar Orbital Precession
SSC - sunspot cycle
SST – sea surface temperature
SV – secular variation
TD - tide-driven (dynamo)
USJL = $\mathrm{SJL} \times 16 = \mathrm{USL} \times 7$
USJR = $USJL \times 9$
USL - Ura/Sat laps
WS – westward drift

NCGT Journal
New Concepts in Global Tectonics

New Concepts in Global Tectonics Journal
Volume 14, Number 6, June 2026

ISSN number; ISSN 2202-0039

AN OCEAN IN GEOLOGICAL HISTORY

Vadim V. Gordienko

S.I. Subbotin Institute of Geophysics, NASU, Kiev, Ukraine

Corresponding Author: Vadim V. Gordienko *S.I. Subbotin Institute of Geophysics, NASU, Kiev, Ukraine*

Email: gordienkovadim39@gmail.com

Abstract The problem of the ocean as a deep-water basin with a specific type of crust, which differs from continental crust by its smaller thickness and more mafic composition, is considered mainly on the basis of the well-known results reported by B.A. Bluman and E.M. Rudich for oceans and by M.I. Budyko and co-authors for continents. Their conclusions are in fairly good agreement with the models of deep-seated processes in the tectonosphere of oceans as discussed by the author. The said processes are consistent with a series of geological phenomena and geophysical field anomalies. The processes in question represent heat and mass transfer within a eugeosyncline overlying an anomalously mafic continental crust, followed by subsequent activation. The increased maficity of the crust is a result of mass exchange with the mantle, accompanied by subduction of eclogitized crustal blocks and an increase in radiogenic heat generation in mantle rocks. Thus, a fairly consistent model of modern ocean formation is viewed as a result of the preceding evolution of the Earth's tectonosphere during the Mesozoic--Cenozoic period.

Keywords: oceanization of the Earth's crust, concentration of water in the oceans.

INTRODUCTION

The results reported in [Gordienko, 2025] suggest that the total volume of water on planet Earth has not changed significantly over its geological history. However, it is unlikely that it has always been located mainly at the surface in the form of H_2O. The events that occurred in the ocean can be inferred from preserved sediments, predominantly those located on continents. Continents together with their shelves and continental slopes account for 42% of the Earth's surface but contain 91% of the sediment volume, whereas the ocean floor (58% of the surface) contains just 9% of sediments. Oceanic sediments, however, are unlikely to be older than about 200 million years (excluding the consolidated crust buried beneath them, which may, in principle, incompass older sedimentary rocks). There are assumptions about the oceanic origin of certain formations with an age of about 3.8 billion years; however, not all characteristics of those rocks are consistent with those typical of the Phanerozoic oceanic crust [Budyko et al., 1987].

The total salinity of ocean water changes in a rather complex manner. Halite deposits, periodically accumulated in the sedimentary sequence, are buried at depths inaccessible to dissolution and are later brought to the erosion level by changes in the direction of epeirogenic movements, and so on (Fig. 1).

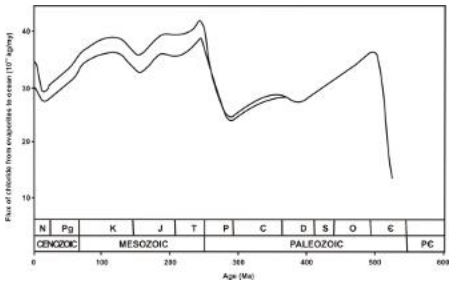

Fig. 1. Input of chlorine (maximum and minimum estimates) into the ocean during the Phanerozoic as a result of erosion of evaporite deposits [Hay et al., 2017].

It is problematic to speak about any directional change in salinity. The models proposed in the literature [Hay et al., 2017, etc.] also include hypothetical elements. Therefore, taking into account the corresponding dataset would be hardly useful for solving the problem posed. It might be more reasonable to focus on an analysis of the deep-seated processes in the tectonosphere reflected in the evolution of sediments, for most of geological history primarily on the continents.

ENDOGENOUS REGIME OF OCEANIZATION

The information presented in [Budyko et al., 1987] regarding the distribution of geosynclines and platforms on present-day continents over the interval 0–3.5 Ga (Fig. 2) is fundamentally consistent with the author's results supported by a quantitative explanation of the decrease in radiogenic heat generation in mantle rocks over the course of geological history [Gordienko, 2017].

NCGT Journal
New Concepts in Global Tectonics

New Concepts in Global Tectonics Journal
Volume 14, Number 6, June 2026

ISSN number; ISSN 2202-0039

With a change in the method of presentation, this agreement can become visually evident. This is important, since other similar comparisons will also be considered below.

Figure 3 shows that seas occupied a significant part of present-day continents during the Phanerozoic. Unfortunately, the depth of epicontinental seas is still not known with certainty, and it is impossible to estimate the proportion of surface water contained within them [Budyko et al., 1987]. Variations in the distribution of seas on platforms reflect, in a smoothed and attenuated form, variations in geosynclines, which, during the early stages of their cycles, represented extensive long-lived reservoirs. Of particular interest is the latest (Late Alpine) rapid reduction in the area of continental seas, which is close in age to the radical deepening of the ocean.

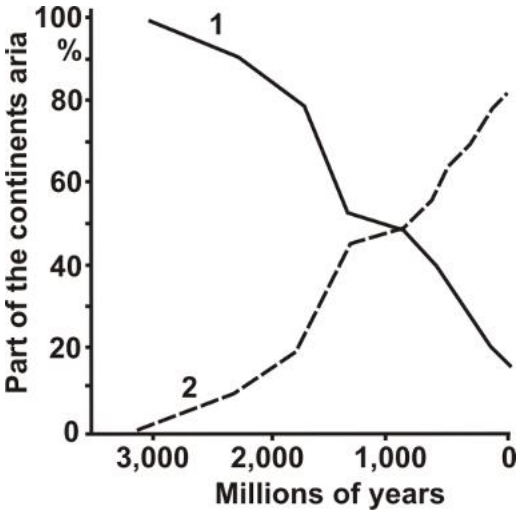

Fig. 2. General trend of changes in the areas of geosynclines (1) and platforms (2) on present-day continents.

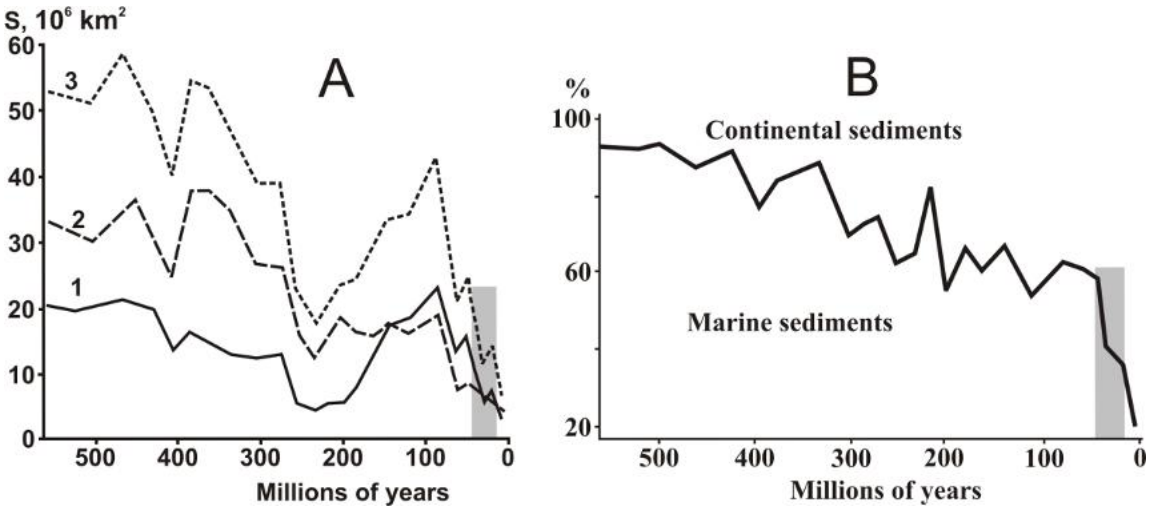

Fig. 3. Areas of seas on present-day continents during the Phanerozoic within platforms (1), geosynclines (2), and overall (3) (A). Changes in the areas of marine and continental sedimentation on present-day continents [Budyko et al., 1987] (B). The grey band marks the period of anomalously rapid subsidence of the ocean floor (see Fig. 4).

It is possible that the amount of liquid water at the planet's surface remained significantly smaller than at present for a long time. It may have been distributed rather evenly and not concentrated in deep basins similar to modern oceans (Fig. 3A). During that period of time, geosynclines that were widespread over the entire Earth's surface were gradually replaced by platforms. The earliest (pre-Riphean) platforms often include granitic batholiths within their thick crust and appear as minimally active shields. The replacement of geosynclines by platforms was accompanied by riftogenesis, including repeated episodes, which also affected segments of geosynclinal regions. Gradually, a part of the Earth developed a crust that was significantly more mafic than that typical of other continental regions. It can be noted that such type of crust has been encountered near the present-day margins of the oceans.

The preceding decrease in the area of continental seas can be more conveniently considered using other data. For comparison with known geological information, the youngest part of Fig. 3 can be used. These are the data from [Rudich, 1984, etc.] regarding the behavior of the ocean floor over the recent tens of millions of years (Fig. 4).

NCGT Journal
New Concepts in Global Tectonics

New Concepts in Global Tectonics Journal
Volume 14, Number 6, June 2026

ISSN number; ISSN 2202-0039

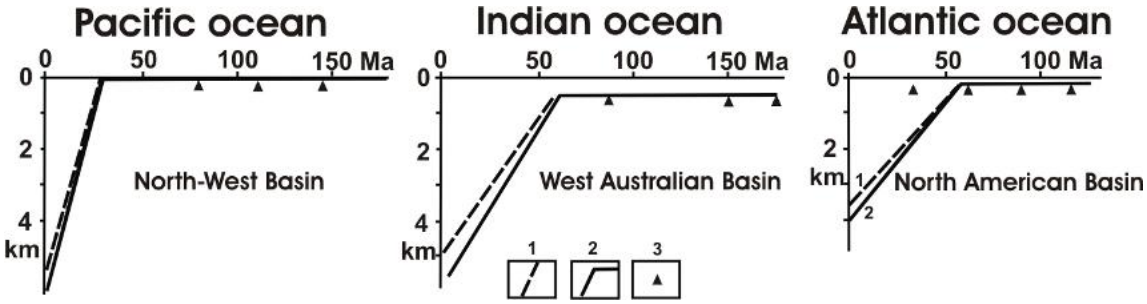

Fig. 4. Changes in the depth of the ocean floor during the period of 200 million years. 1 – depth of the ocean floor; 2 – depth of the basement surface; 3 – manifestations of magmatism.

These data (as well as information presented in publications by B.A. Bluman [Bluman, 2008]) indicate that since the Triassic–Jurassic Boundary the modern ocean experienced a long period of shallow-water or even subaerial conditions with accumulation of sedimentary-volcanogenic deposits. Those conditions were replaced about 30 ± 15 million years ago by a very rapid subsidence of the ocean floor. In the author's view, that deepening was largely related to the final stage of oceanization -- the eclogitization of a basic part of the continental crust [Gordienko, 2017]. The average magnitude "of the ocean floor collapse" is estimated at about 3 ± 0.8 km. It should be noted that this estimate is based on a limited dataset obtained more than 40 years ago. Approximately half of the water required to fill the resulting basin may have been produced during the replacement of the crustal portion by mantle material (which contains less water in its rocks [Gordienko, 2025]). The second part could have come from epicontinental seas. In the latter case, however, this remains just a hypothesis, since the data required for the calculation are lacking.

The episode considered above shows that it is also possible to make inferences about oceanic processes from the data on sediment formation on continents, which is obviously desirable. On the continents, in the modern epoch, encompassing the final stage of the Alpine geosynclinal cycle, it also represents a period of riftogenesis (possibly, a single-stage activation), accompanied by a widespread uplift and extensive magmatism. This triggers the "runoff" of water from the continents into the deepened ocean. It is likely that such processes did occur at the end of the Hercynian and Caledonian cycles (Fig. 3).

E.M. Rudich, analyzing the data presented in Fig. 4, concluded: "…the extensive development of Late Mesozoic and Cenozoic shallow-water sediments within the present-day abyssal zones and the similarity of their lithological–facies to those in coeval deposits occurring in marginal regions of the continents clearly indicate that the boundaries of the latter had until relatively recently been located much more seawards than today" [Rudich, 1983, p. 262]. In other words, subsidence also affected the continental margin, and the ocean advanced onto the continent.

The flood basalts of the Paraná Province (~130 Ma) extend into the continental shelf of eastern South America, while the traps of the Etendeka Province (~120 Ma) in southern Africa continue into the Walvis Ridge (Atlantic Ocean). The same tendency can be traced even in the most recent episodes of geological history. Continental flood basalts (~50 Ma), together with the weathering crusts formed upon them, have been traced by deep-sea drilling into the adjacent waters of the eastern continental shelf of Greenland and the Outer Hebrides; the basalts of the Columbia Plateau (~15 Ma) extend into the Raposos Bay area; and the Afar traps (~35 Ma) extend into the Red Sea [Bluman, 2008]. Obviously, the eruption of large volumes of basaltic melt from the mantle alone is insufficient for producing oceanization.

At the end of the Caledonian and Hercynian cycles (Fig. 3), vast areas of the continents were affected by riftogenesis, examples of which are shown in Fig. 5.

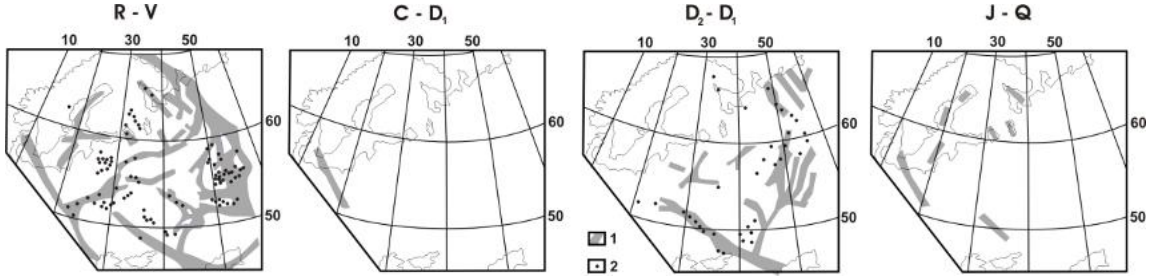

Fig. 5. Manifestations of riftogenesis on the East European Platform (EEP) [Milanovsky, 1983, etc.]. 1 – outlines of rifts; 2 – manifestations of magmatism.

NCGT Journal
New Concepts in Global Tectonics
New Concepts in Global Tectonics Journal
Volume 14, Number 6, June 2026

ISSN number; ISSN 2202-0039

Within the territory of the EEP, the process affected most of the platform area (taking into account the fact that a considerable portion of magmatic rocks there is buried beneath the sedimentary cover and many occurrences remain undiscovered). Within one of the Hercynian rifts -- the Dnieper–Donets Depression (DDD) -- the results of crustal transformation during riftogenesis can be examined in detail. A reduction in thickness of the consolidated crust and its basification are evident (some of those effects may relate to the Riphean --Vendian riftogenesis), i.e., components of the oceanization process. V.V. Belousov referred to such regions as failed oceans [Belousov, 1991]. Recent activation also affected the same territory of the DDD (without magmatism, at least so far). Thus, even at least three episodes of influence do not lead to oceanization. In other words, the observed correlation between continental and oceanic events manifests itself only in the synchronicity of activity, but not in a clear relationship between the endogenous regimes. The geological history of the ocean (a region with an oceanic type of crust) cannot be reliably traced earlier than the Mesozoic.

The increase in heat generation in the rocks of the upper mantle associated with the influx of crustal material gradually created a new type of endogenous regime. At present, its initial manifestations alone can be observed.

OCEANIZATION OF THE EARTH'S CRUST

It is obvious that the regions shown in Fig. 5 cannot as yet become "successful oceans." Information available on the advance of the oceanization front [Bluman, 2008; Dickins,1994; Krasny,1983; Storetvedt,1997, etc.] allows the order-of-magnitude rate of the process to be estimated at about 1cm per year. This value is consistent with the velocity of the Aubouin wave propagating across a geosynclinal region. The same rate is also characteristic of the eclogitic crustal blocks' sinking into the mantle of an active region [Gordienko, 2022]. Naturally, such velocity estimates are approximate, and both the centrifugal and centripetal directions of the oceanization fronts for oceans with active and passive margins, as established by B.A. Bluman [Bluman, 2008], should be regarded as preliminary. Nevertheless, it may be assumed that formation of a modern ocean could require just 200–250 million years (the Mesozoic–Cenozoic).

As noted earlier [Gordienko, 2017], the process in question comprises substantial elements of mantle heat and mass transfer within a geosyncline, supplemented by post-geosynclinal activation. Obviously, this refers to a geosyncline of Cimmerian age. When constructing a thermal model, it is important to know the initial temperature prior to the onset of the process. Such information is unavailable for oceanic regions. Therefore, the Carpathian geosyncline of approximately suitable age, specifically its central (eugeosynclinal) part, was used as an analogue. According to available data, a similar sequence of active geological events may have occurred in the South Okhotsk Basin. Differences could only be traced at the final stage -- rapid subsidence and the accumulation of a thick sedimentary sequence. It might therefore be of interest to compare the seismic velocity sections for the crust in the above regions (as well as in the Dnieper-Donets Depression) with the section typical of an oceanic basin. For this purpose, the Angola–Brazil geotraverse provided convenient data. If information from both sides of the Mid-Atlantic Ridge over a distance of about 2,000 km is combined, a fairly dense system of Vp values could be obtained (Fig. 6; [Pavlenkova et al.,1993]). The velocity structure is close to the well-known model [Spudich et al.,1980], constructed to a depth of 12 km.

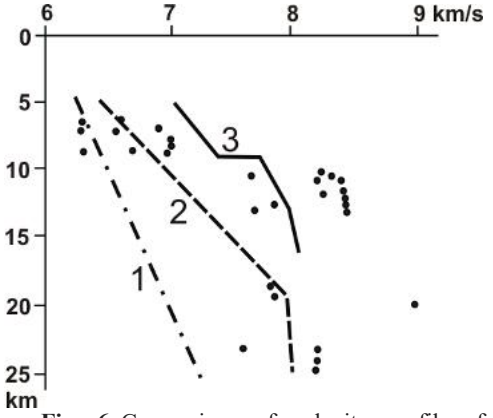

Fig. 6. Comparison of velocity profiles for consolidated crust in different regions with the data from the Angola–Brazil geotraverse.

1–Dnieper–Donets Depression; 2 – Central part of the Carpathian geosyncline (Pannonian Massif, Karcag, Hungary); 3–South Okhotsk Basin; 4 – The data from the Angola–Brazil geotraverse.

Velocity profiles 1–3 were corrected (including allowance for partial-melting zones)

NCGT Journal
New Concepts in Global Tectonics

New Concepts in Global Tectonics Journal
Volume 14, Number 6, June 2026

ISSN number; ISSN 2202-0039

to adjust the Vp values to the P–T conditions typical of the Angola–Brazil geotraverse.

It is evident that the velocity section of the crust in the Dnieper–Donets Depression differs from the oceanic one, whereas beneath the Pannonian Massif and the South Okhotsk Basin they are quite similar. In both cases, eugeosynclinal processes started in the Cimmerian time and were supplemented by Alpine events.

For the Carpathian region considered, the preceding geological history is known back to about 1,200 Ma. The ages of activity stages accompanied by volcanic manifestations have been determined; a young activation stage and a sharp decrease in crustal thickness are also known [Gordienko et al., 2011, etc.]. In the heat and mass transfer model, the quanta of tectonic action (QTA) [Gordienko, 2017, 2022] were assigned to 200, 150, 100, and 50 Ma. Calculation of the effects of the advective events was supplemented by modification of the initial temperature distribution due to surface cooling of the Earth and by the influence of radiogenic heat generation in mantle rocks at the geosynclinal level (0.06 μW/m³). During the second half of the activation sequence, heat generation was assumed to increase due to crust–mantle exchange down to depths of about 100 km (0.08 μW/m³), reaching the oceanic level.

In the consolidated crust of platforms, the complex of physical properties can be explained by the presence of up to 30% of ultrabasic rocks in the lower one-third portion of the crust [Gordienko et al., 2005]. In Phanerozoic geosynclines, a decrease in heat generation of the consolidated crustal rocks is observed; this may be due to the presence of ultrabasic rocks throughout its thickness in concentrations of about 20% [Gordienko, 2017].

Let us consider the content of deep-seated processes during that period. The first QTA arose from the depth interval of 230–470 km to 230–170 km, with an anomalous temperature of about 320°C, while the lower reservoir cooled down by 80°C. The initial magmatism was relatively small in volume, and the surface displacement caused by thermal anomalies of opposite sign was close to zero. The polymorphic transformation of rocks at the base of the upper mantle was virtually negligible: temperature changes at that depth did not exceed the calculation error (Fig. 7). Changes in the crust were limited to the formation of mafic dikes that penetrated the consolidated crust and the sedimentary layer. When heated (mainly during subsequent stages), sedimentary rocks reached the catagenesis stage, and the velocity of longitudinal seismic waves increased to about 6 km/s. Saturation of the layer with dikes resulted in Vp ≈ 6–6.5 km/s.

The second QTA rose from the depths of 170–460 km to 110–170 km with an anomalous temperature of about 300°C, cooling the source by 60°C. In that case too, the uplift and subsidence of the surface, caused by thermal anomalies, virtually compensate one another. The thickness of the effusive-sedimentary surface layer increases by the first hundreds of meters, and the swarm of dikes in the crust becomes denser.

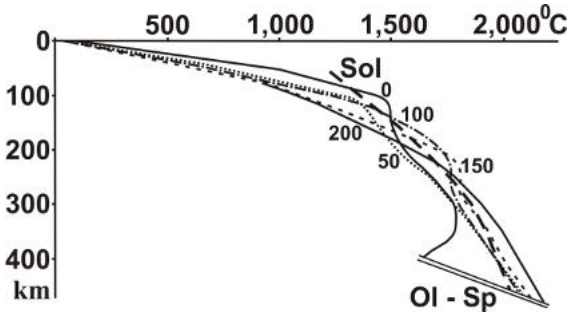

Fig. 7. Temperatures in the crust and upper mantle during the oceanization period. Numbers next to the curves indicate age in Ma. *Sol* – peridotite solidus; *Ol--Sp* – the olivine--wadsleyite transition zone.

The third QTA (completing the geosynclinal process) rose from 130–250 km to 70–130 km, with an anomalous temperature of about 400°C, cooling the source down by 200°C. Some of the partially molten material from the newly formed subcrustal asthenosphere (a layer of about 7–8 km in thickness) moved into the crust at depths of 20–30 km (occupying about half of its volume) and 10–20 km (about one quarter). The material that sank into the asthenosphere cooled it down by about 150°C. Final magmatism continued to build up the upper volcanic layer.

Figure 7 shows temperature distributions before each successive activation event. By that time the heating of the crust, produced by the second and third QTA, became less pronounced than shortly after the beginning of each stage, especially after the injection of large masses of partially molten mantle material into the crust. Granulite-facies metamorphic conditions were reached throughout the consolidated crust, which continued to be

ISSN number; ISSN 2202-0039

enriched with ultrabasic material, and seismic wave velocities exceeded 7 km/s.

The post-geosynclinal stage of heat and mass transfer was prepared by heating up of rocks overlying the base of the upper mantle (Fig. 7). About 50 Ma ago, a 70-km thick partially-melting layer formed there. It was sufficient to generate another QTA. It rose toward the crust (to depths of 40–100 km) with an anomalous temperature of about 950°C, cooling the source down by 800°C. By the present time, the anomalous cooling at the base of the upper mantle has significantly decreased, and the boundary of the polymorphic transformation of peridotite lies at a depth of about 395 km. Compaction of olivine and transformation of part of the pyroxenes into garnet rocks caused an overall density increase of about 0.22 g/cm³ within a depth interval of about 70 km. There is no reliable information about the rate of this process, but it appears highly probable that the process has been completed. According to [Korolyuk et al., 2004], at shallower depths, corresponding changes in P–T conditions are sufficient for geologically rapid transformations.

The described compaction caused subsidence of the entire crust–mantle block by about 4.5 km. Beneath the crust, during the ascent of the QTA, temperatures exceeded the peridotite solidus, forming a zone of intense partial melting (up to 30% [Kadik et al., 1990]). Powerful volcanism caused an increase in the thickness of the surface effusive layer to about 1.5 km. Together with the weight of the water filling the depression, this pushed the lower crust beyond the eclogitization boundary by about 3 km, stimulating thereby an additional 0.5 km of subsidence.

The subcrustal asthenosphere generated intrusion of partially molten peridotite into the crust (a 7–8 km layer) with the volume sufficient for triggering processes with anomalous temperatures of about 350°C in the upper half of the consolidated crust and 700°C in the lower half. Upon cooling, the transformed crust became somewhat denser and subsided by several hundreds of meters. The material descending into the subcrustal asthenosphere reduced its temperature by 60°C and, upon cooling, became transformed into eclogite, bringing the total subsidence of the surface to about 5.5 km. The Vp values in the consolidated crust reach approximately 7.7 km/s.

The scenario of crustal transformation during the process of oceanization, as described above, does not cover phenomena related to the formation of UHP blocks [Gordienko, 2017; 2022, etc.]. However, the fact of mafic rocks' eclogitization during the crust–mantle exchange processes is beyond doubt. Intrusion of the peridotite melt into the crust, with an increase in the degree of melting from 5 to 30%, replacing almost 40% of basic granulites, must be accompanied by a strong densification. However, a mechanism causing formation of sufficiently high-pressure zones around magma intrusions in the crust has hardly been detailed in the literature (except for prograde transformations of gabbro outside the peak stage [Oh, 1990; Zhang et al., 1995]).

Therefore, considered here are only conditions of eclogitization under sufficient lithostatic pressure (>1 GPa). It may be assumed that intrusions during the final magmatism of the geosynclinal stage and the activation stage were accompanied by the formation of eclogites and a corresponding additional increase in Vp at depths larger than 12 km. Shortly after intrusion, thermoelastic stress alone may reach hundreds of MPa [Grinfeld et al., 1988; Turcotte et al., 1985, etc.]. According to seismological data, this portion of the lithosphere is not usually referred to as part of the Earth's crust.

Eclogites with pyropes may sink to depths of 250–300 km, whereas those with almandines may reach the base of the upper mantle. In this way an increased level of radiogenic heat generation may be established throughout the upper mantle beneath the ocean, producing a new type of endogenous regime. The most recent geological events in the oceans may not yet include the full set of phenomena characteristic of that regime.

The upper portion of the crust is represented by the first oceanic layer of young unconsolidated sediments with thicknesses in the first hundreds of meters, formed after accumulation of effusive rocks from the second layer. According to reference data, seismic velocities in the first layer are about 2.0–3.5 km/s, whereas in the second layer they depend on porosity and vary widely between 3.5 and 5.0 km/s [Density…, Dobrynin, 2004; Handbook…, 1969; Mineral…, 1995; Petrophysics…, 1992, etc.]. The rocks of the third layer should have Vp ≈ 6.5 km/s.

Let us compare the above results with experimental data. For this purpose, we selected about 200 Vp values from velocity profiles of the crust in the Atlantic and Pacific oceans, as well as similar data for the subcrustal layer down to 40 km depth. Approximately this level may correspond to the base of the crust affected

NCGT Journal
New Concepts in Global Tectonics

New Concepts in Global Tectonics Journal
Volume 14, Number 6, June 2026

ISSN number; ISSN 2202-0039

by oceanization and plunged down by 5–6 km. The results are as follows:

The first crustal layer: 2.75 ± 0.15 km/s,

The second layer: 4.25 ± 0.15 km/s,

The third layer: 6.5 ± 0.1 km/s.

These values agree well with predicted ones.

At depths larger than 12 km, velocities determined at 12–20 km predominate, although larger depths are also represented. It should be noted that the distribution pattern of velocities is quite similar to that observed beneath the Angola–Brazil geotraverse (Fig. 6). The average velocity in the 12–30 km depth interval is about 7.7–7.8 km/s. However, the dataset actually indicates the presence of two types of rock blocks with different mean Vp values (Fig. 8).

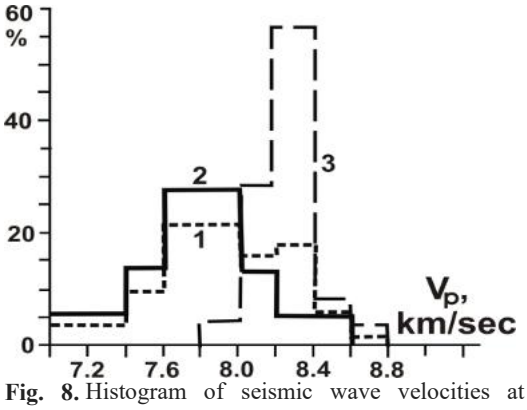

Fig. 8. Histogram of seismic wave velocities at depths of 12–30 km beneath oceanic basins. 1 – entire dataset; 2, 3 – interpreted components (2 – basic granulites and lherzolites; 3 – eclogites).

Crustal thickness in the northwestern Pacific, reaching 25–30 km (including the water layer), can be inferred directly from a complex of geological and geophysical studies [Krasny et al., 1983; Lomtev, 2008].

There is yet another argument in favor of incorporating the depth interval usually attributed to the mantle within the oceanic crust. When interpreting magnetic anomalies in oceans using realistic magnetization values of their sources, the lower boundaries of these bodies must often be placed within rocks considered mantle. This feature is particularly valid for anomalies large in area and intensity, for example the Broken anomaly west of Australia and the South Kuril anomaly (Fig. 9).

Experimental data indicate that typical magnetization of lower-crustal rocks is about 3–3.5 A/m.

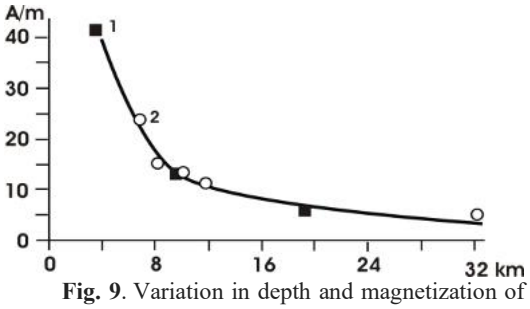

Fig. 9. Variation in depth and magnetization of the magnetic anomaly sources explaining the Broken (1) and South Kuril (2) anomalies.

Thus, in the depth interval **~12–30 km**, the rock complex does not correspond to the usual concept of mantle composition. It is more likely the lower portion of the oceanic crust. Following the intrusion of basic melts from the underlying mantle, those rocks were serpentinized and acquired noticeable magnetization. It is there that sources of linear magnetic anomalies are located [Gordienko, 2023, etc.].

In general, the modeling that was performed has made it possible to view the process in more broad terms than in [Gordienko, 2017]. The test of the possibility that oceanic crust may have been formed on the basis of continental crust can be regarded as valid.

CONCLUSIONS

In continental regions, the deep-seated process corresponding to the eugeosynclinal stage and the subsequent activation over a period of about 200 million years leads to a series of geological events that are recorded in present-day oceans. These include prolonged preservation of level land or shelf conditions, periodic renewal of magmatism, and restructuring of the crust (its basification with transformation of the lower part into a depth interval possessing physical properties close to those of the mantle). This stage was followed by a period of rapid subsidence of the surface (within several tens of millions of years), associated with a shift of the boundary between the upper and lower mantle. The calculated results of studies performed on this process are in good agreement with experimental data on the structure of the oceanic crust. Processes of recent activation (mid-ocean ridges, abyssal hills, deep-sea trenches, and extensive basins filled with young sediments) are superimposed upon the already formed oceanic crust. The crustal material that has subsided into the mantle increases its radiogenic heat generation, thereby forming a new type of endogenous regime.

ISSN number; ISSN 2202-0039

ACKNOWLEDGEMENTS

The author would like to express his special thanks to Mrs. Rita Schneider for her help in translating this paper from Russian.

REFERENCES

Belousov, V.V. (1991). *Earth's tectonosphere: Interaction between the upper mantle and the crust.* Moscow: MGK USSR, 72 p. (in Russian).

Bluman, B.A. (2008). Weathering of basalts and unconformities in the oceanic crust: Possible geodynamic implications. *Regional Geology and Metallogeny*, 35, 72–86 (in Russian). http://www.evgengusev.narod.ru/tecto/bluman-2008.html

Budyko, M.I., Ronov, A.B., & Yanshin, A.L. (1987). *History of the Earth's atmosphere.* Berlin–New York: Springer-Verlag, 139 p.

Density and composition of the upper mantle (in Russian) . http://www.geologam.ru/geophysics/lithosphere/plotnost-i-sostav-verhney-mantii

Dobrynin, V.M., Vendelstein, B.Yu., & Kozhevnikov, D.A. (2004). *Petrophysics (Physics of rocks).* Moscow: Russian State University of Oil and Gas Publ. House, 368 p. (in Russian). geokniga-dobrynin-petrophysics2004.pdf

Gordienko, V.V. (2017). *Thermal processes, geodynamics, deposits.* 283 p. https://ivangord2000.wixsite.com/tectonos

Gordienko, V.V. (2022). About geological theory. *Geophysical Journal*, 44(2), 68–92. https://doi.org/10.24028/gj.v44i2.256266

Gordienko, V. (2025). History of ocean water. *NCGT Journal*, 10, 1566–1573.

Gordienko, V.V., Gordienko, I.V., Zavgorodnyaya, O.V., et al. (2005). *Ukrainian Shield (geophysics, deep processes).* Kyiv: Korvin Press, 210 p. (in Russian).

Gordienko, V.V., Gordienko, I.V., Zavgorodnyaya, O.V., et al. (2011). *Ukrainian Carpathians (geophysics, deep processes).* Kyiv: Logos, 128 p. (in Russian).

Grinfeld, M.A., & Langman, S.A. (1988). Thermoelastic displacements in a homogeneous isotropic half-space with a buried ellipsoid inclusion. *Izvestiya, Physics of the Solid Earth*, 9, 15–28.

Handbook of Physical Constants (1969). S. Clark (Ed.). Moscow: Mir, 544 p. (in Russian).

Hay, W., Migdisov, A., Balukhovsky, A., et al. (2006). Evaporites and the salinity of the ocean during the Phanerozoic: Implications for climate, ocean circulation and life. *Palaeogeography, Palaeoclimatology, Palaeoecology*, 240, 3–46.

Kadik, A.A., Lukanin, O.A., & Portnyagin, A.L. (1990). Magma formation during the ascent of mantle material: Temperature regime and composition of melts formed during adiabatic decompression of mantle ultrabasites. *Geochemistry*, 9, 1263–1276 (in Russian).

Korolyuk, V.N., Lepegin, G.G., & Korsakov, A.V. (2004). Reconstruction of the thermal history of metamorphic rocks based on exchange-diffusion zoning in minerals. *Russian Geology and Geophysics*, 45(4), 501–512 (in Russian).

Krasny, M.L. (1983). System of paleo-island arcs of Northeast Asia. In: *Structure and dynamics of transition zones.* Moscow, p. 49 (in Russian).

Lomtev, V.L. (2008). New data on tectonics and magmatism of the NW Pacific region. *Geology and Mineral Resources of the World Ocean*, 4, 93–105 (in Russian).

Milanovsky, E.E. (1983). *Rifting in the history of the Earth (rifting on ancient platforms).* Moscow: Nedra, 280 p. (in Russian).

Mineral Physics and Crystallography: A Handbook of Physical Constants (1995). T.J. Ahrens (Ed.). Washington: American Geophysical Union, 354 p.

Oh, C.-W. (1990). Metamorphic evolution of two different eclogites in the Franciscan Complex, California, USA. *Lithos*, 25, 41–53.

Pavlenkova, N.I., Pogrebitsky, Yu.E., & Romanyuk, T.V. (1993). Seismic-density model of the crust and upper mantle in the South Atlantic along the Angola–Brazil Geotraverse. *Physics of the Solid Earth*, 29(10), 27–38 (in Russian).

Petrophysics: Handbook. In three volumes. Vol. 1: Rocks and minerals. (1992). Dortman N.B. (Ed.), Moscow: Nedra, 391 p. (in Russian). https://www.geokniga.org/books/2704

Rudich, E.M. (1984). *Expanding oceans: Facts and hypotheses.* Moscow: Nedra, 252 p. (in Russian).

Spudich, P., & Orcutt, J. (1980). A new look at the seismic velocity structure of the oceanic crust. *Reviews of Geophysics*, 18(3), 627–645. https://doi.org/10.1029/RG018i003p00627

Turcotte, D.L., & Schubert, G. (1985). *Geodynamics: Geological applications of continuum physics.* Moscow: Mir, 730 p. (in Russian translation).

Zhang, R.-Y., Hirajima, T., & Banno, S. (1995). Petrology of ultrahigh-pressure rocks from the southern Su-Lu region, eastern China. *Journal of Metamorphic Geology*, 13, 659–675.

NCGT Journal
New Concepts in Global Tectonics

New Concepts in Global Tectonics Journal
Volume 14, Number 6, June 2026

ISSN number; ISSN 2202-0039

ENERGY BALANCE OF THE TECTONOSPHERE DURING OCEANIZATION

Vadim V. Gordienko, Ivan V. Gordienko
S.I. Subbotin Institute of Geophysics, National Academy of Sciences of Ukraine, Kiev

Corresponding Author: Vadim V. Gordienko *S.I. Subbotin Institute of Geophysics, NASU, Kiev, Ukraine*

Email: gordienkovadim39@gmail.com

Abstract: A scenario of maximum variations in radiogenic heat production within the Earth's crust and upper mantle is examined. Comparisons between continental and oceanic tectonospheres usually emphasize pronounced differences in crustal structure and thickness. However, analysis of U, Th, and K contents in mantle rocks indicates that radiogenic heat production within the corresponding depth range also varies no less dramatically. The total heat generation of the tectonosphere remains approximately constant across regions with different endogenic regimes; its variations likely do not exceed ~20%. Thus, transitions between regimes reflect crust–mantle exchange processes, in which heat production in the upper mantle increases at the expense of the crust. The replacement of a continental region with a thick crust containing many low-basic rocks by an oceanic region with a thin, mafic crust results in an approximately twofold increase in upper mantle heat production (from ~0.04 to ~0.08 μW/m³). It appears to be a necessary condition for the development of energy-intensive deep processes in the tectonosphere. According to the authors' model, this transformation proceeds within a eugeosynclinal regime followed by post-geosynclinal activation. The study uses experimental data on the crustal structure of the platform part of Ukraine, the Carpathian geosyncline, and several regions of the Pacific and Atlantic Oceans. The results are consistent with the proposed crust–mantle exchange model. At the same time, further study of the problem is required, particularly about the accuracy of seismic velocity models and processes related to recent oceanic activation.

Keywords: *radiogenic heat production; tectonosphere; Earth's crust; upper mantle*

INTRODUCTION

Results obtained from ocean studies over recent decades [Bluman, 2011; Dickins, 1994; Frolov et al., 2011; Krasnyi, 1983; Lomtev et al., 2016; Pogrebitsky et al., 1990; Rudich, 1984; Storetvedt, 1997; Udintsev, 1987; Vasilyev, 1989; etc.] leave little doubt that oceanic crust has formed based on continental crust. It is evidenced, in particular, by the presence of relics of continental crust in all oceans, spanning at least a quarter of their areas (Fig. 1). The "andesite line" also points to a continental origin [Menard, 1964; Macdonald, 1949; etc.]. In the area between this line and the continent, rocks of intermediate composition occur, which should not be present in typical oceanic crust.

V.V. Belousov related the origin of oceans to the problem of crustal activation: "Ocean formation represents a major turning point in the development of the Earth's crust, in some respects analogous to platform activation, although of a different nature. The significance of this turning point and its deep causes remain unclear" [Belousov, 1954, p. 24]. He further suggested that this turning point allows the Earth's geological history be divided into two stages: the granitic and the basaltic. The granitic stage corresponds to geosynclinal–platform development, involving the formation of continental crust and the gradual reduction of geosynclines, accompanied by the expansion of platforms. Beginning in the Mesozoic, this stage was replaced by a "basaltic" stage, characterized by the transformation of the Earth's crust over half of the planet's surface, seems unfounded.

The "basaltic" stage is marked by the following features: tectonic activation of continental regions that had undergone platform development; massive outpouring of plateau basalts onto continents; and basification and oceanization of the crust both in individual grabens and in Mediterranean-type seas as a result of destruction of the "granitic" crust and its replacement by "basaltic" material.

The evolution of endogenic regimes on continents is quite evident [Budyko et al., 1987]. Over 3.6 Ga, the area of geosynclines, where active tectonic and magmatic processes occur, decreases

NCGT Journal
New Concepts in Global Tectonics

New Concepts in Global Tectonics Journal
Volume 14, Number 6, June 2026

ISSN number; ISSN 2202-0039

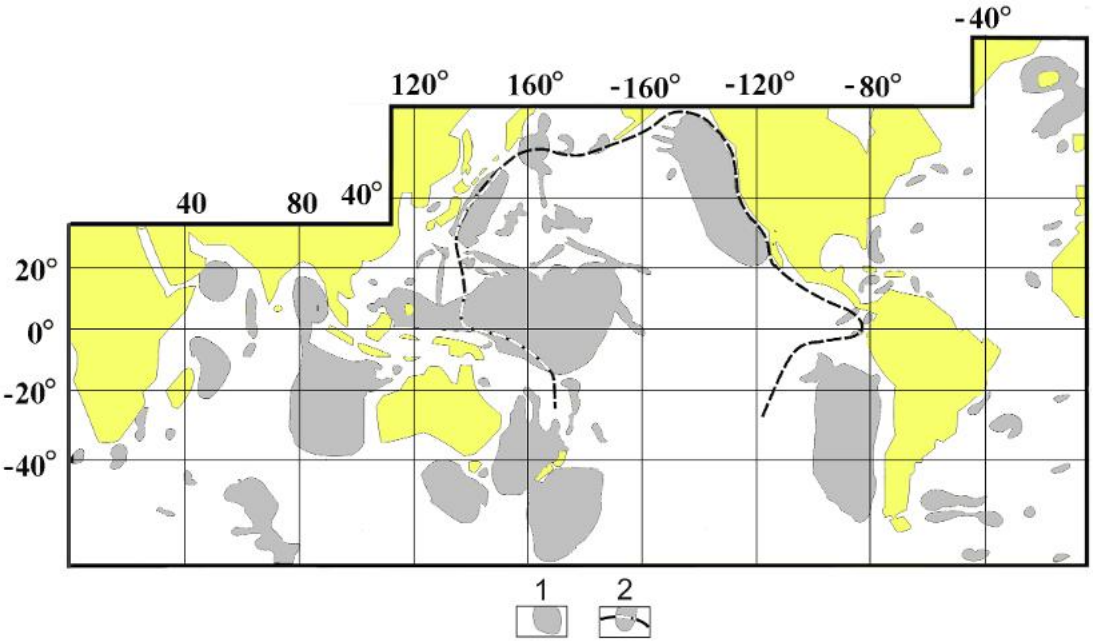

Fig. 1. Regions of the World Ocean showing evidence of formerly existing continental crust (1) and the Pacific "andesite line" (2).

from 100% to 20%. At the same time, the area of platforms correspondingly increases and remains free from such manifestations over long periods (except for episodes of single-stage activation and rifting). This pattern appears logical, since the release of radiogenic energy decreases with time.

The onset of a new stage of development, characterized by pronounced activation and radical emplacement of vast volumes of basalt and the destruction of granitic crust.

However, from the standpoint of the geological theory developed by the authors [Gordienko, 2022; etc.], no contradiction arises. The principal cause of active processes occurring at observable crustal depths is heat and mass transfer in the upper mantle. It has been demonstrated for all types of endogenic regimes in both continental and oceanic settings [Gordienko, 2012; etc.]. In general, this trend is evident when comparing the time-dependent variation in the number of activation events on shields (where their traces are best preserved) with the decrease in radiogenic heat production (RH) in the crust and mantle (Fig. 2).

The association of activation events specifically with mantle energy is evident. During the Phanerozoic, when mantle heat production beneath platforms and geosynclines differ significantly (in the early Precambrian, it was relatively similar), the formation of a more energy-rich mantle is possible only by transferring radioactive sources from the geosynclinal crust into the mantle. Similarly, heat production in the mantle beneath a geosyncline is established during its

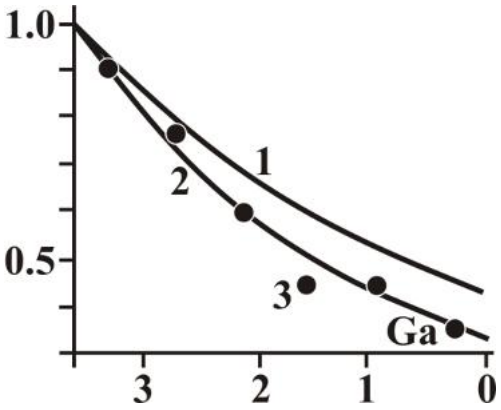

Fig. 2. Relative variation of radiogenic heat production in the crust (1) and mantle (2) of platforms, and the average energy requirements of active processes over time intervals of 0.6 billion years (3).

formation on a platform due to the thick platform crust. It also applies to geosynclines of island arcs. Rifting processes within platform crust are not suitable for such transformation. Post-rift activations do not lead to further modification of the crust. It appears that rifting develops in platform regions with slightly elevated heat production and represents an intensified form of single-stage platform activation. In [Gordienko, 2023a,b; etc.], a model of deep processes in a Cimmerian–Alpine eugeosyncline, supplemented by post-geosynclinal activation, was proposed, leading

NCGT Journal
New Concepts in Global Tectonics

New Concepts in Global Tectonics Journal
Volume 14, Number 6, June 2026

ISSN number; ISSN 2202-0039

to the formation of a mantle with higher heat production beneath oceanic crust. The present paper focuses specifically on this energetic aspect of the deep process, preceded by a brief overview of the corresponding geodynamic events.

DEEP PROCESS AND ITS RESULTS (MAIN ELEMENTS)

In the previous authors' publications [Gordienko, 2022; 2023a,b; etc.], the schemes of heat and mass transfer in the tectonosphere required for oceanization were considered in sufficient detail. Naturally, their application required a reasonably accurate reconstruction of the initial temperature (T) distribution in the mantle and crust of Precambrian platforms and geosynclines, as well as the composition of deep-seated rocks. Several candidate regions with both types of endogenic regimes on different continents were considered. A part of the Eastern European Platform within Ukraine and the Carpathian geosyncline proved to be the most suitable for the present study. In these regions, the geological history preceding the Cimmerian–Alpine geosynclinal process is relatively well constrained, dating back to ~3600 Ma and ~1200 Ma, respectively. It allows us to specify the initial conditions for mantle (and subsequently crustal) material movement, thereby generating thermal anomalies and, in turn, triggering geodynamic processes.

In constructing the model, the timing of the movements of quanta of tectonic action (QTA) was attributed to periods of 200, 150, 100, and 50 Ma. The initial thermal model corresponds to that of the Carpathian region. In the calculations, radiogenic heat production (HG) of mantle rocks evolves from platform to geosynclinal and subsequently to oceanic values (0.04–0.06–0.08 μW/m³) [Gordienko, 2023a].

Without describing all details of the process (presented, in particular, in [Gordienko, 2012; Gordienko et al., 2011; etc.]), we summarize the overall results (Fig. 3).

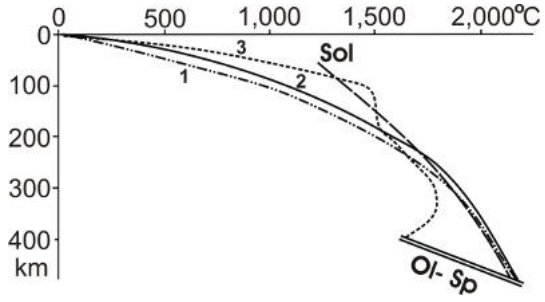

Fig. 3. Temperatures in the crust and upper mantle during the period before and after oceanization. Sol—peridotite solidus; Ol–Sp—olivine to wadsleyite transition zone. Temperature distributions: (1) beneath a Phanerozoic platform; (2) before the onset of the geosynclinal process in the Carpathian Cimmerian–Alpine geosyncline; (3) beneath an oceanic plate.

The geological history of the Carpathian geosyncline before the Cimmerian–Alpine stage included several geosynclinal and rifting events during the Riphean and Paleozoic. The heat generation in its upper mantle likely differed noticeably from that beneath platforms. Accordingly, the initial temperature distribution is somewhat higher. To verify the reliability of the calculated temperatures, they were compared with experimentally determined values derived from the compositions of rocks associated with the final magmatism of the Paleozoic and Cenozoic geosynclines of the Carpathians (Fig. 4).

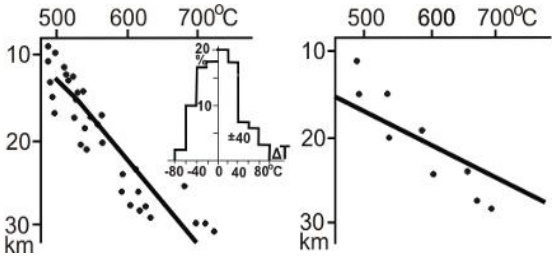

Fig. 4. Temperature distributions during the periods of final magmatism of the Paleozoic (A) and Cenozoic (B) geosynclines of the Carpathians [Gordienko et al., 2011]. Lines indicate calculated temperatures; dots represent experimental values. The inset shows a histogram of deviations between experimental and calculated values.

The differences between the calculated and experimental temperature values (on average ~40°C) do not exceed the typical uncertainties in determining this parameter. The agreement can be considered satisfactory.

We can assume that intrusions associated with the final magmatic stage of the geosynclinal process and the subsequent activation stage are accompanied by the formation of eclogites and, consequently, by a local increase in seismic velocity (Vp) at depths greater than 12 km. Indeed, shortly after intrusion, thermoelastic stresses alone may reach hundreds of MPa [Turcotte et al., 1985; etc.]. According to seismic data, this part of the lithosphere is generally not interpreted as the crust.

Eclogites containing pyrope may sink to depths of 250–300 km, whereas those containing almandine may reach the base of the upper mantle. As a result, enhanced radiogenic heat production may develop throughout the geosynclinal and subsequently oceanic upper mantle, giving rise to a new type of endogenic regime. The youngest events in the geological history of the oceans may not yet fully reflect all features of this regime.

As a result of the entire process, the modeled upper part of the crust consists of the first oceanic

NCGT Journal
New Concepts in Global Tectonics

New Concepts in Global Tectonics Journal
Volume 14, Number 6, June 2026

ISSN number; ISSN 2202-0039

layer of unconsolidated young sediments, several hundred meters thick, formed after the accumulation of effusive rocks of the second layer. According to reference data, seismic velocities in the first layer range from 2.0 to 3.5 km/s, while in the second layer they depend on porosity and vary widely from 3.5 to 5.0 km/s [Density…, 2026; Dobrynin, 2004; Handbook…, 1969; Mineral…, 1995; Petrophysics…, 1992; etc.]. The rocks of the third layer are expected to have Vp values of about 6.5 km/s. Below lies a layer commonly attributed to the mantle. However, according to the authors and many others [Krasnyi, 1983; Lomtev et al., 2016; etc.], down to depths of ~30 km, it still represents a specific type of the crust, with an average seismic velocity of about 7.9 km/s.

TRANSITION FROM PLATFORM TO GEOSYNCLINE

Within the Earth's tectonosphere, the total amount of radiogenic heat sources is approximately the same beneath all regions (the currently observed variations do not exceed ~20%) [Gordienko, 2023a]. During the transition from a region with one type of endogenic regime to another, changes in crustal heat generation (HG) must be compensated by opposite changes in heat production within the upper mantle. These changes are naturally proportional to the volumes of the respective geospheres. In the following, the volume of the crust is taken to be approximately 10% of that of the upper mantle.

Radiogenic heat production in the upper mantle beneath Precambrian platforms and Phanerozoic geosynclines is estimated at 0.04 and 0.06 μW/m³, respectively [Gordienko, 2023a; etc.].

This result has been obtained experimentally. Let us examine, using a specific example, how well these estimates agree with data for the crust of platforms and geosynclines. For this purpose, we consider results from seismic velocity models constructed along deep seismic sounding (DSS) profiles. The locations of the profiles and the relevant bibliography are given in [Gordienko et al., 2025a]. The total terrestrial heat flow (HF) generated by the crust is calculated using the relationship between heat generation and P-wave velocity (Vp), shown in Fig. 5.

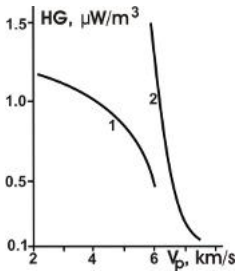

Fig. 5. Relationship between heat generation and P-wave velocity under pressure–temperature conditions typical of platform crust for primary sedimentary, diagenetically and paragenetically altered rocks (1) and crystalline rocks (2).

The results are presented in Fig. 6.

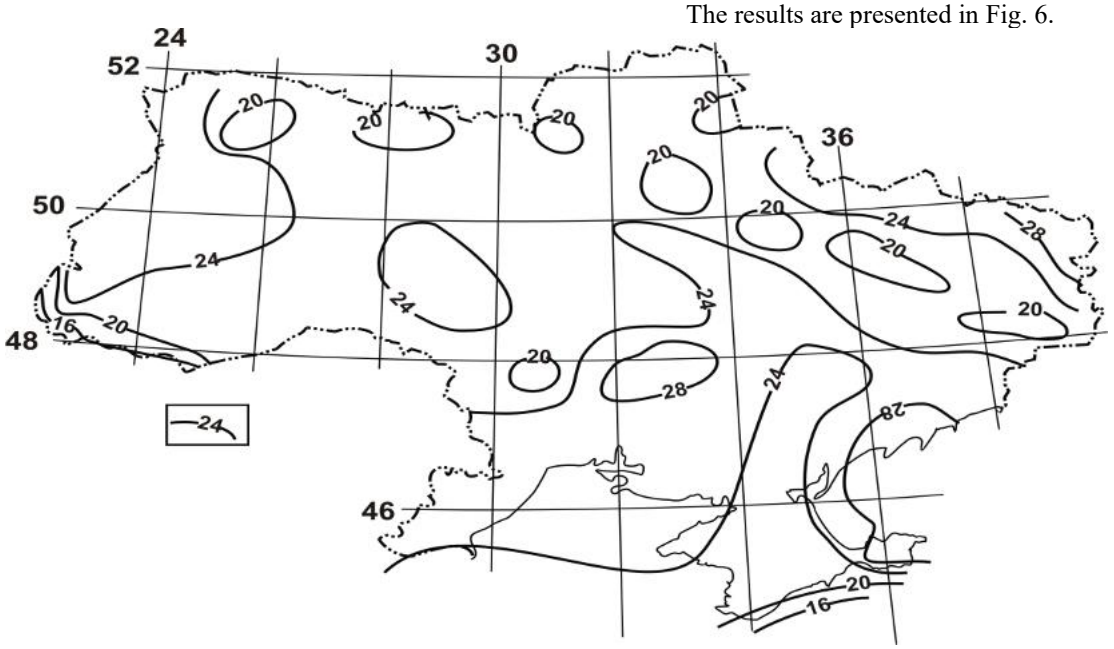

Fig. 6. Distribution of crustal heat flow (mW/m²) in the territory of Ukraine. 1—heat flow isolines; 2—boundary between the Carpathian Alpine geosyncline and the platform; 3—boundary between the Hercynian–Cimmerian geosyncline of the Scythian Plate and the platform.

NCGT Journal
New Concepts in Global Tectonics

New Concepts in Global Tectonics Journal
Volume 14, Number 6, June 2026

ISSN number; ISSN 2202-0039

The platform domain also includes the Donbas parageosyncline, which differs little in crustal structure from the rift-related Dnieper–Donets Basin of the East European Platform. The resulting distribution of HF is shown in Fig. 7.

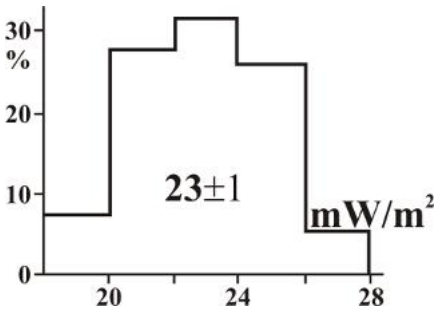

Fig. 7. Histogram of crustal heat flow distribution within the platform area of Ukraine.

In general, variations in crustal HF are small, despite the presence in the western part of the region of an area with anomalously low heat flow (extending north of Ukraine). Recalculation to average volumetric heat generation (for a crustal thickness of ~40 km) yields a value of 0.57 μW/m³.

Data for the Carpathian geosyncline (partly shown in Fig. 6) are considerably less detailed [Belyayevsky, 1981; Grad et al., 2006; Pozhgay, 1977; Sollogub et al., 1979; Starostenko et al., 2013; etc.]. Within this region, it is not meaningful to construct isolines of crustal heat flow due to the uneven distribution of DSS profiles. The level of crustal HF can be estimated from the data in Fig. 5. In other parts of the region, similar results have been obtained: the calculated heat flow decreases toward the center of the Pannonian median massif to values slightly below 10 mW/m². All seismic velocity values in crustal sections were adjusted to ensure comparability with platform conditions. The magnitude of temperature differences is illustrated in [Gordienko et al., 2025b]. Corrections accounting for elevated temperatures and partial melting in the crust, which increase seismic velocities in the Carpathians, reach several tenths of km/s. The calculated crustal HF is shown in Fig. 8.

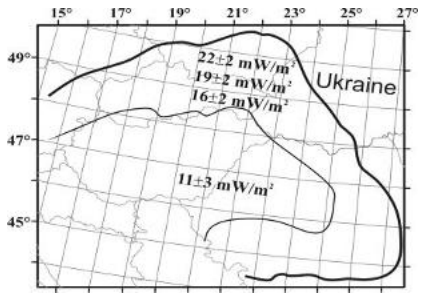

Fig. 8. Distribution of crustal heat flow in the Carpathian geosyncline.

Mean HF values were determined for four zones: the Pre-Carpathian marginal deflection, the Outer and Inner fold belts, and the Pannonian median massif. Taking into account their areal extent, the mean value for the entire geosyncline is 15 mW/m². The corresponding radiogenic heat production in the crust is 0.37 μW/m³.

Thus, during crust–mantle exchange, basification, and reduction of crustal thickness, the crust loses approximately 0.2 μW/m³, while the underlying mantle gains about 0.02 μW/m³. It is in good agreement with experimental data.

TRANSITION FROM A GEOSYNCLINE TO AN OCEAN

The authors' view of the structure of the oceanic crust differs from the conventional one. The brief information presented above on its formation makes it reasonable to assume that at depths from about 10–15 km to ~30 km, along with peridotites, a significant amount of relic continental crust is preserved. It is represented by mafic granulites and eclogites that by this time have subsided to relatively shallow depths, as well as by intrusions of mafic melts derived from the upper mantle. The latter are most likely serpentinized. Thus, this depth interval differs from typical mantle material in both composition and level of radiogenic heat generation. This difference is small (HG reaches only 0.10–0.12 μW/m³), and the total contribution to the radiogenic crustal heat flow is about 2 mW/m². The idea of a relatively thick oceanic crust is also present in studies [Krasnyi, 1983; Lomtev et al, 2016; Vasilyev, 1989, etc.].

To assess the validity of this viewpoint, about 200 Vp values were selected from seismic velocity sections in the Atlantic and Pacific Oceans within the subcrustal layer down to depths of 40 km. At depths greater than 12 km, velocities determined for 12–20 km dominate, although deeper levels are also significantly represented. Notably, the pattern of velocity distribution is quite similar to that observed beneath the Angola–Brazil Geotraverse (see below). The average velocity in the 12–30 km depth interval is about 7.9 km/s. However, the dataset as a whole rather indicates the presence of two types of rock blocks with different mean Vp values. In this study, information on the distribution of seismic wave velocities at depths greater than 12 km was supplemented with data from numerous DSS (deep seismic sounding) profiles in the Pacific and Atlantic oceans (see Fig. 11); the total number exceeded 300 (Fig. 9).

NCGT Journal
New Concepts in Global Tectonics

New Concepts in Global Tectonics Journal
Volume 14, Number 6, June 2026

ISSN number; ISSN 2202-0039

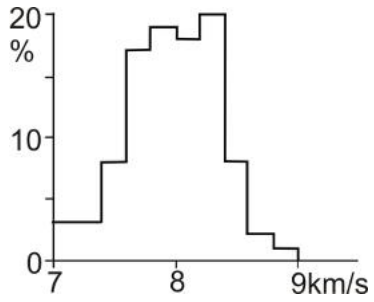

Fig. 9. Histogram of seismic-wave velocities at depths of 12–30 km beneath oceanic basins.

The obtained distribution most likely reflects a superposition of two datasets with mean Vp values of approximately 7.9 and 8.4 km/s.

Information on the depth of the Moho discontinuity derived from seismic data also shows a wide range of values in the Pacific Ocean [Deep…, 1987, etc.]. However, the criteria used by different authors to define the base of the crust vary considerably, making these differences difficult to regard as reliable. More well-founded are the distributions of seismic velocities below this boundary (Fig. 10).

Thus, significant variations in seismic-wave velocities at the considered depths beneath the oceans are well established.

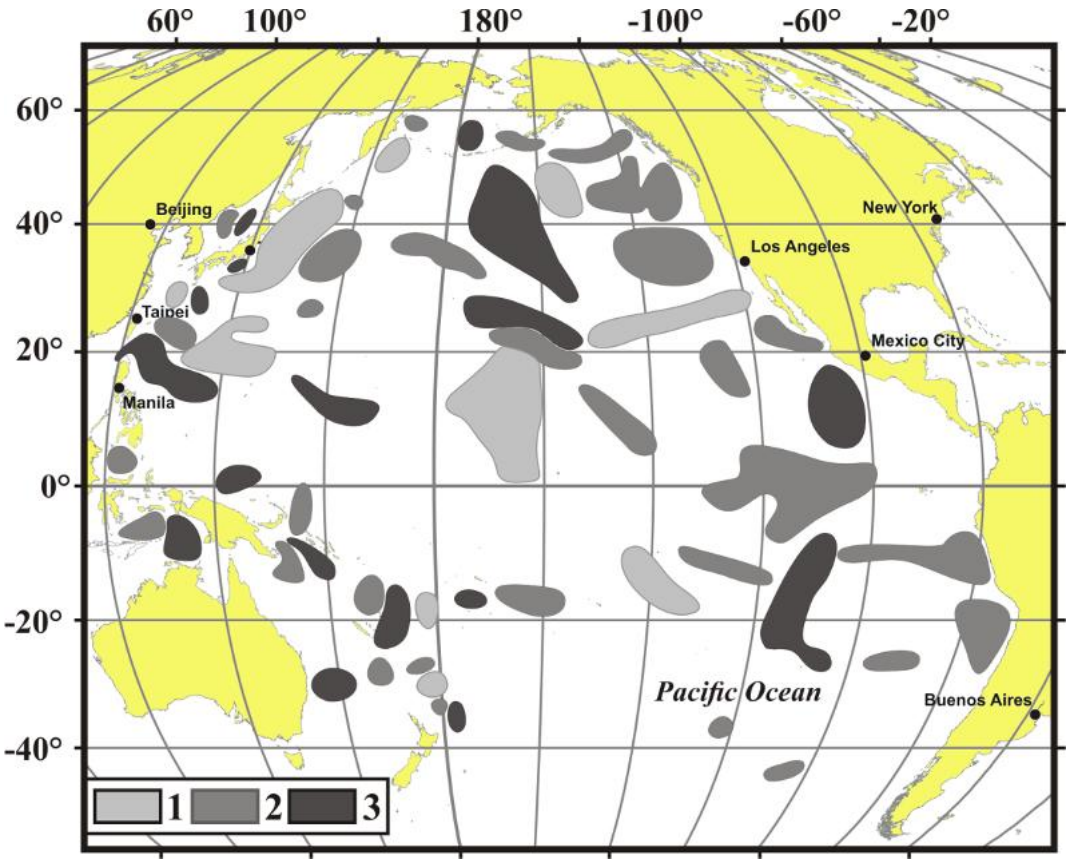

Fig. 10. Areas with different Vp values at depths greater than 10 km in the Pacific Ocean [Deep…, 1987]. 1 – 8.4 km/s and higher; 2 – 8.0–8.3 km/s; 3 – 7.9 km/s and lower.

Figure 11 shows the locations of DSS (deep seismic sounding) profiles along which velocity sections of the crust in the Pacific and Atlantic Oceans were constructed and used to calculate crustal heat flow. The calculations are for depth intervals of about 10–15 km below the seafloor. An additional 2 mW/m² (see above) was added to all results. In cases of high seismic velocities in the 12–30 km interval, where a higher concentration of eclogites may be assumed, no significant change occurs. The HG value for eclogites is ~0.12 μW/m³.

NCGT Journal
New Concepts in Global Tectonics

New Concepts in Global Tectonics Journal
Volume 14, Number 6, June 2026

ISSN number; ISSN 2202-0039

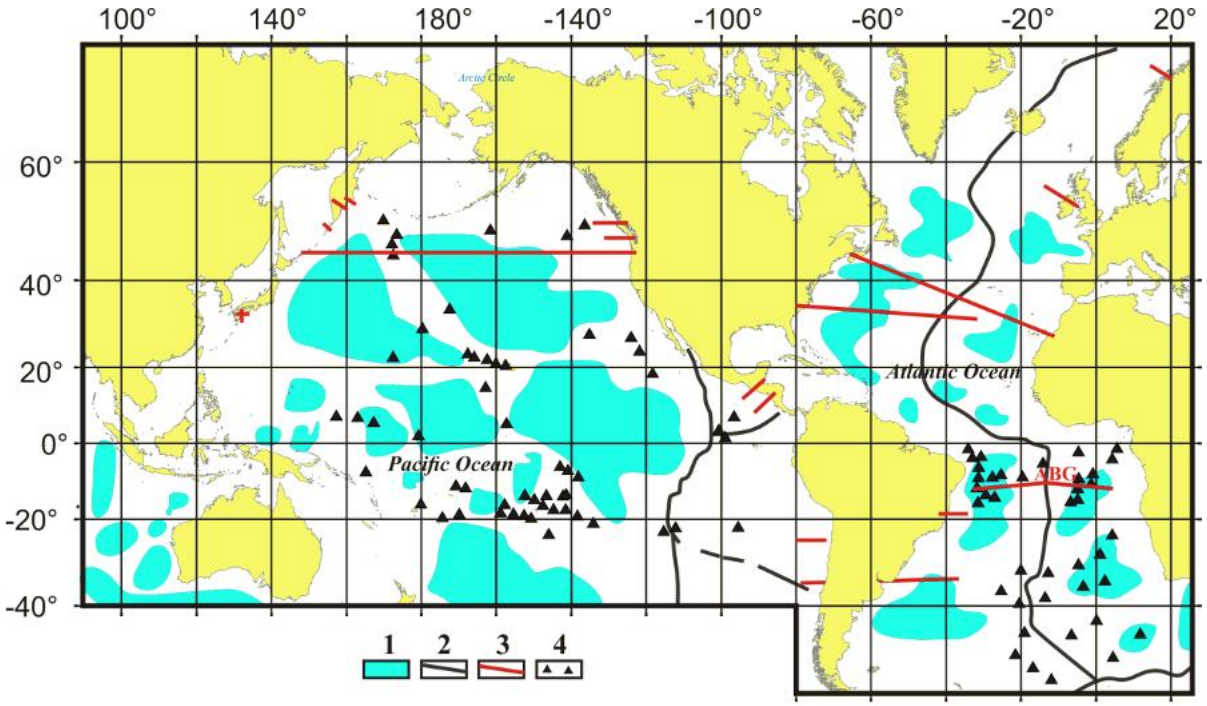

Fig. 11. Locations of DSS profiles in the Pacific and Atlantic Oceans used to calculate crustal heat flow from velocity sections [Belyayevsky, 1981; Deep…, 1987; Geology…, 1978; Golubeva, 2009; Gordienko et al., 2023; Mjelde et al., 1992; Menard, 1964; Pogrebitsky et al., 1990; Pavlenkova et al., 1993; Vasilyev, 1989, etc.]. ABG – Angola–Brazil Geotraverse.

The calculated values of crustal heat flow are remarkably stable: 7 ± 1 mW/m². Accordingly, their difference from the average HF for the geosyncline is about 8 mW/m². The amount of radiogenic sources transferred from the crust to the mantle is about 0.02 μW/m³, bringing the average HG in the upper mantle beneath the oceans to ~0.08 μW/m³.

Along long DSS profiles, information on the distribution of seismic velocities in the crust is often sparse. An exception is the Angola–Brazil Geotraverse, where not only is a much denser set of Vp values available at depths up to 10–15 km, but data are also provided down to 27 and 80 km [Pavlenkova et al., 1993; Pogrebitsky et al., 1990] (Fig. 12).

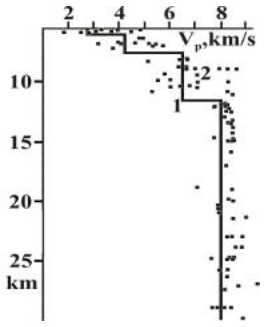

Fig. 12. Velocity sections of the crust and upper mantle along the Angola–Brazil Geotraverse. Vp distributions: 1 – calculated (see above); 2 – experimental [Pavlenkova et al., 1993; Pogrebitsky et al., 1990].

The Vp values shown in Fig. 12 are projected onto a single section along the entire length of the geotraverse, excluding the ridge zone of the Mid-Atlantic Ridge. Agreement with calculated values derived from the oceanization model may be considered satisfactory down to depths of ~12 km. However, deviations are large, averaging ±0.8 km/s. At greater depths, discrepancies increase, with experimental Vp values predominantly exceeding calculated ones. Velocities in the range 8.4–8.8 km/s are widely observed—significantly higher than expected for mantle rocks at the relevant temperatures. In the mantle, the average velocity difference at the same depth is ~0.6 km/s. Various explanations have been proposed for such variations, but in any case, they should be regarded as sources of uncertainty. Therefore, these data are unsuitable for rigorous quantitative validation of the model.

A clearer picture emerges from the study of magnetic field anomalies in the oceans. The thin upper basaltic layer is insufficient to account for their intensity. The sources must be placed, at least in part, at depths commonly attributed to the mantle, for which the presence of magnetically active minerals is generally considered uncharacteristic. In fact, such minerals are quite widespread within this depth interval beneath oceanic plates. Beneath major anomalies (e.g., the Broken anomaly west of Australia or the South Kuril anomaly), the lower

ISSN number; ISSN 2202-0039

boundaries of the sources are interpreted to lie much deeper than the commonly accepted Moho discontinuity.

Experimental data indicate that the typical magnetization of lower crustal rocks is about 3–3.5 A/m. In this case, the anomalies can be explained assuming a crustal base depth of about 25–30 km. As shown in Fig. 3, beneath oceanic basins at these depths, the Curie temperature of magnetite has not been exceeded.

Thus, in the 12–30 km depth interval, the rock assemblage does not correspond to a mantle composition but rather represents the lower part of the oceanic crust. Following the intrusion of mafic melts from the underlying mantle, these rocks were serpentinized and acquired significant magnetization. It is likely where the linear magnetic anomaly sources are located [Gordienko, 2023b, etc.].

The difficulty in reconciling calculated and observed seismic velocities may also indicate that the proposed oceanization model is incomplete. As noted in [Shlezinger et al., 2014, etc.], regions of modern (Late Cenozoic) activation occur in the oceans, including possibly near the Angola–Brazil Geotraverse. As on the continents, zones of modern activation are widespread in the oceans. One manifestation is rifting of mid-ocean ridges (MORs). Comparison of young basalts from the Mid-Atlantic Ridge with those from oceanic basins reveals significant differences. The latter show contamination of mantle-derived melts by remnants of continental crust still present at the time of their formation, and MOR basalts do not, having interacted only with oceanic crust [Frolov et al., 2011, etc.]. Direct contact between rift zones and less intense forms of activation (based on current data) is absent; inactive marginal plateaus lie between them. No present-day heat and mass transfer is observed in the mantle beneath deep-sea trenches. Their anomalously rapid, sediment-uncompensated subsidence is related to polymorphic transformations of rocks occurring simultaneously beneath both active Alpine geosynclines and oceanic plates. Comparisons with gravity and heat-flow data support such a complex model of deep processes [Gordienko, 2012, 2022; Gordienko et al., 2023a,b, etc.]. Thermal models of the tectonosphere allow estimates of ocean floor' uplift and subsidence amplitudes that are broadly consistent with observations. However, these estimates remain approximate and largely qualitative; they do not yet allow reconstruction of the full temporal evolution of seafloor movements. A comprehensive understanding of deep processes still requires further study.

CONCLUSION

The use of data on the contents of U, Th, and K in rocks of the Earth's crust and upper mantle reveals that the total heat production (during the Phanerozoic) is essentially the same for the principal types of endogenic regimes observed on continents and in oceans. Given the fundamental differences in thickness and composition between continental platform crust and oceanic crust, together with clear evidence that the latter formed based on the former, the necessity of intensive crust–mantle exchange becomes evident. The deep processes responsible for this exchange have been examined in the present study within the framework of the authors' general geological theory. Their effects, expressed in terms of crustal heat generation, have been evaluated using a substantial body of experimental data from continental platforms, Alpine geosynclines, and oceanic basins of the Pacific and Atlantic Oceans. Thus, it was possible to demonstrate the sufficient justification of the forecast made.

Less successful, however, was the attempt to validate the calculated velocity model of the Earth's crust and the uppermost mantle beneath oceanic basins using observational data on P-wave velocities. The available empirical data for the upper mantle lack sufficient resolution and accuracy. Nevertheless, the assumption that rocks in the depth range from 10-15 km to approximately 30 km are crustal is confirmed by geological and magnetometric information.

REFERENCES

Belousov V.V. (1954). The next problem of geotectonics. *Sovietskaya Geologiya*, Collected Works, no. 41, 3–25 (in Russian).

Budyko M.I., Ronov A.B., Yanshin A.L. (1987). *History of the Earth's atmosphere*. Berlin, Springer-Verlag, 139 p.

Deep seismic probing, Pacific data (1987). *Materials of the World Data Center*. Moscow, Geophysical Committee of the USSR, 104 p. (in Russian).

Density and composition of the upper mantle. http://www.geologam.ru/geophysics/lithosphere/plotnost-i-sostav-verhney-mantii (accessed March 2026) (in Russian).

Dickins J.M. (1994). The nature of the oceans or Gondwanaland: fact and fiction. In: *Proceedings of the Gondwana Nine Symposium*. Rotterdam, Balkema, 387–396.

Dobrynin V.M., Vendelstein B.Yu., Kozhevnikov D.A. (2004). *Petrophysics (physics of rocks)*. Moscow, Russian State University of Oil and Gas, 368 p. (in Russian).

ISSN number; ISSN 2202-0039

Frolov V.T., Frolova T.I. (2011). *Origin of the Pacific*. Moscow, MAKS Press, 52 p. (in Russian).

Geology of continental margins (1978). Vol. 2. Eds C. Burke, C. Drake. Moscow, Mir, 372 p. (in Russian).

Golubeva E.D. (2009). *Evolution of Pacific magmatism*. Vladivostok, Dalnauka, 132 p. (in Russian).

Gordienko V.V., Gordienko I.V., Zavgorodnya O.V. et al. (2011). *Ukrainian Carpathians (geophysics, deep-seated processes)*. Kyiv, Logos, 129 p. (in Russian).

Gordienko V.V. (2012). *Processes in the Earth's tectonosphere (advection–polymorphic hypothesis)*. Saarbrücken, LAP, 256 p. (in Russian).

Gordienko V. (2022). About geological theory. *Geofizicheskiy Zhurnal* 44(2), 68–92, https://doi.org/10.24028/gj.v44i2.25626

Gordienko V., Gordienko L. (2023). Mantle gravitational anomalies in zones of different endogenous regimes. *NCGT Journal* (1), 63–77.

Gordienko V. (2023a). On the energy balance of the tectonosphere. *Geodynamics* (2), 62–71.

Gordienko V.V. (2023b): Earth's crust and physical fields of the oceans. *Geofizicheskiy Zhurnal* 45(1), 36–54, https://doi.org/10.24028/gj.v45i1.275176

Gordienko V.V., Gordienko I.V. (2025a). Crustal heat flow in Ukraine. *Geofizychnyi Zhurnal* 47(1), 108–119, https://doi.org/10.24028/gj.v47i1.311435

Gordienko V.V., Gordienko I.V. (2025b). Temperatures of the tectonosphere of Ukraine. *Geofizychnyi Zhurnal* 47(4), 122–133, https://doi.org/10.24028/gj.v47i4.330049

Grad M., Guterch A., Keller G. et al. (2006). Lithospheric structure beneath the Trans-Carpathian transect from the Precambrian Platform to the Pannonian Basin: CELEBRATION 2000 seismic profile CEL05. *Journal of Geophysical Research* 111(B3), https://doi.org/10.1029/2005JB003647

Handbook of Physical Constants (1969): Ed. S. Clark. Moscow, Mir, 544 p. (in Russian).

Krasny M.L. (1983). *System of paleo-island arcs of Northeast Asia*. *Structure and dynamics of transition zones*. Moscow, Nauka, 49 p. (in Russian).

Lomtev V.L., Veselov O.V., Kozlov D.N. et al. (2016). Features of the structure and geodynamics of the tectonosphere of the northwestern Pacific Ocean and Far Eastern seas: a collective monograph. Vladivostok:Dalnauka 148p. (in Russian).

Macdonald G. (1949). Hawaiian petrographic province. *Bulletin of the Geological Society of America* 60, 1541–1590.

Menard H.W. (1964). *Geology of the Pacific Ocean floor*. New York, McGraw-Hill, 276 p.

Mineral Physics and Crystallography. A Handbook of Physical Constants (1995): Ed. T.J. Ahrens. Washington, AGU, 354 p.

Mjelde R., Sellevoll M.A., Shimamura H. et al. (1992). A crustal study of Lofoten, N. Norway, by use of 3-component Ocean Bottom Seismographs. *Tectonophysics* 212, 269–288.

Pavlenkova N.I., Pogrebitsky Yu.E., Romanyuk T.V. (1993). Seismic–density model of the crust and upper mantle in the South Atlantic along the Angola–Brazil Geotraverse. *Fizika Zemli* (10), 27–38 (in Russian).

Petrophysics (1992): Ed. N.B. Dortman. Vol. 1. Moscow, Nedra, 391 p. (in Russian).

Pogrebitsky Yu.E., Goryachev Yu.V., Osipov V.A. et al. (1990). Structure of the oceanic lithosphere based on research from the Angola–Brazil Geotraverse. *Sovietskaya Geologiya* (12), 8–22 (in Russian).

Pozhgay K. (1977). Seismic reflectors and velocity distribution in the Earth's crust and upper mantle. In: *Structure of the Earth's crust and upper mantle from seismic data*. Kyiv, Naukova Dumka, 228–230 (in Russian).

Rudich E.M. (1984). *Expanding oceans: facts and hypotheses*. Moscow, Nedra, 251 p.

Shlezinger A., Khortov A., Korneva R., Patrikeev V. (2014). Yu.M. Pushcharovsky's views on deep oceanic basins. *NCGT Journal* (4), 11–12.

Sollogub V.B., Guterch A., Prosen D. et al. (1979). *Structure of the Earth's crust of Central and Eastern Europe based on geophysical data*. Kyiv, Naukova Dumka, 208 p.

Starostenko V., Janik T., Kolomiyets K. et al. (2013). Seismic velocity model of the crust and upper mantle along the PANCAKE profile across the Carpathians between the Pannonian Basin and the East European Craton. *Tectonophysics* 608, 1049–1072, https://doi.org/10.1016/j.tecto.2013.07.008

Storetvedt K. (1997). *Our evolving planet: Earth history in a new perspective*. Bergen, Alma Mater, 456 p.

Turcotte D.L., Schubert G. (1985): *Geodynamics: applications of continuum physics to geological problems*. Moscow, Mir, 730 p. (in Russian).

Udintsev G.B. (1987). *Topography and structure of the ocean floor*. Moscow, Nedra, 240 p. (in Russian).

Vasilyev B.I. (1989). On the structure and evolution of the Pacific Ocean floor. *Tikhookeanskaya Geologiya* 4, 3–10 (in Russian).

ISSN number; ISSN 2202-0039

ABOUT THE NCGT JOURNAL

The NCGT Newsletter , the predecessor of the NCGT Journal , was begun as a result of discussions at the symposium "Alternative Theories to Plate Tectonics " held at the 30th International Geological Congress in Beijing in August 1996 . The name is taken from an earlier symposium held in association with the 28th International Geological Congress in Washington , D. C. in 1989. The first issue of the NCGT Newsletter was December 1996. The NCGT Newsletter changed its name in 2013 to the NCGT Journal . Aims of the NCGT Journal include:

1. Providing an international forum for the open exchange of new ideas and approaches in the fields of geology, geophysics , solar and planetary physics , cosmology , climatology , oceanography , electric universe , and other fields that affect or are closely related to physical processes occurring on Earth from its core to the top of its atmosphere.
2. Forming an organizational focus for creative ideas not fitting readily within the scope of dominant tectonic models.
3. Forming the basis for the reproduction and publication of such work, especially where there has been censorship or discrimination.

https://www.GeoplasmaResearchInstitute.org/